Max Planck Institute
of Colloids and Interfaces

Universität Potsdam

Chemomechanical coupling and motor cycles of the molecular motor myosin V

von

Veronika Bierbaum

Dissertation

zur Erlangung des akademischen Grades

"doctor rerum naturalium"

(Dr. rer. nat.)

in der Wissenschaftsdisziplin Physik

Max-Planck-Institut für Kolloid- und Grenzflächenforschung
Theorie und Bio-Systeme

Potsdam, Februar 2011

Published online at the
Institutional Repository of the University of Potsdam:
URL http://opus.kobv.de/ubp/volltexte/2011/5361/
URN urn:nbn:de:kobv:517-opus-53614
http://nbn-resolving.de/urn:nbn:de:kobv:517-opus-53614

Erklärung

Hiermit versichere ich, dass ich die vorliegende Arbeit selbstständig verfasst und keine anderen als die angegebenen Quellen und Hilfsmittel benutzt habe.

Potsdam, den 15. Januar 2011

Contents

Abstract

In the living cell, the organization of the complex internal structure relies to a large extent on molecular motors. Molecular motors are proteins that are able to convert chemical energy from the hydrolysis of adenosine triphosphate (ATP) into mechanical work. Being about 10 to 100 nanometers in size, the molecules act on a length scale, for which thermal collisions have a considerable impact onto their motion. In this way, they constitute paradigmatic examples of thermodynamic machines out of equilibrium.

This study develops a theoretical description for the energy conversion by the molecular motor myosin V, using many different aspects of theoretical physics. Myosin V has been studied extensively in both bulk and single molecule experiments. Its stepping velocity has been characterized as a function of external control parameters such as nucleotide concentration and applied forces. In addition, numerous kinetic rates involved in the enzymatic reaction of the molecule have been determined. For forces that exceed the stall force of the motor, myosin V exhibits a 'ratcheting' behaviour: For loads in the direction of forward stepping, the velocity depends on the concentration of ATP, while for backward loads there is no such influence.

Based on the chemical states of the motor, we construct a general network theory that incorporates experimental observations about the stepping behaviour of myosin V. The motor's motion is captured through the network description supplemented by a Markov process to describe the motor dynamics. This approach has the advantage of directly addressing the chemical kinetics of the molecule, and treating the mechanical and chemical processes on equal grounds. We utilize constraints arising from nonequilibrium thermodynamics to determine motor parameters and demonstrate that the motor behaviour is governed by several chemomechanical motor cycles. In addition, we investigate the functional dependence of stepping rates on force by deducing the motor's response to external loads via an appropriate Fokker-Planck equation. For substall forces, the dominant pathway of the motor network is profoundly different from the one for superstall forces, which leads to a stepping behaviour that is in agreement with the experimental observations. The extension of our analysis to Markov processes with absorbing boundaries allows for the calculation of the motor's dwell time distributions. These reveal aspects of the coordination of the motor's heads and contain direct information about the backsteps of the motor. Our theory provides a unified description for the myosin V motor as studied in single motor experiments.

1 Introduction

1.1 A first glance at molecular motors

This study characterizes the stepping dynamics of myosin V, a linear molecular motor that converts chemical energy into mechanical work by means of an enzymatic reaction. In general, an enzyme is a protein that acts as a catalyst to a chemical reaction by supporting the conversion of a chemical substrate into its product.

In the cell, thousands of different molecules are constantly being converted through chemical reactions. Among these, enzymatic reactions play an important role as they enhance and therefore select a specific chemical reaction. This establishes a hierarchy of chemical reactions in the cell. The series of these reactions are called metabolic pathways. The set of all pathways constitutes the metabolic network, which is of basic importance for the homeostasis, or self-regulation, of an organism. Another particular feature of an enzymatic reaction is its tuneability with respect to a variety of external parameters like the chemical environment and the temperature. The function of an enzyme can, in addition, be regulated by co-factors, helper molecules that enhance or suppress its activity. A variety of enzymes that perform different tasks and are linked through their substrates or products thus establish a highly elaborate, yet controlled process. A comprehensive discussion of the molecular biology of the cell including all its complex processes can be found in the book of Alberts [1]. For condensed information about enzymatic processes in the cell, we refer to the atlas of biochemical pathways [2] and a map of the metabolic pathways [3].

Molecular motors fall into a category of enzymes that are able to generate mechanical motion, ranging from cargo transport to the induction of fluid flows or molecule assembly. The cellular machinery comprises a fascinating variety of motors such as ion pumps, cargo transporting motors, or machines for the manipulation of DNA. Each of these motors has a specific and often very elaborate fashion to perform its task despite the noisy environment it is exposed to. The size of molecular machines, typically several tens to a few hundred nanometers, is on a length scale of the physical world where random collisions with surrounding molecules govern the motion of a free particle.

Linear molecular motors move along the different filaments that form the cytoskeleton, the complex structure that constitutes the solid part of the eucaryotic cell. It consists of mainly two types of filaments, microtubules and actin. The microtubules are oriented from the centrosome with their positive end towards the cell periphery. They lead to a

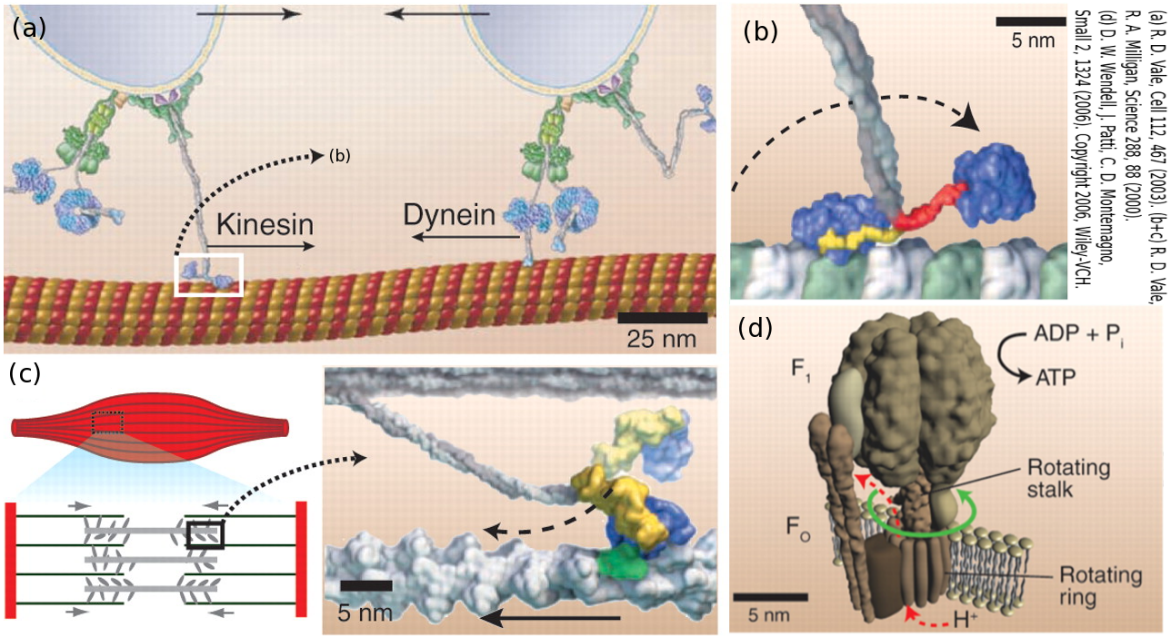

Figure 1.1 : Examples of motor proteins in the cell. (a) Conventional kinesin and dynein serve as cargo transporters in opposite directions along microtubules. (b) Kinesin is a linear motor, whose two heads walk in a hand-over-hand fashion in steps of 8 nm along microtubules. (c) Muscle contraction is caused by by the power stroke of myosin II attached to actin in a sarcomere unit. The nonprocessive myosin II detaches after each power stroke. (d) The rotary motor F0F1-ATPase. For a substrate concentration that results in ATP hydrolysis, to motor drives a proton flux through a rotary motion of its subunits. With changing the substrate concentration, the motor performs a proton-driven synthesis of ATP. Figure adapted from [4], with the original sources listed on the right hand side.

network of actin filaments that stabilizes the cell shape. Kinesin and dynein are linear molecular motors that transport cargo along microtubules, whereas the motors myosin V and VI move in opposite directions along actin filaments. The nonprocessive myosin II serves as a linker of the actin network.

Fig. 1.1 shows a selection of motor proteins in the cell. Kinesin and dynein, depicted in panels (a) and (b), walk along microtubules in opposite directions in a hand-over-hand fashion, and may be attached to the same cargo. Panel (c) shows the most prominent relative of myosin V, myosin II, typically referred to as the muscle myosin. Besides its function as a linker in the cytoskeleton, it is involved in the contraction of muscles. By means of a stroke, driven by ATP hydrolysis, an assembly of myosin II motors on actin causes a sliding motion of the filaments that leads to muscle contraction. In (d), a rotary motor, the F0F1-ATPase, is shown. It serves, depending on the concentration of its substrate and products, either as a proton pump that is fueled by ATP hydrolysis or a proton-driven machine for ATP synthesis.

A common element to all motor proteins is that they consume a fuel, typically ATP or GTP, that releases energy by means of a chemical reaction and is used by the motor to perform its work. The biological details of molecular motors exhibit all features of nature's ingenious diversity, but their function is based on fundamental principles of energy conversion, for instance, enzymatic activity.

Molecular motors pose a challenge for researchers ranging from experiment to theory, from biology to chemistry and physics. The fascination arising from molecular motors is, last but not least, based on the fact that their work in progress can nowadays be observed by means of advanced experimental techniques in high resolution and real time. This level of insight has been around only two decades, and is taken further as different elaborate methods of modern microscopy are combined to investigate biomolecules.

1.2 The physics of molecular motors

The physics to describe the function of the cellular machinery is the physics of nonequilibrium thermodynamics. Therfore, molecular motors provide a *live* example of a thermodynamic machine far from equilibrium.

Experimentally, an *in vitro* observation allows for separation of the motor from its natural environment, the cell, and testing it in a controlled fashion with a limited set of parameters. From a theoretical point of view, the motor provides an example of a dynamical system with non-negligible thermal noise. This is of particular interest with respect to the formulation of thermodynamic rules, the constraints they evoke for the system, and its fluctuation theorems. The motor is exposed to a flux of energy to and from other systems, a situation which poses the fundamental difficulty of defining entropy for systems out of thermodynamic equilibrium. In case of stationarity, this definition becomes feasible, and the interplay of chemical and mechanical energy along

with the production of entropy can be accessed. A variety of concepts established for nonequilibrium thermodynamics have been formulated with respect to molecular motors, like fluctuation theorems [5], the Onsager reciprocal relations [6] or the motor efficiency [7, 8, 9]. A general approach to molecular motors both experimentally and theoretically can be found in the book of Howard [10].

For the theoretical treatment of the cellular machinery, two complementary concepts have emerged in the past years. One approach is based on a continuous description called thermal ratchets, and the other one, used in this work, relies on discrete chemomechanical networks. General reviews of these concepts can be found in [11, 12, 13, 14, 15].

The description of the motor as a thermal ratchet provides a simplistic approach based on minimal parameter input to generate a directed motion [16]. With a focus on the motor's motion that is modelled through an effective potential, the chemical reaction is used to trigger a motion by inducing a change of the potential in form of a periodically changing signal. This signal facilitates the motor's mechanical displacement into a given direction and thus results in a directed motion. Ratchets are continuous in time and space, and their mathematical treatment, apart from a few simple cases, can turn rather elaborate. As the underlying potentials may not be accessible to experiment, the ratchet's parameters sometimes can not directly be mapped onto experimental observables.

The use of an enzymatic network to model the motor's motion relies on a set of chemical states that form the network. Both the chemical reaction and the motor's motion are treated on an equal footing through transitions between these states. One assumption that allows for this procedure relies on the separation of timescales of the chemical reactions and the motor's mechanical transitions. A second requirement is that thermal equilibrium is acquired for each designated state, which means that after a transition from one state to another, the system relaxes into thermal equilibrium on a timescale that is fast compared to the transition in itself. Compared to thermal ratchets, the amount of the model's parameters, like transition rates, rises with the complexity of the network. It is, however, possible to relate these parameters to measurable quantities that can in principle be accessed experimentally, and in most cases have indeed been measured. As the network description is discrete in space, the identification of relevant states that connect dominating pathways to the enzymatic reaction is crucial for the network's quality. This problem is similar to finding a good finite approximation to an infinite Hamiltionian in quantum mechanics, and often, the techniques used rely on an educated guess that is taken with respect to the system's inherent constraints like its symmetries.

In our approach to molecular motors [17, 18], the constraints are posed by thermodynamics, and the educated guess has a footing on experimental observations. Our guidance to find a network description follows the principle of Occam's razor, *entia non sunt multiplicanda sine necessitate - entities must not be multiplied beyond necessity.*

1.3 Experimental characterization of the molecular motor myosin V

In a chemomechanical description, the motor is treated as a system whose motion is characterized by its center of mass and its ability to move forward by means of passing through several interacting chemical states. One can think of the motor as a moving particle with a specific internal functionality, which corresponds to the level of observation as given in single-molecule experiments carried out with optical tweezers. Its performance is captured by a sequence of chemical reactions with mechanical transitions that constitute different pathways the motor explores for its work. We are therefore interested in chemical and stepping variables of the motor rather than its atomic or molecular details. Myosin V is a motor protein that processively moves along actin

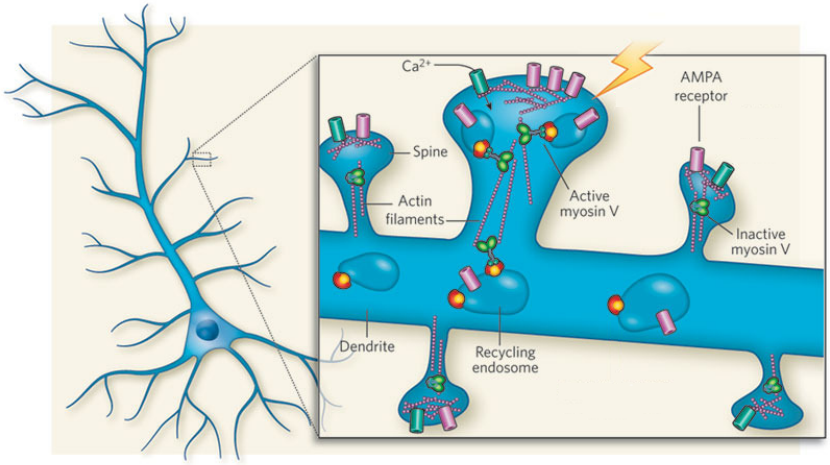

Figure 1.2 : Cell function of myosin V. The figure depicts a neuron with a dentritic spine, a membrane protrusion that receives input from a synapse. For strengthening (yellow flash), the synapses need to be supplied by membrane pieces and receptors (AMPA). Through influx of Ca^{2+} at the spines, the myosin V is activated. At the dendrite shaft, it binds, at the recycling endosome, to a protein (red and yellow bead) containing AMPA receptors (lila). Subsequently, it transports cargo into and along spines through processive motion on actin filaments to mediate insertion of the receptors at the cell surface. In the subsynaptic region, the actin filaments are not oriented and thus allow for transport in various directions. Figure adapted from [19].

filaments in a hand-over-hand fashion. By virtue of its extraordinary step size of 36 nm, it has experienced deep interest since the first observations of its processive motion [20, 21]. A great variety of experimental methods has been applied for the characterization of the molecule ranging from bulk chemokinetic experiments to single-molecule

methods with both fluorescence techniques and optical traps. It is believed to serve as a cargo transporter, but little is known about the actual details of its function. However, it has been discovered only recently that myosin V is part of the molecular machinery in neurons that is responsible for the regulation of active transport of receptors into synapses [22, 23, 19], as illustrated in Fig. 1.2.

Myosin V is approximately 100 nm in size, and consists of a tail domain that binds the cargo, a light chain neck region and two lever arms of the motor that are build of 6 IQ motifs, i. e., calmodulin binding sequences of amino acids, with heads at their ends. The heads are responsible for both binding to the motor's track, the actin filament, and for energy conversion. Each head has a nucleotide binding pocket that is able to bind ATP and support its hydrolysis. Fig. 1.3 sketches some important experiments for the motor‘s characterization and a schematic drawing of the motor in panel (e).

The knowledge about the motor has been summarized in numerous reviews, [28, 29, 30, 31, 32, 33, 34, 35]. They include the coupling of its fuel consumption to its motion, its stepping details, like the distribution of step sizes, waiting times and thus velocities, as a function of a variety of control parameters. The latter are primarily nucleotide concentration and an external load force, but the influence by the length of its lever [36, 37, 38, 39] or the regulatory impact of Ca^{2+} have also been tested [40, 41, 42].

Most of the stepping properties of the molecule have been investigated using optical traps [43, 44, 45, 46, 47], where an external force can be exerted on the molecule via a roughly micrometer-sized polystyrene bead that is attached to myosin V, as sketched in Fig. 1.3 (a). The motor walks on an actin filament that is immobilized on a glass coverslip with myosin II or held in a second trap by its ends. In feedback traps, it is possible to keep the external force at a constant level. The bead is observed using an optical microscope that is usually coupled to a quadrant photodiode. A particularly elaborate feedback trap is used for the experimental observations in [47], where the motion of the bead in both vertical and horizontal direction is monitored at a resolution of nanometers. The data set for kinetic rates that form the main input to our model is based on the work of de la Cruz [48]. These are the rates of binding or release of ATP, ADP and phosphate. They are quantified using techniques to determine the kinetics of chemical reactions: The equilibrium binding constants for single-headed constructs of myosin V both in the presence and absence of actin are measured using a quench and a stopped flow apparatus with fluorescent titration.

The structural information about myosin V, with an example shown in Fig. 1.3 (b), stems from cryoelectronmicroscopy [25]. It directly visualizes the frozen motor molecules that can be attached to their tracks and initialized the debate about the motor's powerstroke or telemark conformation [49]. One way to explicitly monitor the motion of the molecule is the use of fluorescence microscopy, where both the motor and the actin filament are fluorescently labelled, as shown in panel (c). The newest highly spectacular experiment that directly observes the molecule at work includes movies that have

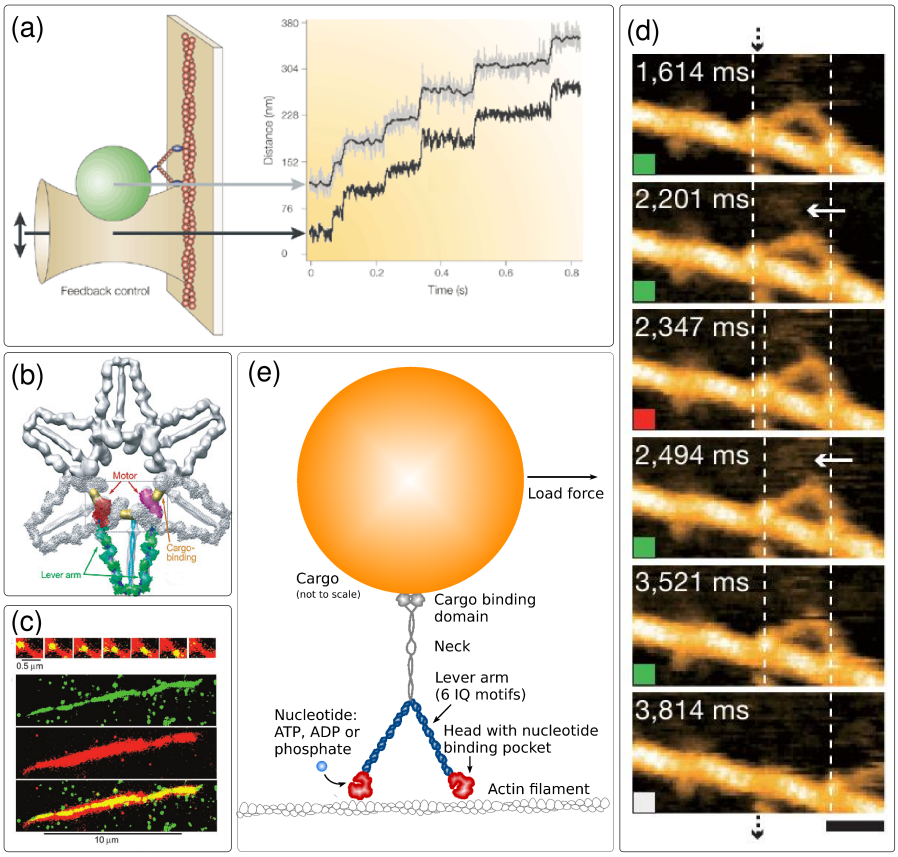

Figure 1.3 : Experiments carried out with myosin V and a schematic view of the molecule. (a) Sketch of a feedback-controlled optical trap. A bead (green) is captured in a laser trap (brown), thus allowing to extert forces up to several pN on the myosin V, that is fixed to the bead and moves along the immobilized actin filament. Monitoring the position of the bead results in the grey/black signal, and the feedback signal of the trap is shown in black. Taken from [24]. (b) Structure of a folded and thus inactive state of myosin V as observed in cryoelectromicroscopy [25]. (c) Fluorescently labelled myosin V molecules (green) moving along actin filaments (red), and their overlap (yellow), taken from [26]. (d) Time-series of video-imaging of moving myosin V by high-speed atomic force microscopy [27] The molecule has performed a step in the last picture. (e) Sketch of myosin V with indication of its molecular details.

been obtained with rapid atomic force microscopy [27], providing high-resolution images of the moving motor. A snapshot of the motion is shown in Fig. 1.3 (d). Taking the scale down to molecular details, conformational changes in the actin-binding region have been observed using fluorescence resonance energy transfer (FRET) [50]. In addition, Molecular Dynamics (MD) simulations have been used to investigate the conformational changes in the molecule's head upon the binding of nucleotides [51].

The details of the stepping mechanism that are observable due to the molecule's large step size have been elucidated in an elaborate fashion and conclude on the mechanism as being a combination of a power stroke and a subsequent diffusive search of the next binding site on the filament [52]. This mechanism is perceptible as substeps of the motor, which have been characterized by various groups [53, 47, 54, 55, 56]. Fluorophore and quantum dot labelling or the use of gold nanoparticles allow for the direct observation of the motor's hand-over-hand motion [57, 58, 59].

1.4 Outline of the thesis

This thesis is organized as follows.

Chapter 2 provides the theoretical framework of Markov processes and Markov chains with absorbing boundaries. We link the kinetics of an enzyme to a stochastic process, and show how the concept of stationarity can be used to calculate the motor's dynamic properties. For calculation of the stationary state of a given network, we introduce the corresponding matrix algebra and a method from graph theory. Finally, the theory of Markov chains with absorbing states will be used to determine dwell time distributions, i. e., the distribution of waiting times between two successive steps of the motor.

Chapter 3 gives an overview about thermal ratchets and sets the mathematical basis for deduction of mechanical stepping rates from the Fokker-Planck equation.

Chapter 4 deals with the application of the theory for the molecular motor myosin V. A network representation for the stepping motion of the motor is established based on experimental observations.

Chapter 5 focuses on macroscopic observables like the average velocity of the motor subject to different external parameters like the concentration of nucleotides or an external force. These quantities are calculated and compared with experimental data. In particular, the functional form of transition rates that are not accessible experimentally is deduced from basic physical principles.

Chapter 6 turns to the distributions of dwell times that can be determined analyti-

cally when splitting our network representation into single cycles. The influence of these as a function of an external load force is discussed and compared with results from simulations obtained for the complete network representation.

Chapter 7 concludes with a summary and provides an outlook into further prospects of the field. Different extensions of the model to capture further characteristic properties of myosin V will be discussed.

Appendix A deals with the details of the network's stationary state. Appendix B contains further information about the network properties in relation to experimental information. Appendix C provides information about the Gillespie algorithm, that has been used for the simulation of dwell time distributions. Appendix D gives the full form of the analytical solutions of the dwell time distributions.

2 Networks

This chapter motivates the use of networks for the description of enzymatic activity. It contains a short introduction to the enzymatic networks and their kinetics, followed by some aspects of graph theory, with the formal definitions restricted to our specific needs. To determine the stationary states of the master equation, we use a graph-theoretical method based on probability fluxes that are related to a method used by Kirchhoff [60]. Thereafter, we establish a connection to nonequilibrium thermodynamics, that relates the probability fluxes of discrete networks to the enzyme kinetics of molecular motors. Finally, we discuss the algebraic formalism for Markov processes, that can be found, for instance, in van Kampen [61], and its extension to Markov chains with absorbing states to describe the mathematical foundations for the calculation the motor's dwell time distribution.

2.1 Enzymatic networks

The activity of an enzyme or molecular motor can be described as a series of chemical reactions that involves the binding and release of chemical species, which results in their transformation from educts to products and vice versa. These chemical reactions may lead to conformational changes of the molecule that result in the motor's motion.

The motor typically moves along its filamentous track in a discrete fashion. Thus, its position can be specified by a discrete, one-dimensional coordinate that is parametrized along the filament. At a specific position, the motor can attain different conformational states, and have a different chemical composition at its catalytic domains. As a catalytic domain, the so-called nucleotide binding pocket, typically binds a single nucleotide, one can characterize the state of the molecule by the chemical state of its binding pocket. An empty binding pocket that supports ATP hydrolysis may bind an ATP molecule, which is cleaved to an ADP*P complex with subsequent release of phosphate, with bound ADP remaining, and the release of ADP leads to the empty pocket again. The possible chemical states are thus characterized by bound ATP, ADP*P, ADP, or an empty state, which leads to the chemical reaction cycle shown in Fig. 2.1 (a). The corresponding states are denoted by T (ATP bound), Θ (ADP*P bound), D (ADP bound), and E (empty). In principle, the binding pocket can have more than one conformational state that belongs to a bound nucleotide. As these conformational states require experimental knowledge about the molecular details of the binding pocket, and can not be resolved in

single-molecule experiments, we rely on a description with a state space determined by its chemical states. Moreover, it is hard to experimentally distinguish the ATP cleavage and phosphate release, i.e., the transition between the states T→ Θ → D, one combines the state Θ into the transition T → D, as shown in Fig. 2.1 (b) [11]. The remaining three

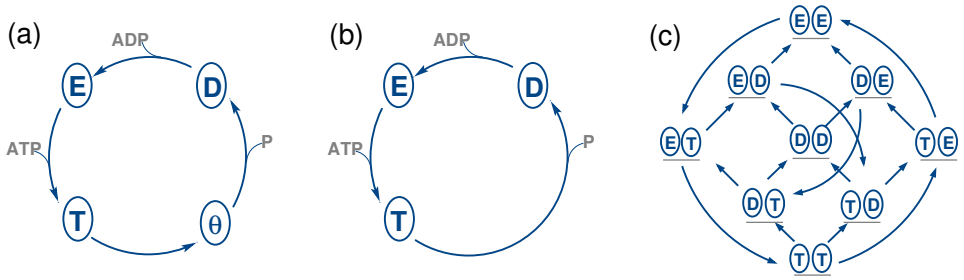

Figure 2.1 : Chemical networks for a single (a, b) catalytic domain and for two domains (c), with chemical transitions between the states in both directions, with arrows indicating the direction of hydrolysis. (a) Four chemical states characterized by an empty (E) domain, with ATP or ADP bound (D, T), and with the complex ADP*P (Θ). (b) Reduced version of the network where the cleavage transition and phosphate release have been combined into a single transition T → D. (c) For $M = 2$ catalytic domains, the chemical network consists of $3^M = 9$ states. When identifying the two domains as the heads of a molecular motor moving along a filament towards the right hand side (grey line), the trailing and the leading head can be associated with the left and right domain.

states of the binding pocket are thus denoted by T, D, or E, and the transitions between these states happen by binding or release of ATP, ADP, or phosphate. The extension to a motor molecule with multiple nucleotide binding pockets M, leads to a chemical state space that is composed by all 3^M combinations of the chemical states of the single pockets, as shown in Fig. 2.1 (c) for $M = 2$. Adding a spatial coordinate to the system to incorporate the motor's position leads to a network that consists of repeated copies of the chemical network along x_i, with mechanical transitions connecting specific chemical states. For a motor that moves in a hand-over-hand fashion, a mechanical transition is characterized by the interchange of the leading and the trailing head, such that the possible mechanical transitions for the network shown in Fig. 2.1 can happen between the states DT ⇌ TD, ET ⇌ TE, and ED ⇌ DE, as well as EE ⇌ EE, DD ⇌ DD, and TT ⇌ TT. As a motor repeatedly moves along its filament, and all chemical states can be attained at each position, we will impose periodic boundary conditions on the spatial coordinate of the system. The specific form of a network representation will be discussed in chapter 4.

Prior to discussing the general properties of networks, let us outline the motor's dynamics. We characterize the motor by chemical states, with both chemical and mechani-

cal transitions between two connected states taking place in a stochastic manner. These states form a probabilistic network, for which the probability $P_i(t)$ to find the motor in state i at time t evolves according to a master equation

$$\frac{\mathrm{d}}{\mathrm{dt}}P_i(t) = -\sum_j \Delta J_{ij}(t), \tag{2.1}$$

with

$$\Delta J_{ij}(t) \equiv P_i(t)\ \omega_{ij} - P_j(t)\ \omega_{ji} \tag{2.2}$$

being the local excess fluxes through the transition between two states i and j, where the transition rate ω_{ij} is given by the number of transitions from i to j per unit time. In the case of continuous energy supply and stepping, the motor resides in a steady state, which allows for calculation of its macroscopic properties like stepping velocity or hydrolysis rate. In the steady state, the probabilities P_i^{st} of the motor do not depend on time,

$$\frac{\mathrm{d}}{\mathrm{dt}}P_i^{\mathrm{st}} = 0, \tag{2.3}$$

and the dynamics of the system is determined by the corresponding steady state fluxes J_{ij}^{st} . We will return to the transition rates ω_{ij} in chapter 4, where they will be discussed in detail with respect to myosin V, and in the following focus on the graph-theoretical properties of networks.

2.2 Elements of graph theory

A graph $\mathcal{G}$= $\mathcal{G}(V, L)$ consists of two finite sets $V = \{v_1, ...v_n\}$ and $L = \{l_1, ...l_m\}$, where V contains n elements called vertices or nodes, and L is a two-element subset with m elements called links or edges connecting the nodes. An introduction into graph theory can be found in the book of Volkmann [62]. The graphs used throughout this work are connected graphs, i. e., graphs that do not contain isolated subgraphs.

A connection between two nodes i and j is established by two directed edges or di-edges $|ij\rangle$ and $|ji\rangle$. Between two connected nodes, transitions with rates ω_{ij} and ω_{ji} take place. In graph theory, these rates are referred to as weights of the graph. The degree k_i of a node i is given by the number of edges connected to that node. A cycle $\mathcal{C}$ of a connected graph $\mathcal{G}$ consists of a subset of nodes with degree two.

For the specification of connections between the vertices $\{v_1...v_n\}$ of a graph $\mathcal{G}$, we define a discrete map called adjacency matrix $\mathbf{A} = A_{ij}$ with elements A_{ij} that contain the number $k = 0, 1, ...$ of links connecting two nodes j and j. The adjacency matrix

A is a square matrix of order n, and its Laplacian or connectivity matrix $\mathbf{C} = C_{ij}$ is defined by the difference of the graph's degree matrix, a diagonal matrix with elements given by the degrees k_i, and its adjacency matrix,

$$C_{ij} = \begin{cases} k_i, & \text{for } i = j, \\ -1 & \text{for } i \neq j \text{ and } i, j \text{ connected} \\ 0 & \text{otherwise.} \end{cases} \tag{2.4}$$

If the transitions ω_{ij} are understood as the weights of a graph, the connectivity matrix **C** is identical with the matrix **T** associated with the master equation, as will be discussed in section 2.5.

Let us turn to Kirchhoff's method for the calculation of the steady state distribution of the Master equation, Eq. (2.1). The inspiration to utilize it in the present work arises from its application in the context of enzyme kinetics by T. Hill [63] and a network formulation for the molecular motor kinesin by Lipowsky and coworkers, as reviewed e.g. in [11].

The steady state that we will use for the characterization of the motor‘s motion can be obtained from the spanning trees $\mathcal{T}_s$ of a given graph $\mathcal{G}$. A spanning tree $\mathcal{T}_s$ is a subgraph of $\mathcal{G}$ that contains all vertices $v_i \in V$and a subset of edges $l_i \in V$such that $\mathcal{T}_s$ is connected but does not contain any cycles. Here, s refers to the different trees that belong to the same graph $\mathcal{G}$. A subset of $\mathcal{T}_s$ that contains solely edges pointing towards a given node i is called a directed or rooted spanning tree $\vec{\mathcal{T}}_s^{\,i}$. An example for a graph $\mathcal{G}$, a spanning tree $\mathcal{T}_s$ associated with that graph and a directed spanning tree $\vec{\mathcal{T}}_s^{\,i}$ is shown in Fig. 2.2. The transition rates ω_{ij} that belong to the graph define a measure $\Omega(\vec{\mathcal{T}}_s^{\,i})$ on each of directed spanning tree $\vec{\mathcal{T}}_s^{\,i}$ given by

$$\Omega(\vec{\mathcal{T}}_s^{\,i}) = \prod_{|kl\rangle}^{\vec{\mathcal{T}}_s^{\,i}} \omega_{kl}. \tag{2.5}$$

The sum of all measures of the directed spanning trees associated with a certain node i, $\Omega_i = \sum_s \Omega(\vec{\mathcal{T}}_s^{\,i})$, is directly related to the steady state probability distribution of the system. The steady state probability P_i^{st} for a given state i corresponds to the fraction of all measures associated with state i, Ω_i, with respect to the total number of measures of *all* states, $\sum_i \Omega_i$,

$$P_i^{\text{st}} = \frac{\Omega_i}{\sum_i \Omega_i} = \frac{\sum_s \Omega(\vec{\mathcal{T}}_s^{\,i})}{\sum_{i,s} \Omega(\vec{\mathcal{T}}_s^{\,i})}, \tag{2.6}$$

and $\sum_i \Omega_i$ acts as a normalization factor.

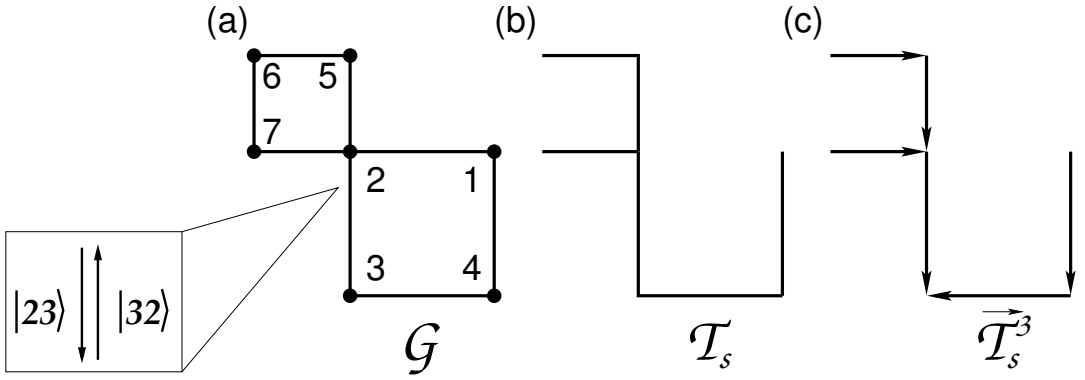

Figure 2.2 : (a) A graph $\mathcal{G}$ that contains $i = 6$ vertices or nodes, with connections established by pairs of directed edges, $|ij\rangle$ and $|ji\rangle$, as illustrated for the nodes 2 and 3. (b) One of the spanning trees $\mathcal{T}_s$ that belong to $\mathcal{G}$ and the corresponding directed spanning tree $\vec{\mathcal{T}}_s^{\,i}$ for node $i = 3$ (c).

Hence, the inspection of directed spanning trees of a given graph leads to the steady state probability distribution in an intuitive way. As the number of spanning trees increases dramatically with the complexity of the underlying graph, the feasibility of this concept is restricted to rather small systems. The construction of spanning trees, however, is convenient because of its intimate linkage to network cycles.

There is no straightforward way for the construction of spanning trees, but their total number for a given graph can be calculated with the use of Kirchhoff's matrix-tree theorem. The theorem is based on the Laplacian matrix $\mathbf{C}$ associated with a connected graph $\mathcal{G}$. Let $\mathcal{G}$ have n vertices, and let $\lambda_1, \lambda_2, \cdots, \lambda_{n-1}$ be the non-zero eigenvalues of $\mathbf{C}$. Then the number of spanning trees of $\mathcal{G}$ is

$$m(\mathcal{G}) = \frac{1}{n}\lambda_1\lambda_2\cdots\lambda_{n-1}. \tag{2.7}$$

In Fig. 2.3, the Laplacian matrix and the corresponding eigenvalues λ_i are shown for the graph that has been used before. Using Eq. (2.7), we find that $m(\mathcal{G}) = 16$, which can be easily seen for the example, because the subgraphs consisting of nodes 1, 2, 3, 4 and 2, 5, 6, 7 have four spanning trees each and the total number of trees for the graph involves $4 \cdot 4 = 16$ combinations of these.

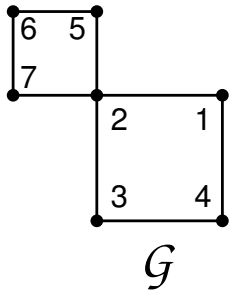

$$\mathbf{C} = \begin{pmatrix} 2 & -1 & 0 & -1 & 0 & 0 & 0 \\ -1 & 4 & -1 & 0 & -1 & 0 & -1 \\ 0 & -1 & 2 & -1 & 0 & 0 & 0 \\ -1 & 0 & -1 & 2 & 0 & 0 & 0 \\ 0 & -1 & 0 & 0 & 2 & -1 & 0 \\ 0 & 0 & 0 & 0 & -1 & 2 & -1 \\ 0 & -1 & 0 & 0 & 0 & -1 & 2 \end{pmatrix}$$

$$\lambda_i = \left\{0, 2-\sqrt{2}, 2, 2, 4-\sqrt{2}, 2+\sqrt{2}, 4+\sqrt{2}\right\}$$

Figure 2.3 : Example graph $\mathcal{G}$ (left panel), with the corresponding Laplacian matrix $\mathbf{C}$ and the eigenvalues λ_i associated with $\mathbf{C}$ in ascending order (right panel).

2.3 Network cycles and probability fluxes

We will now turn to the concept of cyclic probability fluxes as a step towards the description of the dynamics of enzymatic networks. A graph can be split into two subsets, one of which contains one of its spanning trees and the other one the set of edges $\{\kappa_\nu\}$ that belong to the graph, but not the spanning tree,

$$\mathcal{G} = \{\kappa_\nu\} \cup \mathcal{T}_s. \tag{2.8}$$

These edges κ_ν are called chords. Adding a chord to a spanning tree $\mathcal{T}_s$ results in a graph that has exactly one closed pathway or cycle $\mathcal{C}$, and the resulting graph is formed by the cycle and tree-like branches $\mathcal{T}_s^{\mathcal{C}_\nu}$. The addition and subtraction of cycles is defined by

$$\mathcal{C}_\nu \oplus \mathcal{C}_\gamma = \mathcal{C}_\nu \cup \mathcal{C}_\gamma - \mathcal{C}_\nu \cap \mathcal{C}_\gamma \tag{2.9}$$

$$\mathcal{C}_\nu \ominus \mathcal{C}_\gamma = \mathcal{C}_\nu \setminus \mathcal{C}_\gamma + \mathcal{C}_\nu \cap \mathcal{C}_\gamma. \tag{2.10}$$

For a given spanning tree, each chord added to this tree leads to a different cycle. The set $\{\mathcal{C}_\nu\}$ of all cycles obtained by adding a single chord to the spanning tree provides a so-called *fundamental set of cycles*. It has the property that any cycle in a network can be constructed by linear combination of cycles from its fundamental set. A fundamental set is not unique, as different spanning trees can lead to different sets of fundamental

cycles. Each cycle consists of a closed loop of *nondirected* edges. A closed loop of *directed edges* within a given cycle carries an orientation d, where d can be positive $(+)$ or negative $(-)$. As our approach is based on directed probability fluxes along these cycles, it is convenient to define a directed cycle $\mathcal{C}_\nu^d$ or dicycle formed by a set of directed edges $\{|ij\rangle, |jk\rangle, ...\}$. For $d = (+)$, we have $\mathcal{C}_\nu^+ = \{|12\rangle, ... |ij\rangle, |j1\rangle\}$ and for $d = (-)$, we have $\mathcal{C}_\nu^- = \{|j1\rangle, |ji\rangle, ... |12\rangle\}$, respectively. Throughout this work, we will use a short notation for both cycles and dicycles, given by

$$\begin{aligned} \mathcal{C}_\nu &= \langle 12..ij1\rangle && (2.11)\\ \mathcal{C}_\nu^+ &= |12...ij1\rangle && (2.12)\\ \mathcal{C}_\nu^- &= |1ji...21\rangle\,. && (2.13) \end{aligned}$$

In analogy to Eq. (2.5), the measure $\Omega(\mathcal{C}_\nu^d)$ of a directed cycle along both directions is given by

$$\Omega(\mathcal{C}_\nu^+) = \prod_{|ij\rangle}^{\mathcal{C}_\nu^+} \omega_{ij} \quad \text{and} \quad \Omega(\mathcal{C}_\nu^-) = \prod_{|ij\rangle}^{\mathcal{C}_\nu^-} \omega_{ij} = \prod_{|ij\rangle}^{\mathcal{C}_\nu^+} \omega_{ji}. \tag{2.14}$$

For the addition and subtraction of the measures around cycles, the combination of Eqs. (2.9, 2.10) and (2.14, 2.14) leads to

$$\begin{aligned} \Omega(\mathcal{C}_\nu^+ \oplus \mathcal{C}_\gamma^+) &= \Omega(\mathcal{C}_\nu^+)\Omega(\mathcal{C}_\gamma^+) \quad \text{and} && (2.15)\\ \Omega(\mathcal{C}_\nu^+ \ominus \mathcal{C}_\gamma^+) &= \frac{\Omega(\mathcal{C}_\nu^+)}{\Omega(\mathcal{C}_\gamma^+)}. && (2.16) \end{aligned}$$

In the following, let us establish the connection between the steady state probability fluxes, $J_{ij}^{\rm st}$, and the measure Ω_i. In addition, the definition of dicycles allows for determination of a cyclic probability flux $\Delta J^{\rm st}(\mathcal{C}_\nu^d)$. Starting from the master equation, Eq. (2.1) in the stationary state, we have, in combination with Eq. (2.6) a steady state probability flux, $\Delta J_{ij}^{\rm st}$, which is given by

$$\begin{aligned} \Delta J_{ij}^{\rm st} &= P_i^{\rm st}\,\omega_{ij} - P_j^{\rm st}\,\omega_{ji} && (2.17)\\ &= \frac{1}{\sum_i \Omega_i}\left(\Omega_i\omega_{ij} - \Omega_j\omega_{ji}\right) && (2.18)\\ &= \frac{1}{\sum_i \Omega_i}\left(\sum_\nu c_{ij,\nu}\left(\Omega(\mathcal{C}_\nu^+) - \Omega(\mathcal{C}_\nu^-)\right)\sum_s \Omega(\vec{\mathcal{T}}_s^{\mathcal{C}_\nu})\right). && (2.19) \end{aligned}$$

Here, $c_{ij,\nu}$ is an index that determines the sign of the contribution to the probability flux, where ν stands for the cycles of the graph $\mathcal{G}$. It is $+1$ if the transition $|ij\rangle$ is part of $\mathcal{C}_\nu^+$,

and -1 if it belongs to $\mathcal{C}_\nu^-$, and 0 if $|ij\rangle$ is not part of the cycle. Note that this requires some care about the definition of the orientation d, as all cycles that are part of $\mathcal{G}$ have to be oriented with consistent handedness. In our description, $d = +$ corresponds to counterclockwise and $d = -$ to a clockwise orientation. Through inspection of Eq. (2.19), one can define a cyclic probability flux as

$$\Delta J^{\mathrm{st}}(\mathcal{C}_\nu) = \frac{1}{\sum_i \Omega_i} \left(\Omega(\mathcal{C}_\nu^+) - \Omega(\mathcal{C}_\nu^-)\right) \sum_s \Omega(\vec{\mathcal{T}}_s^{\mathcal{C}_\nu}). \tag{2.20}$$

This infers that any flux through a given edge can be expressed as a linear combination of probability fluxes of dicycles $\Delta J^{\mathrm{st}}(\mathcal{C}_\nu)$.

Cycle completions

An important connection between the cyclic probability fluxes and macroscopically observable quantities can be established when focusing on the completion of trajectories along specific di-cycles for a stochastic process in the stationary state. The probability fluxes through a cycle $\mathcal{C}$ can be split into their dicycle contributions,

$$\Delta J^{\mathrm{st}}(\mathcal{C}_\nu) = J^{\mathrm{st}}(\mathcal{C}_\nu^+) - J^{\mathrm{st}}(\mathcal{C}_\nu^-). \tag{2.21}$$

These dicycle fluxes are, for long observation times t, linked to the average number of cycle completions via $\langle n_{\mathcal{C}^\pm}(t)\rangle \approx \Delta J^{\mathrm{st}}(\mathcal{C}_\nu^\pm)t$ [64]. The mean time for a cycle completion is given by

$$\tau_{\mathcal{C}^\pm} = \frac{t}{\langle n_{\mathcal{C}^\pm}(t)\rangle} = \frac{1}{\Delta J^{\mathrm{st}}(\mathcal{C}^\pm)}, \tag{2.22}$$

and the average number of effectively completed cycles after a time t can again be split into the contribution from the dicycles,

$$\langle n_{\mathcal{C}}(t)\rangle = \langle n_{\mathcal{C}^+}(t)\rangle - \langle n_{\mathcal{C}^-}(t)\rangle = \frac{t}{\tau_{\mathcal{C}^+}} - \frac{t}{\tau_{\mathcal{C}^-}}. \tag{2.23}$$

Let us turn back to enzyme kinetics, where the enzyme's work is described as a sequence of chemical states with transitions that correspond to chemical reactions. As the enzyme in itself is not altered by the chemical reaction, a closed pathway can be identified as one catalytic cycle of the enzyme. Thus, the enzyme's velocity is related to the number of cycle completions,

$$v = \ell \lim_{t\to\infty} \frac{n_{\mathcal{C}}}{t}. \tag{2.24}$$

The variance $\sigma^2_{n_\mathcal{C}}(t) = \left\langle (n_\mathcal{C}(t) - \langle n_\mathcal{C}(t)\rangle)^2 \right\rangle$ can be used to obtain the diffusion constant of the process, given by

$$D = \lim_{t\to\infty} \frac{\sigma^2_{n_\mathcal{C}}(t)}{2t}. \tag{2.25}$$

To quantify the competition between drift and diffusion in a stochastic system, the Peclet number $Pe = \ell v/2D$ can, in this way, be determined for the network. In the context of molecular motors, the randomness parameter, given by its inverse, $r = 1/Pe$, is more common. In the case of a random walk on a single cycle, the diffusion constant can be calculated analytically from the transition rates ω_{ij}, as shown by Derrida [65]. The evaluation of the variance of stepping trajectories measured for a molecular motor and the conclusions about the underlying process can be found in [66].

2.4 Nonequilibrium thermodynamics

Stationarity and balance conditions

Here, we discuss the relation between biochemical thermodynamics and kinetics, and establish a connection between kinetic parameters that describe processes far from equilibrium with thermodynamic quantities that characterize the system in equilibrium. These relations have first been deduced for chemical networks and are known as the Haldane relations, as emphasized by Hill [63], and have been extended for general chemomechanical networks by Liepelt and Lipowsky [67].

True equilibrium is, in our formulation, the total the absence of steady state probability fluxes, $\Delta J^{\rm eq}_{ij} = 0$ for all egdes $\langle ij\rangle$. Consequently, $\Delta J^{\rm eq}(\mathcal{C}_\nu) = 0$ for all ν. The vanishing local and cycle fluxes lead to a formulation of detailed balance that is based on cyclic fluxes,

$$\left.\frac{\Omega(\mathcal{C}^+_\nu)}{\Omega(\mathcal{C}^-_\nu)}\right|_{\rm db} = 1 \quad \text{or} \quad \left.\ln\frac{\Omega(\mathcal{C}^+_\nu)}{\Omega(\mathcal{C}^-_\nu)}\right|_{\rm db} = 0 \quad \text{for all } \nu, \tag{2.26}$$

respectively. In contrast to the local formulation of detailed balance,

$$\left.\frac{\omega_{ij}}{\omega_{ji}}\right|_{\rm db} = \frac{P^{\rm eq}_j}{P^{\rm eq}_i}, \tag{2.27}$$

Eq. (2.26) does not include the probability distribution. For true equilibrium, the transition rates must obey Eq. (2.26). If this is not the case, the system contains non-vanishing cyclic probability fluxes, which can be seen from Eq. (2.20). A message to remember is that non-zero cyclic fluxes constitute a sign of a system out of equilibrium.

Entropy production

Our final goal is to link the dynamics of the steady state to thermodynamic properties of the system. The formulation of entropy for networks that have a dynamics described by the master equation is discussed in [68, 69, 70] and has been adressed in the context of kinesin [71, 72]. Gibb's entropy postulate or the definition of Shannon entropy reads

$$S = S(t) = -k_{\mathrm{B}} \sum_i P_i(t) \ln P_i(t), \tag{2.28}$$

with the derivative

$$\frac{\mathrm{d}}{\mathrm{dt}} S(t) = -k_{\mathrm{B}} \sum_i \partial_t P_i(t) \ln P_i(t) = \frac{k_{\mathrm{B}}}{2} \sum_{i,j} \Delta J_{ij}(t) \ln \frac{P_i(t)}{P_j(t)}. \tag{2.29}$$

With using the second law of thermodynamics, one can split this sum into parts referred to as the production of internal and external entropy, S^{i} and S^{e}, where

$$\partial_t S^{\mathrm{i}} = \frac{k_{\mathrm{B}}}{2} \sum_{i,j} \Delta J_{ij}(t) \ln \frac{P_i(t)\omega_{ij}}{P_j(t)\omega_{ji}} \quad \text{and} \tag{2.30}$$

$$\partial_t S^{\mathrm{e}} = -\frac{k_{\mathrm{B}}}{2} \sum_{i,j} \Delta J_{ij}(t) \ln \frac{\omega_{ij}}{\omega_{ji}}. \tag{2.31}$$

These two terms represent the entropy production and the flux of entropy that arises from the heat flux of the surrounding medium. In the steady state, the change in entropy equals zero, $\frac{\mathrm{d}}{\mathrm{dt}} S(t) = 0$. Then, the entropy flux out of the system into the environment is equal to the production of entropy, and we have

$$\partial_t S^{\mathrm{i}} = \frac{k_{\mathrm{B}}}{2} \sum_{i,j} \Delta J^{\mathrm{st}}_{ij} \ln \frac{\omega_{ij}}{\omega_{ji}} = \frac{k_{\mathrm{B}}}{2} \sum_{\nu} \Delta J^{\mathrm{st}}(\mathcal{C}_\nu) \sum_{i,j} c_{ij\ \nu} \ln \frac{\omega_{ij}}{\omega_{ji}} \tag{2.32}$$

$$= \sum_{\nu} \partial_t S^{\mathrm{i}}(\mathcal{C}_\nu) = \sum_{\nu} \left(\partial_t S^{\mathrm{i}}(\mathcal{C}^+_\nu) + \partial_t S^{\mathrm{i}}(\mathcal{C}^-_\nu) \right), \tag{2.33}$$

where Eq. (2.33) defines the mean rate of entropy production along a pathway $\mathcal{C}_\nu$. By integration over the time interval $[0, \tau_{\mathcal{C}^\pm_\nu}]$, which corresponds to the average time it takes for one cycle completion along its direction $d = \pm$, we obtain the amount of entropy that is produced, on average, during the completion of a single dicycle,

$$\Delta S^{\mathrm{i}}(\mathcal{C}^\pm_\nu) = \int_0^{\tau_{\mathcal{C}^\pm_\nu}} \partial_t S^{\mathrm{i}}(\mathcal{C}^\pm_\nu) \mathrm{dt} = k_{\mathrm{B}} \ln \prod_{|ij\rangle}^{\mathcal{C}^\pm_\nu} \frac{\omega_{ij}}{\omega_{ji}} = \pm k_{\mathrm{B}} \ln \frac{\Omega(\mathcal{C}^+_\nu)}{\Omega(\mathcal{C}^-_\nu)}. \tag{2.34}$$

As the transition rates ω_{ij} are positive, Eq. (2.34) can turn negative. This feature stems from the fact that a cycle can be completed in its less favourable direction. Eq. (2.33) can be used to determine the mean rate of entropy production,

$$\partial_t S^{\mathrm{i}}(\mathcal{C}_\nu) = k_{\mathrm{B}} \Delta J^{\mathrm{st}}(\mathcal{C}_\nu) \ln \frac{\Omega(\mathcal{C}_\nu^+)}{\Omega(\mathcal{C}_\nu^-)} \geq 0. \tag{2.35}$$

The equality holds in the case of equilibrium, which can be seen from the condition for the equilibrium detailed balance given by Eq. (2.26). The production of entropy for closed trajectories has been used with respect to of kinesin [72, 73, 11], and for special cases of cyclic networks in [74]. Under the assumption that each state has an identical entropy, the entropy production has been quantified for systems with arbitrary trajectories [5].

Energy balance

The concept of entropy production turns out a powerful and descriptive tool for the enzyme kinetics of molecular motors. A linear molecular motor walks along its track in a processive manner, by means of chemical energy that is released in a chemical reaction, in this case, hydrolysis of ATP. The change in internal energy is thus quantified by the balance of chemical energy, mechanical work and heat release. Fig. 2.4 sketches this exchange of energy by viewing the motor as a system coupled to different reservoirs, like the nucleotide concentration, the temperature T and a force F. In a stationary state of the motor, its internal energy does not change during completion of a cycle, i.e., the motor can attain a set of internal states it repeatedly visits during an enzymatic turnover. For a closed trajectory on a cycle $\mathcal{C}_\nu^+$ or $\mathcal{C}_\nu^-$, the first law of thermodynamics reads

$$\Delta U(\mathcal{C}_\nu^\pm) = \Delta\mu(\mathcal{C}_\nu^\pm) - \Delta W(\mathcal{C}_\nu^\pm) - \Delta Q(\mathcal{C}_\nu^\pm) = 0, \tag{2.36}$$

where $U(\mathcal{C}_\nu^\pm)$ is the internal energy, $\mu(\mathcal{C}_\nu^\pm)$ is the chemical energy, $W(\mathcal{C}_\nu^\pm)$ is mechanical work and $Q(\mathcal{C}_\nu^\pm)$ the heat. The chemical energy balance along a path $\mathcal{C}_\nu^\pm$ during a reaction can be quantified by the energy μ_α the motor gains or loses by binding a specific nucleotide α, and the number $\Delta n_\alpha(\mathcal{C}_\nu^+) = n_\alpha^+(\mathcal{C}_\nu^+) - n_\alpha^-(\mathcal{C}_\nu^+)$ of nucleotides that is bound $(+)$ or released $(-)$ during the revolution of a cycle,

$$\Delta\mu(\mathcal{C}_\nu^+) = \sum_\alpha \mu_\alpha \Delta n_\alpha(\mathcal{C}_\nu^+). \tag{2.37}$$

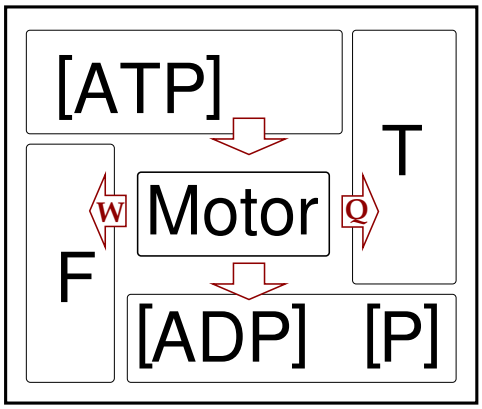

Figure 2.4 : Motor as a system connected to different energy reservoirs. For the motor, the in- and outflux of chemical energy is controlled by the presence of nucleotide concentrations of ATP, ADP and P. It is coupled to a thermal reservoir, and can exert or be influenced by a force F. The red arrows indicate the flux of energy. The motor gains chemical energy by ATP hydrolysis, and releases ADP and P. It is able to perform a work W, and releases thermal energy Q.

The mechanical work performed along a closed path can be characterized in a similar way,

$$\Delta W(\mathcal{C}_\nu^+) = -F \sum_\beta \ell_\beta \Delta n_\beta(\mathcal{C}_\nu^+). \tag{2.38}$$

Here, F is an external load applied to the motor, and $\Delta n_\beta(\mathcal{C}_\nu^+) = n_\beta^f(\mathcal{C}_\nu^+) - n_\beta^b(\mathcal{C}_\nu^+)$ corresponds to the difference of forward (f) and backward (b) steps of length ℓ_β.
Because of microscopic reversibility, we have $n_\alpha^+(\mathcal{C}_\nu^+) = n_\alpha^-(\mathcal{C}_\nu^-)$ and likewise $n_\alpha^-(\mathcal{C}_\nu^+) = n_\alpha^+(\mathcal{C}_\nu^-)$, and thus $\Delta\mu(\mathcal{C}_\nu^+) = -\Delta\mu(\mathcal{C}_\nu^-)$. The same holds for the mechanical work, where the direction of steps changes when following the reverse path, $f \to b$, or $n_\beta^f(\mathcal{C}_\nu^-) = n_\beta^b(\mathcal{C}_\nu^+)$ and $n_\beta^b(\mathcal{C}_\nu^-) = n_\beta^f(\mathcal{C}_\nu^+)$. Therefore, $\Delta W(\mathcal{C}_\nu^+) = -\Delta W(\mathcal{C}_\nu^-)$.
The amount of heat that is released during motor motion in the stationary state is given by

$$\Delta Q(\mathcal{C}_\nu^\pm) = -T\Delta S^{\mathrm{e}}(\mathcal{C}_\nu^\pm) = T\Delta S^{\mathrm{i}}(\mathcal{C}_\nu^\pm). \tag{2.39}$$

The second law of thermodynamics in the cycle formulation, Eq. (2.36) can be combined with the principle of entropy production, Eq. (2.29) into

$$\ln \frac{\Omega(\mathcal{C}_\nu^+)}{\Omega(\mathcal{C}_\nu^-)} = \frac{1}{k_{\mathrm{B}}T}\left(\Delta\mu(\mathcal{C}_\nu^+) - \Delta W(\mathcal{C}_\nu^+)\right), \tag{2.40}$$

for any cycle $\mathcal{C}_\nu$. Eq. (2.40) constitutes a generalization of detailed balance for non-equilibrium steady states, [72]. For each cycle of the network, it imposes one constraint to the transition rates of the underlying network.
The equilibrium situation, Eq. (2.26), is fulfilled for the case where both the stepping and the chemical reactions are equally likely in the forward and the backward direction. We then have, for all ν, $\Delta\mu(\mathcal{C}_\nu^+) = \Delta W(\mathcal{C}_\nu^+) = 0$. The case where the chemical energy difference balances the difference in work, $\Delta\mu(\mathcal{C}_\nu^+) = \Delta W(\mathcal{C}_\nu^+)$, where the energy difference is not necessarily equal to zero, is given by the stall condition in the context of molecular motors.
Eq. (2.40) reflects the features of the second law of thermodynamics. A positive balance that is obtained in the case where the cycle $\mathcal{C}_\nu^+$ dominates over $\mathcal{C}_\nu^-$ corresponds to heat release. The dominance of $\mathcal{C}_\nu^+$ states that the process is more prone to evolving along the positive direction of the cycle, i.e., the system evolves spontaneously into the direction where heat is released. In the context of a molecular motor, we will have a directed motion of the molecule through the supply of ATP in the absence of an external load.

2.5 Networks with absorbing states

So far, we have shown how networks are used to model the motion of a molecular motor that constitutes a system out of thermal equilibrium. The concept of stationarity allows for calculation of the steady state properties of the motor. For more detailed information about the motor's kinetics, it is instructive to analyze the distributions of the motor's waiting times rather than its step velocity. As a single molecule experiment typically monitors the motor's motion as a discrete, equally spaced displacement, the distributions of dwell times between the steps can be directly accessed and provide the probably most valuable source of experimental data. For the analytical calculation of these distributions, the Markov formalism is extended to networks with absorbing boundaries. Prior to the introduction of such boundaries, let us outline the correspoding matrix algebra for Markov processes.

Matrix formulation

The master equation introduced in the beginning of this chapter, as given by the combination of Eq. 2.1 and 2.2, reads

$$\frac{\mathrm{d}}{\mathrm{dt}} P_i(t) = -\sum_j P_i(t)\ \omega_{ij} - P_j(t)\ \omega_{ji}. \tag{2.41}$$

It can be cast into a matrix form

$$\frac{\mathrm{d}}{\mathrm{dt}}\mathbf{P}(t) = \mathbf{P}(t)\mathbf{T}, \tag{2.42}$$

where $\mathbf{P}(t)$ is a vector with components $P_i(t)$ and $\mathbf{T}$ is a transfer matrix that is defined as

$$T_{ij} = \begin{cases} \sum_i \omega_{ij}, & \text{for } i = j, \\ -\omega_{ij} & \text{for } i \neq j \text{ and } i, j \text{ connected} \\ 0 & \text{otherwise.} \end{cases} \tag{2.43}$$

The formal solution to 2.42 is given by

$$\mathbf{P}(t) = \exp(t\mathbf{T})\mathbf{P}(0). \tag{2.44}$$

As $\mathbf{T}$, in general, is not symmetric, a solution in term of eigenvectors and eigenvalues is not feasible for all matrices $\mathbf{T}$. The networks we deal with in this work, however, obey detailed balance, as we have discussed in the course of section 2.4. In this case, the matrices $\mathbf{T}$ fulfill a symmetry condition such that 2.44 can be solved by diagonalization of $\mathbf{T}$, a procedure that we will discuss further below.

Note that the formulation of the equation in terms of $\mathbf{T}$ is discrete in a strict sense, but can be validated by splitting the continuous process into small time steps Δt. A fundamental property of the master equation is, that it has a stationary solution, that is valid for infinite times irrespective of the initial condition $\mathbf{P}(\mathbf{0})$. By use of the above-mentioned discretization procedure, the existence of the stationary solution is assured by the Perron-Frobenius theorem. The steady state probability distribution $\mathbf{P}^{\mathrm{st}}$ is given by the null space of $\mathbf{T}$, i. e., the eigenvector that belongs to the zero eigenvalue $\lambda_0 = 0$. A detailed discussion of these properties can be found in [61], where the matrices $\mathbf{T}$ are referred to as the class of W-matrices.

Dwell time distributions

For an unrestricted random walk on a discrete network, the time in between two successive steps of a molecular motor is analogous to the time it takes for a random walker to start, at time $t = 0$, from a given site i and reach another specific site j at time t. The probability distribution for this time can be obtained using a random walk that has one or more absorbing boundaries. The process starts at a fixed site i at $t = 0$ and is stopped when reaching an absorbing state j. The average time is also referred to as the mean first-passage time of the process. The simplest example of a probability distribution is the exponential distribution, which is obtained for a Markov chain that consists of only

two states, an initial state 0 and an absorbing state 1 that are connected through the transition rate $\omega \equiv \omega_{01}$. A fundamental treatment of the formalism of mean first-passage times can be found in the book of van Kampen [61]. Here, we follow the route of [75] using an approach based on matrix algebra.

For a given Markov chain $X(t)$ with $t \geq 0$, that has N discrete states, let the first n states be transient and the remaining $N - n$ states be absorbing. We denote the conditional probability for the process to dwell in state j at time t given that it started in state i at time $t = 0$ by $P_{ij}(t)$. The corresponding master equation reads

$$\frac{\mathrm{d}}{\mathrm{dt}} P_{ij} = \sum_{k \neq j} \left(P_{ik}\omega_{kj} - P_{ij}\omega_{jk} \right), \tag{2.45}$$

where ω_{ij} is the transition or jump rate from state i to state j. The steady state solution to Eq.(2.45) is given by $P_{ij}^{\mathrm{st}} = 0$ for any transient state $1 \leq i \leq n$, with the normalization condition $\sum_{k=n}^{N} P_{ik}^{\mathrm{st}} = 1$. For an absorbing state k, the steady state solution is equal to the probability for being absorbed in state k given that the walk started in state i,

$$P_{ik}^{\mathrm{st}} = \Pr\{X^{\mathrm{abs}} = k \mid X(0) = i\}, \tag{2.46}$$

where '$_{\mathrm{abs}}$' stands for absorbing. The dynamics of the process prior to absorption is identical to the dynamics of the unrestricted Markov process. Prior to reaching a boundary, the random walk proceeds with an exponentially distributed waiting time in every transient state i,

$$\psi_i(t) = \frac{1}{\tau_i} \exp(-t/\tau_i) \tag{2.47}$$

with an average dwell time $\tau_i = 1/\sum_j \omega_{ij}$. The process starts in a state i, sojourns in each state according to the probability

$$P_{ij} = \frac{\omega_{ij}}{\sum_j \omega_{ij}}, \tag{2.48}$$

until it is eventually absorbed in state k. The time for absorption in any of the states $n < k \leq N$ when starting in state i is given by the lower bound for the time to reach the respective state,

$$t_i^{\mathrm{abs}} = \min\{t \geq 0, X(t) = k \geq n \mid X(0) = i\}. \tag{2.49}$$

This time is referred to as the dwell time of the process.

To obtain the distribution of dwell times, consider the probability that absorption in

any of the states $n...N$ takes place prior to a given time t, i. e.,

$$\Pr\{t^{\rm abs} \leq t\} = \sum_{k=n}^{N} P_{ik}(t). \tag{2.50}$$

This probability can also be expressed as [76, 77]

$$\Pr\{t^{\rm abs} \leq t\} = \int_0^t \rho_i^{\rm abs}(t')\ dt' = \int_0^t \sum_{k=n}^{N} \dot{P}_{ik}(t')\ dt' \tag{2.51}$$

Here, $\rho_i^{\rm abs}(t) = \sum_{k=n}^{N} \dot{P}_{ik}(t)$ is the probability density for absorption with an initial transient state i. The average time to absorption is then given by

$$\tau_i^{\rm abs} = \langle t \rangle_i = \int_0^\infty t'\ \rho_i^{\rm abs}(t')\ dt'. \tag{2.52}$$

The formalism introduced above refers to the case of absorption in any of the absorbing states $n < k \leq N$. For absorption in a *specific* state k, one has to find the subset of those walks that start in i and are absorbed in k, i. e., the conditional probability

$$P_{ij|k} = \Pr\{X(t) = j \mid X(0) = i, X^{\rm abs} = k\} \tag{2.53}$$

for an initial transient state $i < n$ and the absorbing state $k \geq n$. It is given by the fraction of walks that start in i, sojourn in j and are absorbed in k,

$$P_{ij,k}(t) = \Pr\{X(t) = j,\ X^{\rm abs} = k \mid X(0) = i\} = P_{ij,k}(t) P_{jk}^{\rm st} \tag{2.54}$$

with respect to all walks that start in i and are absorbed in k, see Eq. (2.46),

$$P_{ij|k} = \frac{P_{ij,k}(t)}{P_{ik}^{\rm st}} = \frac{P_{ij}(t)\ P_{jk}^{\rm st}}{P_{ik}^{\rm st}}. \tag{2.55}$$

Consequently, the conditional probability density distribution $\rho_{i|k}^{\rm abs}(t)$ that refers to $P_{ij|k}$ is defined as

$$\Pr\{t_{i|k}^{\rm abs} \leq t\} = P_{ik|k}(t) \equiv \int_0^t \rho_{i|k}^{\rm abs}(t')dt'. \tag{2.56}$$

Using Eq. (2.55) and $P_{kk}^{\rm st} = 1$, one gets

$$\rho_{i|k}^{\rm abs}(t) = \dot{P}_{ik|k}(t) = \frac{\dot{P}_{ik}(t)}{P_{ik}^{\rm st}}. \tag{2.57}$$

The conditional distribution of probability density is thus given by the time-dependent derivative of the probability, $\dot{P}_{ik}(t)$, rescaled with the steady state probability for absorption, P_{ik}^{st}. The probability densities for the conditional process and the original one are connected via

$$\rho_i^{\mathrm{abs}}(t) = \sum_{k=n}^{N} P_{ik}^{\mathrm{st}} \rho_{i|k}^{\mathrm{abs}}(t). \tag{2.58}$$

The average absorption time can be decomposed in the same manner,

$$\tau^{\mathrm{abs}} = \sum_{k=n}^{N} P_{ik}^{\mathrm{st}} \tau_{i|k}^{\mathrm{abs}}, \tag{2.59}$$

with

$$\tau_{i|k}^{\mathrm{abs}} = \int_0^\infty t' \ \rho_{i|k}^{\mathrm{abs}}(t') \ dt' \tag{2.60}$$

being the conditional average time to absorption.

Let us now turn to the method for the calculation of the time-dependent transition probabilities $P_{ij}(t)$, and thus $\dot{P}_{ik}(t)$, to obtain an explicit solution to the conditional distributions of dwell times. To determine the conditional distribution of dwell times, $\rho_{i|k}(t)$, one needs to find both the steady state probability P_{ik}^{st} and the time dependent distribution $\dot{P}_{ik}(t)$, which can be obtained by solving the time-dependent master equation, Eq. 2.45. Let $\mathbf{T}$ be the matrix of the given network that contains all transient states $1...n$ as defined in 2.43. Let then $\mathbf{T^0}$ be the matrix that contains the $N-n$ absorbing states, defined as

$$T_{ij}^0 = \begin{cases} -\omega_{ij} & \text{for } i,j \text{ connected and } j \text{ absorbing} \\ 0 & \text{else.} \end{cases} \tag{2.61}$$

The matrix of the transition probabilities that contains the solutions of the unrestricted master equation is given by

$$\mathbf{P}(t) = \mathbf{Q}^{-1} \exp\left(-\mathbf{\Lambda} t\right) \mathbf{Q}. \tag{2.62}$$

Here, $\mathbf{Q}$ and $\mathbf{Q^{-1}}$ are the matrices in the transformation diagonalizing the matrix $\mathbf{T}$,

$$\mathbf{\Lambda} = \mathbf{Q^{-1}} \mathbf{T} \mathbf{Q}, \tag{2.63}$$

where $\mathbf{\Lambda}$ is a diagonal matrix of the n eigenvalues λ_i that belong to $\mathbf{T}$, and $\mathbf{Q}$ is con-

structed from the eigenvectors of $\mathbf{T}$.

The derivative of the time-dependent probability distribution to arrive in an absorbing state k, $\dot{P}_{ik}(t)$, is, in general, given by the probability to jump into that state from a neighbouring site, times the transition rate into the absorbing state. Hence,

$$\dot{P}_{ik}(t) = \sum_{m,j} (T^0)^T_{km} P_{mj}(t) \mathbb{I}_{ji}, \tag{2.64}$$

where $\mathbb{I}$ is an n-by-n identity matrix, for an initial state i and an absorbing state k. The corresponding steady state solution follows by integration,

$$P^{\text{st}}_{ik} = \int_0^\infty \dot{P}_{ik}(t) dt. \tag{2.65}$$

3 Motors in continuous space

In this chapter, we take a continuous approach to the motion of a molecular motor. The description of the motor's motion as a driven diffusing particle against a load force results in a class of models called ratchets, the mechanisms of which are briefly discussed. As the spatial displacement of the particle is governed by a potential rather than a stepping rate, these models can be used to obtain physical information about the particle's escape over a potential barrier, a classical problem [78, 79] that is of fundamental interest in the context of enzyme kinetics [80, 81, 82, 83, 84]. Here, we aim to arrive at a discretization of the continuous description for the particle's motion which follows the line of [85] and allows to deduce mechanical transition rates that are valid for a wide range of external load forces. The discretization procedure enables us to implement the rates into networks.

3.1 Brownian motors

Using a continuous description for the motor's motion leads to a class of models that are called non-uniform ratchets. In biological physics, these ratchets have been studied in a detailed way to explain the motion of molecular motors, as reviewed in [15]. Many fundamental properties of stochastic motion can be addressed with these models, with a focus on the mechanical displacement of the particle and an implicit treatment of the chemical details. The term 'ratchet' was motivated by Feynman, as a Gedankenexperiment where a directed motion arises from thermal fluctuations [86]. He showed that the thermal ratchet coupled to a single heat bath did not perform work in agreement with the second law of thermodynamics.

A fluctuating force from, e. g., thermal collisions may help the particle to overcome the potential barrier, but as this happens with equal probability in both directions, the average motion of the process is zero. A net motion arises for switching the potentail on and off periodically, which enables the motor to perform work.

Thermal ratchets are described with an overdamped Langevin equation for the motion of a particle in an external potential $V(x,t)$ and noise $\xi(t)$

$$\zeta_{\mathrm{fr}} \frac{\partial}{\partial t} x = -\frac{\partial}{\partial x} V(x,t) + \xi(t), \tag{3.1}$$

where ζ_{fr} is a friction coefficient, and $\xi(t)$ is a randomly fluctuating force from the thermal environment. In the case of white noise, we have

$$\langle \xi(t) \rangle = 0, \ \langle \xi(t)\xi(t') \rangle = 2k_{\mathrm{B}}T \ \delta(t - t') \tag{3.2}$$

and the Langevin equation can be reformulated as a Fokker-Planck-equation. The detailed treatment of these important formulations of stochastic processes can be found in a variety of textbooks, [61, 78, 79, 87]. The rectification of the Brownian motion can

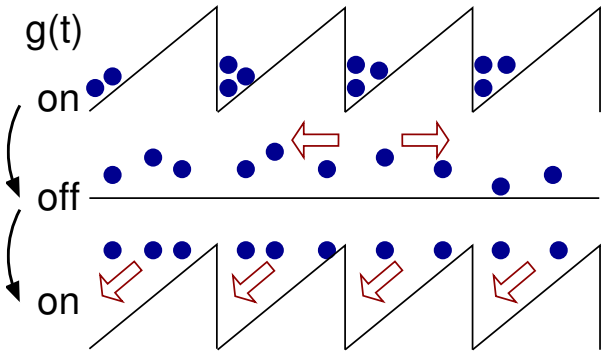

Figure 3.1 : Example of a fluctuating potential ratchet with signal $g(t)$, that periodically switches between states 1 (on) and 0 (off). When the signal is turned off, the particles can freely diffuse and are redistributed in the potential once the signal is turned on again, as indicated by the arrows. This mechanism leads to a net motion of the particles.

be achieved many ways [14]. In the context of molecular motors, the external potential $V(x,t)$ that governs the particle's motion can be rewritten in terms of an inherent potential $U(x,t)$ and a load force F as $V(x,t) = U(x,t) - Fx$, as reviewed in [88]. With explicitly addressing the time-dependence of the process, we have

$$V(x,t) = U(x)g(t) - Fx, \tag{3.3}$$

where $g(t)$ influences the potential $U(x,t)$. One now introduces periodically fluctuating functions $g(t)$, which leads to a 'fluctuating potential' ratchet. By the periodical change of $g(t)$, one defines two states where the particle is subject to different external potentials. Fig. 3.1 shows the example of a fluctuating potential ratchet, that switches between free diffusion and a confining potential. The switching between these states defines a transition rate, and can explicitly be incorporated into the Fokker-Planck equation for the problem to yield a set of reaction-diffusion type of equations. The mathematical feasibility of these equations is facilitated by the fact that the time-dependence for fluctuating potential ratchets can be restricted to the switching signal between potentials that themselves do not depend on time.

3.2 Chemical and mechanical transitions

The situation described above can be expanded to an arbitrary number of different potentials. In the context of a molecular motor, these potentials can be seen as different chemical states that the motor attains when it is bound to the filament. The binding of a nucleotide affects the interaction between the filament and the motor, by strenghtening or weakening the attachtment to the filament. In this way, one can think of each state as having a different potential the motor is exposed to. The motor can be described as a particle moving along a spatial coordinate x with its chemical state characterized by a potential specified by a coordinate m. This means that for each location x, a defined set of chemical reactions described by the coordinate m can take place.

The probability density $P_m(x,t)$ for the particle to be in position x and the chemical state m at time t determines the dynamics of the system. At a given position x, the densities can change through either diffusion, characterized by the lateral current $J_m(x,t)$, or transitions between different chemical states, that results in a transition current with density $I_m(x,t)$. The probability densities satisfy the continuity equation

$$\frac{\partial P_m(x,t)}{\partial t} + \frac{\partial J_m(x,t)}{\partial x} = I_m(x,t). \tag{3.4}$$

The lateral currents $J_m(x,t)$, depend on the underlying potential of molecular interaction, $U_m(x)$, and, if applied, the external force F. This defines an effective force potential

$$V_m(x) = \frac{1}{k_{\mathrm{B}}T}\left(U_m(x) - Fx\right) \tag{3.5}$$

for each chemical state m. A translation along the spatial coordinate x while keeping the chemical state m fixed exposes the motor to the force $-\partial U_m(x)/\partial x$, which corresponds to a ratchet mechanism.

Using the effective potential 3.5, the continuity equation 3.4 can be rewritten and formulated in terms of a Fokker-Planck equation, which results in the lateral current

$$\begin{aligned} J_m(x,t) &= -D_m\left[\frac{\partial}{\partial x}V_m(x) + \frac{\partial}{\partial x}\right]P_m(x,t) && (3.6)\\ &= -D_m \exp\left(V_m(x)\right)\frac{\partial}{\partial x}\left[\exp\left(V_m(x)\right)P_m(x,t)\right]. && (3.7) \end{aligned}$$

Here, D_m is an effective 'small scale' diffusion coefficient. A linear molecular motor typically moves along a filament that has a repeated structure, with a periodicity ℓ that corresponds to the motor's step size. Thus, the potentials and lateral currents obey

periodic boundary conditions of the form

$$P_m(x,t) = P_m(x+\ell,t) \tag{3.8}$$
$$J_m(x,t) = J_m(x+\ell,t). \tag{3.9}$$

The current densities $I_m(x,t)$ can be transformed into a gain and loss equation,

$$I_m(x,t) = \sum_{n\neq m} \left(-P_m(x,t)\Omega_{nm}(x) + P_n(x,t)\Omega_{nm}(x)\right), \tag{3.10}$$

where $\Omega_{nm}(x)$ are transition rate functions for the transition from state n to state m. Summing up Eq. 3.10 over all chemical current densities results in $\sum_m I_m(x,t) = 0$, because each term comes up twice and with opposite sign.

The total probability density, $P_{\text{tot}}(x,t)$, and the total lateral current, $J_{\text{tot}}(x,t)$, are obtained by summation over all internal states,

$$P_{\text{tot}}(x,t) \equiv \sum_m P_m(x,t) \quad \text{and} \quad J_{\text{tot}}(x,t) \equiv \sum_m J_m(x,t). \tag{3.11}$$

For the total probability density, the continuity equation is given by

$$\frac{\partial P_{\text{tot}}(x,t)}{\partial t} + \frac{\partial J_{\text{tot}}(x,t)}{\partial x} = \sum_m I_m(x,t) = 0. \tag{3.12}$$

The latter equality reflects the probability conservation of the motor being in a chemical state bound to the filament, which is implicitly included in the construction of the model. Within our framework, the situation of motor unbinding from the filament will not be used in the context of the continous models.

3.3 From continous to discrete space

The transition rate functions $\Omega_{nm}(x)$, do, in general, depend on the spatial coordinate x. According to the discrete stepping of the motor, one can assign discrete positions x_k with $k = 1...K$ to the transition rate functions,

$$\Omega_{nm}(x) \equiv \sum_k \ell_\Omega \omega_{nm}(x_k)\delta(x-x_k), \tag{3.13}$$

where ℓ_Ω is a localization length, $\delta(x)$ is Dirac's delta function and $\omega_{nm}(x_k)$ are transition rates. In this way, the energy landscape governing the motor's motion is essentially mapped onto a two-dimensional lattice with a chemical coordinate m and a spatial

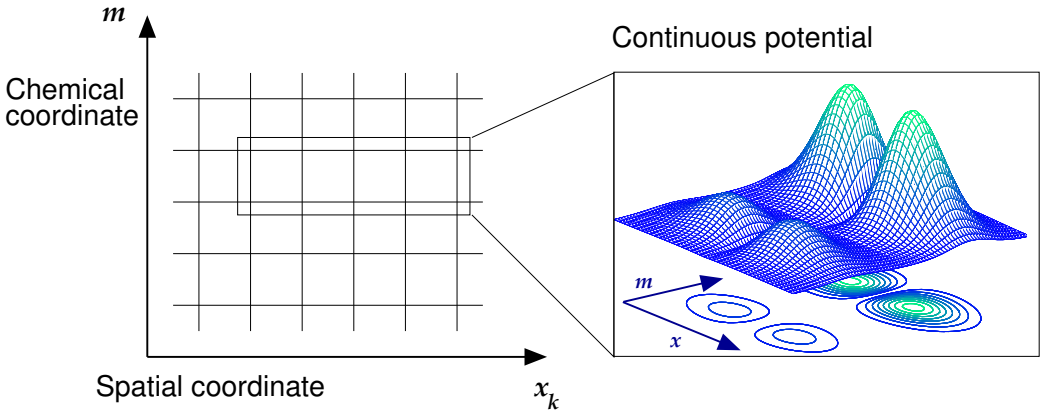

Figure 3.2 : Discrete lattice of states with chemical coordinate m and spatial coordinate x_k. At the right hand side, a continous potential is shown to illustrate the original energy landscape. A transition along the chemical coordinate m leads to a change in the potential the motor is exposed to. Here, the potentials differ considerably in height, while the potentials along the spatial coordinate x repeat periodically.

coordinate x_k, as illustrated in Fig. 3.2. At the moment, we do not specify the exact mapping of these discrete locations onto the motor's filament, but discuss general aspects of this discretization. The confinement to specific sites in terms of delta functions allows for analytical solution for various stochastic models of this type [85, 84].

Let us turn to the stationary case, that corresponds to $\partial P_m/\partial t = 0$, which through Eq. 3.11 implies stationariy for the total probability aswell, $\partial P_{\rm tot}(x,t)/\partial t = 0$. From the continuity equation (3.12), it directly follows that the total lateral current $J_{\rm tot}(x,t)$ is constant. The integration of the FPE formulation for the current density, Eq. 3.6, yields

$$P_m(x) = P_m(x')e(x',m|x,m) = -D_m \int_{x'}^{x} J_m(y)e(y,m|x,m) \tag{3.14}$$

with exponential functions that depend on the transition potentials $V_m(x)$,

$$e(x,m|y,n) \equiv \exp\left(V_m(x) - V_n(y)\right) = \frac{1}{e(y,n|x,m)}. \tag{3.15}$$

From the functional equation of the exponential function, it directly follows that the $e(x,m|y,n)$ obey a product rule of the form

$$e(x_1,m|x_2,m)e(x_2,m|x_3,m) = e(x_1,m|x_3,m). \tag{3.16}$$

The normalization condition is imposed on one spatial repeat of the potential, that with

the use of periodic boundary conditions is given by

$$\int_{x_1}^{x_1+\ell} P_{\rm tot}(x)\ dx = \int_{x_1}^{x_1+\ell} \sum_m P_m(x)\ dx \equiv 1 \tag{3.17}$$

This implements the requirement of one motor to be completely localized within a periodic repeat of the filament. This form of normalization defines a motor velocity given by $v = \ell J_{\rm tot}$.

Detailed balance

In the absence of both an external force and enzymatic activity, the system obeys detailed balance, which we again indicate by use of the superscript '$_{\rm db}$', such that $P_m(x) = P_m^{\rm db}(x)$ and $\Omega_{nm}(x) = \Omega_{nm}^{\rm db}(x)$. The detailed balance condition, in this way, reads

$$P_m^{\rm db}(x)\Omega_{nm}^{\rm db}(x) = P_n^{\rm db}(x)\Omega_{nm}^{\rm db}(x). \tag{3.18}$$

As a consequence, the transition current density vanishes, as can be infered from Eq. 3.10. The absence of an external force, $F = 0$, leads to a vanishing current $J_m(x,t)$ for each chemical state m. In this way, Eq. 3.6 can be easily solved to yield

$$P_m(x,t)^{\rm eq} \sim \exp\left(U_m(x)/k_{\rm B}T\right), \tag{3.19}$$

which is the Boltzmann weight for the equilibrium probability distribution. Using this weight together with Eq. 3.18 leads to a balance for the transition rate functions,

$$\Omega_{nm}^{\rm db}(x) = e^{(1/k_{\rm B}T(U_m(x)-U_n(x)))}\Omega_{nm}^{\rm db}(x) = e^{(V_m(x)-V_n(x))}\Omega_{nm}^{\rm db}(x). \tag{3.20}$$

For transition rate functions that are localized and parametrized in terms of delta functions, as done in Eq. 3.13,

$$\frac{\omega_{mn}^{\rm db}(x_k)}{\omega_{nm}^{\rm db}(x_k)} = e^{(V_m(x_k)-V_n(x_k))},\ \text{or}\ \ln\frac{\omega_{mn}^{\rm db}(x_k)}{\omega_{nm}^{\rm db}(x_k)} = V_m(x_k) - V_n(x_k). \tag{3.21}$$

Note that this relation holds for $F \neq 0$, i. e., for situations out of equilibrium.

Local currents

Up to now, we have set up the framework for mapping the energy landscape for the motor's motion onto a two-dimensional network with a chemical coordinate m and a spatial coordinate x_k. For transition rates between neighbouring states, we outline the

calculation of the corresponding local currents. Let us define the local transition current at a fixed lattice site x_k, from state m to n,

$$J_{mn} \equiv P_m(x_k)\omega_{mn}(x_k)\ell_\Omega \geq 0. \tag{3.22}$$

The corresponding current from state n to m is given by $J_{nm}(x_k)$. These are the two currents through a di-edge along the chemical coordinate, and the total current through this edge is given by $J_{mn}(x_k) - J_{nm}(x_k)$. After a calculation that is based on the integration of the continuity equation and the formulation of local transition density currents in terms of probabilities, Eq. 3.10, one can use the local currents between chemical states m and n to determine a relation for the transition currents between neighbouring *spatial* sites x_k and x_{k+1},

$$J_m(x_k, x_{k+1}) = J_m(x_{k-1}, x_k) + \sum_{n\neq m} \left(-J_{mn}(x_k) + J_{nm}(x_k)\right). \tag{3.23}$$

Reformulation of Eq. 3.14 with using neighbouring coordinates x_k and x_{k+1} for x and x', leads to spatial transition currents of the form

$$J_m(x_k, x_{k+1}) = P_m(x_k)\frac{e_m(x_k, x_{k+1})}{\mathcal{E}_m(x_k, x_{k+1})} - P_m(x_{k+1})\frac{1}{\mathcal{E}_m(x_k, x_{k+1})}, \tag{3.24}$$

with

$$\mathcal{E}(x, y) = 1/D_m \int_x^y dz\ e_m(z, y) = 1/D_m \int_x^y dz\ \exp(V_m(z) - V_m(y)). \tag{3.25}$$

The structure of Eq. 3.24 has the structure of a master equation, when identifying the terms

$$\omega^{\mathrm{f}}(k, k+1) = \frac{e_m(x_k, x_{k+1})}{\mathcal{E}_m(x_k, x_{k+1})\ell_\Omega} \tag{3.26}$$

$$\omega^{\mathrm{b}}(k+1, k) = \frac{1}{\mathcal{E}(x_k, x_{k+1})\ell_\Omega}, \tag{3.27}$$

as the forward (f) and backward (b) transition rates of the system. Note that the rates have to be rescaled by ℓ_Ω in order to turn the corresponding probabilities dimensionless.

4 The molecular motor myosin V

4.1 Introduction

Myosin V is a processive molecular motor that moves along actin filaments in discrete steps of 36 nm [20]. This processive motion is tightly coupled to the hydrolysis of adenosine triphosphate (ATP) [89]. The molecule has a catalytic domain at each of its two heads and proceeds in a 'hand over hand' fashion towards the barbed end of the actin filament [57]. The coordination of hydrolysis between the two heads is thought to be crucial for the processive motion and the high duty ratio of the motor [90, 54]. For external forces opposing the forward motion of the motor that do not exceed its stall force, i.e., the force at which the motor does not exhibit any net motion, a dominant chemomechanical cycle has been identified. The molecule mainly dwells with both heads strongly bound to the filament, with adenosine diphosphate (ADP) bound to both catalytic domains. After release of ADP from the trailing head, ATP binding to the empty domain takes place. This leads to weakening of the actomyosin bond, which in turn allows for unbinding of the head from the actin filament. Subsequently, the free head finds its way to the next binding site via a power stroke, and a subsequent diffusional search until encounter with the next binding site [52], where it rebinds and hydrolyses the ATP molecule [54] to an ADP*P complex with subsequent release of P (phosphate). For high concentrations of ATP, the release of ADP is the rate limiting step of this turnover cycle.

Extensive research has been done on the step size distribution of the molecule [20], its dwell times [44], and its backstepping behaviour [91]. Moreover, the release of ADP has been proposed to be different for the leading and the trailing head of the molecule [92, 93]. Reported data on the stall force range from 1.5 to 3.0 pN for various concentrations of ATP [20, 26, 46, 53, 91]. Three different force regimes have to be distinguished: Assisting forces as well as resisting forces below and above the stall force F_s of the motor. For resisting forces that exceed stall, myosin V has been proposed to act as a mechanical ratchet [46]: When stepping backwards in a forced manner, the stepping velocity does not seem to depend on the concentration of ATP, while this is not the case for the forward motion of the motor under assisting forces.

A variety of theoretical models has been proposed for myosin V, such as a kinetic model [94], and a treatment of the molecule implementing the elastic properties of its lever arms [95]. A stochastic algorithm for the fit of dwell time distributions has been proposed

by [77], and the molecule serves as a model mechanism to evaluate its properties in terms of efficiency [9]. A recent study [96] performs a Brownian dynamics simulation of the forward motion of myosin V, with the aim to investigate the substepping behaviour that has been reported by different groups [47, 53]. A generic class of discrete models addresses the substepping behavior [97] and the reaction of enzymatic activity to high forces [98]. The models, however, are either based on a large number of parameters or do not investigate the force dependence of the myosin V stepping behaviour. In addition, none of them investigates the role of backward steps quantitatively, especially the step ratio and the ratcheting behaviour of the myosin V.

Here, we use a network representation deduced from the enzymatic activity of the myosin motor to explain several sets of experimental data, including those on backward steps. Our approach is based on previous work [11, 67] that provides a general framework for the chemomechanical coupling of molecular motors which is consistent with nonequilibrium thermodynamics.

4.2 Network representations

During processive motion, the motor can attain several states, specified by its location on the motor filament and the chemical composition of its nucleotide binding pockets. The transitions between these states involve binding or release of ATP, ADP or P, or a mechanical displacement. For the definition of discrete motor states that separate the chemical reaction from the step, two requirements have to be fulfilled, *i)* thermal equilibrium has to be reached on a timescale much shorter than the chemical reaction takes place and *ii)* the step in itself has to be much faster than the reaction. This is indeed the case for the myosin V molecule, where the hydrolysis rate is on the order of 10 /s and the mechanical step takes only a few ms to be completed [48, 59, 47]. A single catalytic domain of the motor can contain bound ATP, ADP, or ADP*P, or it can be empty. When combining the ADP*P state with the transition between the ATP and the ADP state, as discussed in chapter 2, each of the two catalytic sites of the motor can attain 3 states that we denote by T (ATP bound), D (ADP bound), and E (empty). This state space for a single motor head leads to 3x3=9 possible states for the two heads. These 9 states are connected by 18 chemical and 6 mechanical transitions. A chemical transition corresponds to the binding or release of a nucleotide, while a mechanical transition results in the interchange of the two motor heads. In general, the possible mechanical transitions are, without specification of the step direction, EE $\rightleftharpoons$ EE, DD $\rightleftharpoons$ DD, TT $\rightleftharpoons$ TT, ET $\rightleftharpoons$ TE, DT $\rightleftharpoons$TD, and DE $\rightleftharpoons$ ED.

Fig. 4.1 shows the chemical network of myosin V repeated with periodic boundary conditions along a filament coordinate x with a discrete spacing of $\ell = 36$ nm. The chemical transitions connect the nine states of the network, while the mechanical transitions connect two copies of the network separated by a step of size ℓ. Only those

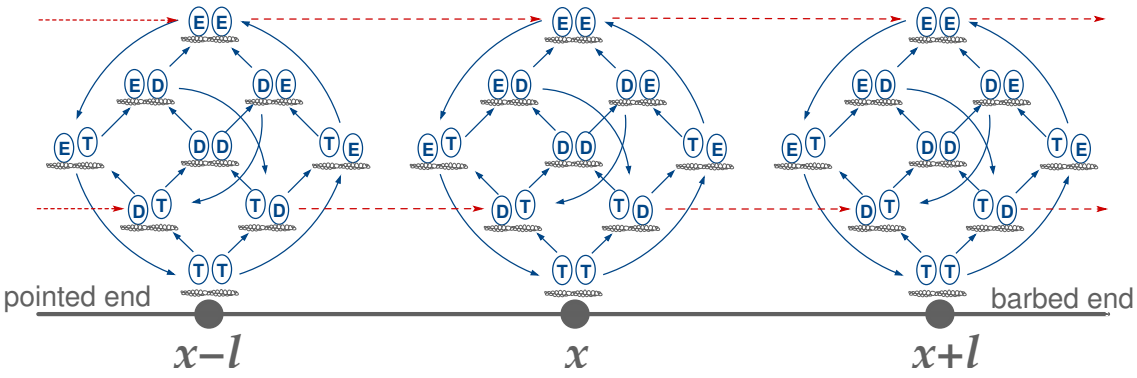

Figure 4.1 : Chemomechanical network for myosin V at different binding sites x of the filament, represented by a thick grey line. The nine states, that are repeated periodically along the filament with a spacing of $\ell = 36$ nm, are defined by the chemical composition of the nucleotide binding pockets of the two motor heads. A head with bound ATP or ADP is denoted by T or D, an empty head by E. Both the E and D states are strongly bound to the actin filament, whereas the T state is only weakly attached [48], as indicated by the gap between the T heads and the filament. All transitions between two connected states can occur both in the forward and the backward direction. Chemical transitions are drawn as solid lines (blue), with arrows indicating the direction of ATP hydrolysis. The broken lines (red) correspond to the mechanical transitions as observed experimentally, with the arrows pointing towards the forward stepping direction [46, 47], i.e., towards the barbed end of the actin filament.

mechanical transitions are included that have been observed in experiments, namely EE $\rightleftharpoons$ EE and TD $\rightleftharpoons$ DT.

The network shown in Fig. 4.1 contains 36 chemical and 4 mechanical transitions which lead, in general, to a rather large number of possible pathways or motor cycles. In the following, we identify the dominant pathways of the motor and, in this way, reduce the network description. This procedure enables us to minimize the number of model parameters and to construct a theory which, on the one hand, describes a large set of experimental data as obtained by different groups and, on the other hand, can be improved if new experimental data become available.

The simplest chemomechanical network that takes both mechanical transitions TD $\rightleftharpoons$ DT and EE $\rightleftharpoons$ EE into account is displayed in Fig. 4.2. Apart from the two mechanical transitions, this network contains six chemical transitions, each of which may proceed in the forward or backward direction. As shown in the following, the available experimental data allow us to determine the corresponding transition rates for vanishing load force in a unique manner.

With the use of periodic boundary conditions for the network, each state can be revisited on a closed path. A network cycle consists of a set of states that are directly connected and have, as a starting and end point, either the same state or the corresponding copy at a neighbouring lattice site of the network. A cycle with a primed state indicates that it contains a mechanical displacement ℓ. The network thus can be characterized by three cycles $\mathcal{M}$, $\mathcal{E}$ and $\mathcal{F}$, two of which contain a stepping transition. Each of these cycles is composed of two directed cycles, i. e., the forward cycles $\mathcal{F}^+ = |1234'\rangle$, $\mathcal{E}^+ = |256\rangle$, $\mathcal{M}^+ = |55'\rangle$ and their corresponding backward cycles $\mathcal{F}^- = |4'321\rangle$, $\mathcal{E}^- = |652\rangle$, and $\mathcal{E}^- = |5'5\rangle$, see App. A. The chemomechanical cycle $\mathcal{F}$ (DD $\rightleftharpoons$ ED $\rightleftharpoons$ TD $\rightleftharpoons$ DT $\rightleftharpoons$ DD) is the one discussed previously in various experimental studies [44, 54], and contains both chemical and stepping transitions. The ratcheting cycle $\mathcal{M}$ contains only the stepping transition EE $\rightleftharpoons$ EE, corresponding to the experimental result in [46] where myosin V was observed to step at superstall forces in the EE state. The third cycle, $\mathcal{E}$ (EE $\rightleftharpoons$ ET $\rightleftharpoons$ ED), is a dissipative cycle, that connects the two stepping cycles $\mathcal{M}$ and $\mathcal{F}$ along two different pathways, one involving ATP hydrolysis, and the other binding of ADP.

The experimental consensus for coordination of the motor's heads is a gating effect that leads to an increased rate of ADP release for the trailing head compared to the leading head [90, 54]. This effect is implicitly included in the network by focusing on the chemomechanical cycle $\mathcal{F}$ for substall load forces, with omitting ADP release from the leading head in the state DD. Including pathways with the state omitted here, DE, as discussed in [99], does not change the quantitative results, a point that we address in App. B.

Myosin V exhibits rather different stepping behavior for load forces below and above the stall force. Our analysis as described below shows that this difference arises from different cycles of the network being dominant for different force regimes. The chemomechanical cycle $\mathcal{F}$, which couples the mechanical forward steps TD $\rightarrow$ DT or $|34'\rangle$ to ATP hydrolysis, is dominant for forces below the stall force. In this regime, the motor also exhibits some backward steps DT $\rightarrow$ TD or $|4'3\rangle$ but these backwards steps are immediately followed by forward steps. Thus, these backward steps are not coupled to ATP synthesis, a process that is rather unlikely for typical nucleotide concentrations. The mechanical slip cycle $\mathcal{M}$ dominates for forces above the stall force. In the latter regime, the motor walks backwards in a processive manner. The stall force itself is determined by the competition between the chemomechanical cycle $\mathcal{F}$ and the mechanical slip cycle $\mathcal{M}$.

It is instructive to compare these operation modes of myosin V with those of kinesin. For the latter motor, the sub- and superstall regimes are governed by two different chemomechanical cycles, one of which couples mechanical backward steps to ATP hydrolysis [67]. The latter coupling has also been discussed for myosin V [99]. In the case of kinesin, the competition between the two chemomechanical cycles leads to a stall force that is essentially independent of ATP concentration [67], in agreement with single molecule

data. In contrast, the experimentally determined values for the stall force of myosin V lie within a relatively broad range [20, 53, 26, 91, 46]. Therefore, at present, the myosin V data do not provide strong evidence for the relevance of another chemomechanical cycle that couples backward steps to ATP hydrolysis. The data for these arguments are given in App. B.

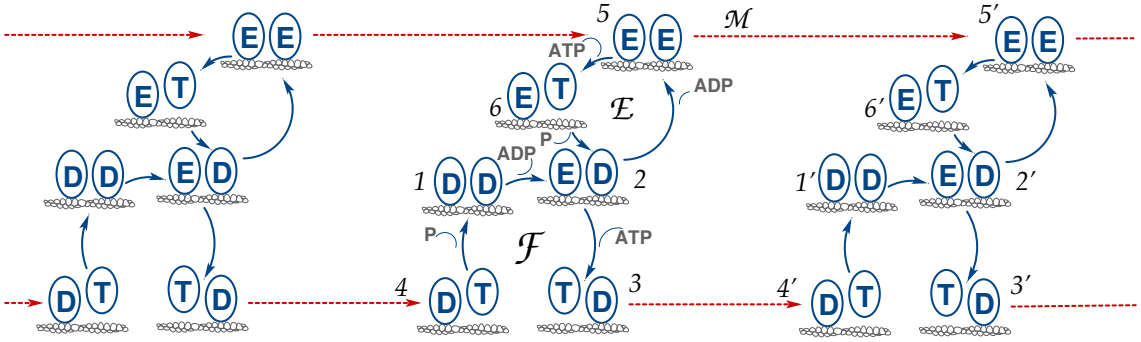

Figure 4.2 : Reduced network for the motion of myosin V, consisting of three copies of six states $i = 1...6$ connected by transitions $|ij\rangle$ from state i to state j, that form three pathways $\mathcal{F}$, $\mathcal{E}$, and $\mathcal{M}$. The chemomechanical forward cycle $\mathcal{F}$ consists of the states $\langle 1234' \rangle$, that contain both chemical and mechanical transitions, while the dissipative or enzymatic slip cycle $\mathcal{E}$ with states $\langle 256 \rangle$ is purely chemical. The ratcheting cycle $\mathcal{M}$, on the other hand, consists only of the mechanical stepping transitions $|55' \rangle$, $|5'5'' \rangle$, and so on. Each state is characterized by the chemical composition of the two motor heads, the one on the right hand side being the leading one. The solid lines (blue) are the chemical transitions for the indicated species X=ATP, ADP, or P, while the broken lines (red) show the stepping transitions. The arrows refer to the direction of forward stepping and ATP hydrolysis, respectively.

Let us briefly outline the considerations that lead to the chemomechanical step cycle $\mathcal{F}$. Because of the high binding affinity of ATP to myosin [48], the motor heads are, for saturating concentrations of ATP, very likely to attain the T state before binding to the filament. As the motor is strongly bound to the filament both in the E and D states but only weakly bound in the T state [48], and ATP hydrolysis is fast compared to ADP release, the motor will end up in the states DE, ED, or DD when binding to the filament to start its processive run. Experiments indicate that the molecule dwells in the DD state for most of the time between two succesive steps [44, 90]. Starting from this state, the release of ADP can lead to two states, ED or DE. For two-headed myosin constructs, the rate of ADP release in the myosin motor has been investigated extensively and is thought to differ for the trailing and the leading head of the motor [92, 100]. The different experiments present highly diverse data, but agree that the rate

of ADP release for the leading head is much slower than for the trailing head. This observation is taken into account by omitting the state DE from the network and will be discussed in more detail as the *gating* mechanism. In the state ED, both heads are strongly bound to the filament. The binding of an ATP molecule to the trailing head leads to the TD state, which, through weakening of the actomyosin bond, is followed by a mechanical step. This results in an interchange of the two heads and in the state DT, and subsequent hydrolysis leads to the state DD and the completion of the forward stepping cycle $\mathcal{F}$.

Before we discuss the functional form of the chemical and mechanical transitions, we focus on the network dynamics that allow us to determine characteristic properties of the motor's motion.

4.3 Motor dynamics

As discussed in chapter 2, the motor's motion can be characterized by the master equation 2.1 for the network shown in Fig.4.2. It connects the probability to find the motor in a given state i with the corresponding local excess flux, $\frac{\mathrm{d}}{\mathrm{dt}}P_i(t) = -\sum_j \Delta J_{ij}(t)$, where the fluxes $\Delta J_{ij}(t) = P_i(t)\ \omega_{ij} - P_j(t)\ \omega_{ji}$ contain the transition rates ω_{ij}, see 2.2.

In general, the transition rates ω_{ij} can depend on both on the load force component parallel to the filament, $F = \vec{F}_{\|}$, and the molar concentrations $[X]$, where X denotes the molecular species ATP, ADP or P. Thus, the transition rates have the general form

$$\omega_{ij} \equiv \omega_{ij,0}\ \Phi_{ij}(F) \quad \text{with} \quad \Phi_{ij}(0) \equiv 1 \tag{4.1}$$

which defines the zero-force transition rates $\omega_{ij,0}$ and the force-dependent factors $\Phi_{ij}(F)$. Moreover, the transitions that include binding of an X-molecule with X = ATP, ADP and P depend on the molar concentration $[X]$ which implies

$$\begin{array}{rcll} \omega_{ij,0} & \equiv & \hat{\kappa}_{ij}\,[X] & \text{for} \quad X-\text{binding} \\ & \equiv & \kappa_{ij} & \text{for} \quad X-\text{release}\,. \end{array} \tag{4.2}$$

The transition rate constants $\hat{\kappa}_{ij}$ have the dimension $1/(\mathrm{s}\,\mu\mathrm{M})$ whereas the transition rates κ_{ij} have the dimension $1/\mathrm{s}$.

In the case of the steady state, given by 2.3, the motor moves persistently through a continuous supply of energy. The steady state fluxes J_{ij}^{st} for our network description have been calculated using Kirchhoff's method, and are given explicitly in Appendix A. Every time the motor undergoes a stepping transition, it performs a step with length $\ell = 36$ nm. The average velocity of the motor is thus given by the probabilistic flux

through the two stepping transitions $|34'\rangle$ and $|55'\rangle$,

$$v = \ell(\Delta J^{st}_{34'} + \Delta J^{st}_{55'}). \tag{4.3}$$

In the following, we discuss the energetic balance of the motor, which can be specified in a quantitative manner in terms of network dicycles $\mathcal{C}^d_\nu$ with orientation $d = \pm 1$, as discussed in section 2.3.

4.4 Cyclic fluxes and balance conditions

The entropy that is produced during the revolution of a cycle can be readily connected to the work performed by the motor. For each dicycle, the average entropy ΔS can be calculated through 2.34. In the steady state, the internal energy, which arises from the chemical reaction and mechanical work during the processive motion of the motor, does not change on a cycle $\mathcal{C}^d_\nu$ of the network, $\Delta U(\mathcal{C}^d_\nu) = 0$. As can be infered from 2.40, the first law of thermodynamics together with the heat $\Delta Q(\mathcal{C}^d_\nu) = T\Delta S(\mathcal{C}^d_\nu)$ released by the motor during one completion of the dicycle $\mathcal{C}^d_\nu$ leads to a balance condition for this dicycle as given by

$$k_{\rm B}T \ln \prod_{|ij\rangle}^{\nu,\pm} \left(\frac{\omega_{ij}}{\omega_{ji}}\right) = E_{\rm ch}(\mathcal{C}^\pm) - W_{\rm me}(\mathcal{C}^\pm). \tag{4.4}$$

Here, $E_{\rm ch}(\mathcal{C}^d_\nu)$ and $W_{\rm me}(\mathcal{C}^d_\nu)$ are the chemical energy supplied to the motor and the mechanical work performed by the motor, respectively, during one completion of dicycle $\mathcal{C}^d_\nu$.

The chemical energy $\Delta\mu$ can be expressed in terms of the chemical potential difference $\Delta\mu$ that arises from addition of one ATP molecule to the system and the subsequent release of one ADP and phosphate, which is, for dilute solutions, given by

$$\Delta\mu = k_{\rm B}T \ln\left(K_{\rm eq}\,\frac{[\rm ATP]}{[\rm ADP][P]}\right), \tag{4.5}$$

with $K_{\rm eq} \simeq 4.9 \times 10^{11}\mu$M being the equilibrium constant of the reaction.
For each of the three cycles $\mathcal{F}$, $\mathcal{M}$, and $\mathcal{E}$ of the network shown in Fig. 4.2, Eq. (4.4) leads to a balance condition. For the cycles $\mathcal{F}$ and $\mathcal{E}$, we obtain, for $F = 0$,

$$K_{\rm eq} = \frac{\kappa_{12}\hat{\kappa}_{23}\kappa_{34'}\kappa_{41}}{\hat{\kappa}_{21}\kappa_{32}\kappa_{4'3}\hat{\kappa}_{14}} = \frac{\kappa_{25}\hat{\kappa}_{56}\kappa_{62}}{\hat{\kappa}_{52}\kappa_{65}\hat{\kappa}_{26}}. \tag{4.6}$$

For $F \neq 0$, substracting the balance condition for $F = 0$, Eq. (4.6) from Eq. (4.4), and

using Eq. (4.1) leads to the general balance condition

$$\frac{\Phi_{12}\Phi_{23}\Phi_{34'}\Phi_{41}}{\Phi_{21}\Phi_{32}\Phi_{4'3}\Phi_{14}} = \exp\left(-\frac{\ell}{k_{\mathrm{B}}T}F\right) \tag{4.7}$$

for the force-dependent factors Φ_{ij}. Here, we have used that $W_{\mathrm{me}}(\mathcal{F}^+) = \ell F$. The enzymatic cycle $\mathcal{E}$ consists of chemical transitions only, and we thus have $W_{\mathrm{me}}(\mathcal{E}^+) = 0$ and, as a consequence,

$$\frac{\Phi_{25}\Phi_{56}\Phi_{62}}{\Phi_{52}\Phi_{65}\Phi_{26}} = 1. \tag{4.8}$$

Since the ratchet cycle $\mathcal{M}$ does not contain any chemical transition, we have, for $F = 0$,

$$\kappa_{55'} \;=\; \kappa_{5'5}, \tag{4.9}$$

which reflects the fact that there is a priori no preferred direction for the motor to perform a forward or a backward step in the state EE. For the chemomechanical cycle $\mathcal{F}$, we take

$$\frac{\Phi_{12}\Phi_{23}\Phi_{41}}{\Phi_{21}\Phi_{32}\Phi_{14}} = 1, \tag{4.10}$$

which is based on the assumption that the displacement of the center of mass of the motor upon ATP hydrolysis and synthesis is negligible. Then, the balance conditions for the cycles $\mathcal{F}$ and $\mathcal{R}$ read, for $F \neq 0$,

$$\frac{\Phi_{34}(F)}{\Phi_{43}(F)} = \frac{\Phi_{55'}(F)}{\Phi_{5'5}(F)} = \exp\left(-\frac{\ell}{k_{\mathrm{B}}T}F\right). \tag{4.11}$$

We use the convention that negative values of F correspond to assisting forces , which act in the preferred direction of forward stepping, i. e., the plus- end of the actin filament, while resisting forces are described by positive values of F. A widely used parametrization for the force dependence of the stepping transitions $|ij\rangle$ is given by [97, 67]

$$\Phi_{ij}(F) \;=\; \exp\left(-\theta_{ij}\frac{\ell}{k_{\mathrm{B}}T}F\right) \quad \text{for forward and} \tag{4.12}$$

$$\Phi_{ji}(F) \;=\; \exp\left((1-\theta_{ij})\frac{\ell}{k_{\mathrm{B}}T}F\right) \quad \text{for backward steps,} \tag{4.13}$$

where $0 < \theta_{ij} < 1$ is a fit parameter. This parametrization does not apply to the limit of large forces. In particular, when the motor motion arises solely from the mechanical cycle $\mathcal{M}$, the parametrization (4.12) and (4.13) would lead to an exponential increase

of the stepping rate, which does not correspond to the expected behavior of the energy barrier and the experimental observation. The failure of this parametrization is due to the fact that Eq. (4.12) is only valid if the deformation energy arising from the force exerted on the motor is much smaller than the energy barrier that has to be overcome to perform a step. We thus keep the parametrization given by Eq. (4.12) and (4.13) only for the stepping rates of the chemomechanical cycle $\mathcal{F}$, ω_{34} and ω_{43}. The force dependence of the stepping transitions $\omega_{55'}$ and $\omega_{5'5}$ is calculated from the escape of a particle over a potential barrier using the Fokker-Planck-equation, as shown in the following section.

4.5 Functional form of mechanical stepping rates

To obtain stepping rates valid for a large range of load forces, we use, as discussed in chapter 3, a coarse graining approach that is based on the discretization of the continuous Fokker-Planck-equation. The stepping rates calculated in this way automatically fulfill the correct balance condition. A different method based on calculations of the mean first passage time can be found in [78, 79]. We start from a Fokker-Planck-equation for the

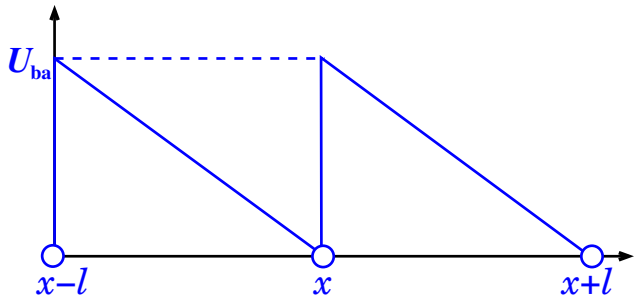

Figure 4.3 : Periodic sawtooth potential with slope $-U_{\mathrm{ba}}/\ell$, barrier height U_{ba} and periodicity ℓ.

diffusion of a particle over a potential $V(x)$ along a continuous variable x. For simplicity, we take a sawtooth potential $U(x)$ with period ℓ, height U_{ba}, and slope U_{ba}/ℓ, and impose periodic boundary conditions on the potential. Here, the chemical coordinate is $m = 1$. The simplest discretization of the continuous equation consists in assigning lattice sites to the potential in two successive minima, i. e., at locations $x_n = n\ell$ and $x_{n+1} = (n+1)\ell$ for integer n, as indicated in Fig. 7.4. $U(x)$ is then given by

$$U(x) = -\frac{U_{\mathrm{ba}}}{\ell}(x - n\ell) \quad \text{for} \quad n\ell \leq x < (n+1)\ell \tag{4.14}$$

The transition rates between two neighbouring sites x_n and x_{n+1} are calculated as

$$\omega_{n,\ n+1} = \frac{e(x_n,\ x_{n+1})}{\mathcal{E}(x_n,\ n_{k+1})\ell_\Omega}, \tag{4.15}$$

$$\omega_{n+1,\ n} = \frac{1}{\mathcal{E}(x_n, x_{n+1})\ell_\Omega}, \tag{4.16}$$

as given in 3.26 and 3.27, with

$$e(x,y) = \exp\left(\frac{1}{k_\mathrm{B}T}(x-y)F\right) \tag{4.17}$$

and

$$\mathcal{E}(x,y) = 1/D \int_x^y dz\ \exp(V(z) - V(y)), \tag{4.18}$$

where D is a diffusion constant, ℓ_Ω a localization and $V(x) = \frac{1}{k_\mathrm{B}T}\left(U(x) + Fx\right)$ is the forced potential, with $F > 0$ being a backward force. Note that $\mathcal{E}(x,y)$ holds for $x < y$, with both x and y being from one interval of the potential. For the sawtooth potential as given by 4.14, the forward and the backward transitions have the form

$$\omega_{n,\ n+1} = \frac{D}{k_\mathrm{B}T} \cdot \frac{U_\mathrm{ba} - F\ell}{\ell^2} \cdot \frac{\exp\left[-\frac{\ell}{k_\mathrm{B}T}F\right]}{1 - \exp\left[\frac{1}{k_\mathrm{B}T}(F\ell - U_\mathrm{ba})\right]}, \tag{4.19}$$

$$\omega_{n+1,\ n} = \frac{D}{k_\mathrm{B}T} \cdot \frac{U_\mathrm{ba} - F\ell}{\ell^2} \cdot \frac{1}{1 - \exp\left[\frac{1}{k_\mathrm{B}T}(F\ell - U_\mathrm{ba})\right]} \tag{4.20}$$

$$\tag{4.21}$$

where we have set $\ell_\Omega = \ell$. The rates automatically obey the requirement that $\frac{\omega_{n,\ n+1}}{\omega_{n+1,\ n}} = \exp(-\frac{\ell}{k_\mathrm{B}T}F)$. In this way, a backward step in the ratchet has the rate $\omega_{55'} = \omega_{n,\ n+1}$ and a forward step is given by $\omega_{5'5} = \omega_{n+1,\ n}$. By definition, we then have $\kappa_{55'} = \omega_{55'}(F=0)$ and $\kappa_{5'5} = \omega_{5'5}(F=0)$, respectively.

4.6 Specification of transition rates

For vanishing load $F = 0$, we use the ATP binding rates $\hat{\kappa}_{23}$ and $\hat{\kappa}_{56}$ as well as the phosphate release rates κ_{41} and κ_{62} as determined experimentally for single-headed myosin V in [48]. The two motor heads of myosin V are believed to be coordinated by a gating

mechanism that leads to an increased rate of ADP release at the trailing head compared to the leading head [54, 101]. The reduced network considered here involves the transition $|12\rangle$ with ADP release from the trailing head and the transition $|25\rangle$ with ADP release from the leading head, see Fig. 4.2. Therefore, in our theory, the gating mechanism is incorporated via the transition rate ratio $\zeta \equiv \kappa_{25}/\kappa_{12}$. We find that average motor properties such as the motor velocity v, the ratio q of forward to backward steps, and the run length Δx can be well described for ζ-values within the range $1/10 \lesssim \zeta \lesssim 1$, consistent with the experimental data in [101]. However, a detailed comparison of calculated and measured dwell time distributions leads to the specific choice $\zeta = 1/10$, as discussed in chapter 6. In addition, the ADP binding rates, $\hat{\kappa}_{21}$ and $\hat{\kappa}_{52}$, are taken to have the values measured in [44]. In addition, we use the rates for ADP binding, $\hat{\kappa}_{21}$ and $\hat{\kappa}_{52}$, measured in [44]. Therefore, the only unknown chemical rates in the chemomechanical cycle $\mathcal{F}$ and the enzymatic slip cycle $\mathcal{E}$ happen to be the ATP release rates, κ_{32} and κ_{65}, and the phosphate binding rates, $\hat{\kappa}_{14}$ and $\hat{\kappa}_{26}$. The rate of ATP release is rather small and thus difficult to measure [102]. In the absence of direct measurements of the ATP release rate for myosin V, we make the plausible assumption that this rate is in the same order of magnitude as the corresponding rate for myosin II. The latter rate has been determined experimentally and is in the order of 10^{-5} s^{-1} [103]. It turns out that increasing this rate by up to three orders of magnitude does not significantly change our calculations, with the exception of the stepping velocity as a function of phosphate concentration, as discussed in the next section.

We use the zero-force balance condition, Eq. (4.6), to determine the phosphate binding rates $\hat{\kappa}_{14}$ and $\hat{\kappa}_{26}$. For the chemomechanical cycle $\mathcal{F}$, the balance condition for $F = 0$ leads to

$$\hat{\kappa}_{14} = \frac{\hat{\kappa}_{23}\kappa_{34'}\kappa_{41}\kappa_{12}}{\hat{\kappa}_{21}\kappa_{4'3}\kappa_{32}K_{\mathrm{eq}}}, \tag{4.22}$$

whereas it implies

$$\hat{\kappa}_{26} = \frac{\kappa_{25}\hat{\kappa}_{56}\kappa_{62}}{\hat{\kappa}_{52}\kappa_{65}K_{\mathrm{eq}}}. \tag{4.23}$$

for the enzymatic slip cycle $\mathcal{E}$. It follows directly from these conditions that $\hat{\kappa}_{14} \neq \hat{\kappa}_{26}$. The latter inequality reflects the differences in the chemical transitions $|14\rangle$ and $|26\rangle$. First, the phosphate is released from the leading head during $|14\rangle$ but from the trailing head during $|26\rangle$. Second, the other head is in the D state during $|14\rangle$ but in the E state during $|26\rangle$. Inspection of Eq. (4.22) and (4.23) shows that the rates of phosphate binding in the cycles $\mathcal{F}$ and $\mathcal{E}$, $\hat{\kappa}_{14}$ and $\hat{\kappa}_{26}$, are proportional to each other and satisfy

the relation

$$\hat{\kappa}_{14} = \hat{\kappa}_{26} \, \frac{\kappa_{34'}}{\kappa_{4'3}}. \tag{4.24}$$

The zero-force rates for the mechanical steps, $\kappa_{34'}$ and $\kappa_{4'3}$ describe the motor's tendency to move in the forward or backward direction, respectively. For the forward stepping rate $\kappa_{34'}$, we use a value deduced from simulations [96], and extract the backward stepping rate $\kappa_{4'3}$ by comparison of our calculations with the measurements in [91] using a procedure explained further below. Once the mechanical stepping rates have been determined, the phosphate binding rate $\hat{\kappa}_{14}$ follows from the balance relation (4.22). The force dependence of the transition rates ω_{ij} is contained within the force-dependent factors $\Phi_{ij}(F)$ as defined by Eq. (4.1). These factors satisfy the balance conditions as described in the previous section, and provide constraints on ratios of the factors $\Phi_{ij}(F)$ but do not determine the force-dependence of the individual factors. In addition, the force dependence $\Phi_{ij}(F)$ of the chemical transition rates is, in general, not accessible to experiment. In single headed constructs of myosin V, the force dependence of the binding and dissociation rates of ADP has been investigated [93]. For a single head, the ADP dissociation rate increases for assisting forces and decreases for resisting forces, and the ADP binding rate decreases for both forces. The implications of these latter observations for the behavior of double-headed myosin are not obvious, however, since internal strain may significantly influence the force exerted on the catalytic site of the molecule [54] and reduce this force dependence to some extent. For the force-dependent factors $\Phi_{ij}(F)$ of the chemical rates, we use the parametrization

$$\Phi_{ij}(F) = \frac{1 + \exp(-\chi_{ij} \, \frac{\ell}{k_{\mathrm{B}}T} F')}{1 + \exp(\chi_{ij} \, \frac{\ell}{k_{\mathrm{B}}T} (F - F'))} \tag{4.25}$$

which involves the dimensionless parameter χ_{ij} and the characteristic force F'. The force-dependent factors Φ_{ij} as given by Eq. (4.25) satisfy $\Phi_{ij}(0) = 1$ as required by Eq. (4.1), fulfill the obvious conditions $0 \leq \Phi_{ij}(F) \leq \infty$ for all F, and decay to zero for large resisting loads $F > 0$. For $F' = 0$, the expression (4.25) reduces to the force-dependent factors Φ_{ij} as previously used in [67] to describe the single motor data for kinesin. A nonzero value of F' as introduced here represents a *threshold value* for the load force F. Indeed, this load force needs to exceed the characteristic force F' in order to have an appreciable effect on the chemical transitions.

We find that the available single motor data can be described if *only two* chemical transition rates are taken to be force-dependent, namely the rates of the transitions $|56\rangle$ and $|52\rangle$ for ATP and ADP binding to the leading head. For these two transitions, we chose the parametrization as given by Eq. (4.25) with $F' = 1.6\,\mathrm{pN}$, comparable to the internal strain estimated in [54], and $\chi_{56} = \chi_{52} = 4$. The latter equality is imposed

by the balance condition 4.8 since all other chemical transition rates are taken to be force-independent with $\Phi_{ij}(F) \equiv 1$, see Table 5.2. It is tempting to interpret the force-dependence of the rates for ATP and ADP binding to the leading head in terms of elastic deformations of the motor molecule. Indeed, if the motor is exposed to the load force F, the leading head should experience a larger elastic stress and, thus, a larger deformation compared to the trailing head. If this deformation induced a partial closure of the nucleotide binding pocket of the leading head, binding of both ATP and ADP would be suppressed.

5 Stepping dynamics

5.1 Motor velocity in the absence of load

The stepping velocity of the motor, given by Eq.(4.3), has the general form

$$v = v(F, [\text{ATP}], [\text{ADP}], [\text{P}]), \tag{5.1}$$

i.e., it depends both on the load force F and on the nucleotide concentrations [ATP], [ADP], and [P]. For $F = 0$, the mechanical step cycle $\mathcal{M}$ does not contribute to the stepping velocity. In the limit of vanishing ADP and P, the stepping velocity arises predominantly through the chemomechanical cycles $\mathcal{F}^+$ and the enzymatic slip cycle $\mathcal{E}^+$, while the backward cycles $\mathcal{F}^-$ and $\mathcal{E}^-$ are suppressed. The competition between the two dicycles $\mathcal{F}^+$ and $\mathcal{E}^+$ is governed by the competition of the rates ω_{23} and ω_{25} corresponding to ATP binding by the trailing head and to ADP release from the leading head, respectively. For saturating values of [ATP], the ATP binding rate associated with $\mathcal{F}^+$ is large compared to the ADP release rate of $\mathcal{E}^+$, and the network can be reduced to the forward cycle $\mathcal{F}$ only. For this uni-cycle network, the velocity exhibits the Michaelis-Menten-like behaviour as given by

$$v = \ell \Delta J^{st}_{34'} = \frac{1}{\Omega} \kappa_{41}\kappa_{12}\hat{\kappa}_{23}\kappa_{34'} \left([\text{ATP}] - \frac{[\text{ADP}][\text{P}]}{K_{\text{eq}}} \right) \approx \frac{v_{sat} \cdot [\text{ATP}]}{K_M + [\text{ATP}]}, \tag{5.2}$$

with Ω being a normalization constant that contains terms that are multilinear in [ATP], [ADP] and [P]. Here, K_M is the effective Michaelis constant and v_{sat} the saturation velocity for large ATP concentration, and the second asymptotic equality in (5.2) applies to the limit of small product concentrations, i.e., small [ADP] and [P]. The calculated values for v_{sat} and K_M are presented in Table 5.1, where we have used the transition rates specified in Table 5.3. Using the complete network, we can also calculate the stepping velocity as a function of other control parameters. Fig. 5.1 shows the velocity dependence on one of the nucleotide concentrations [X] with X=ATP, ADP, or P in the absence of load and when keeping the other two concentrations fixed. In general, the experimental choices for the fixed concentrations were taken to be low [ADP] and [P] and saturating [ATP], as shown in the inset of Fig. 5.1. For experiments carried out in the absence of ADP and phosphate, we chose a minimal value of [ADP]=[P]=0.1 μM if not specified differently to account for small amounts of ADP or P that may be

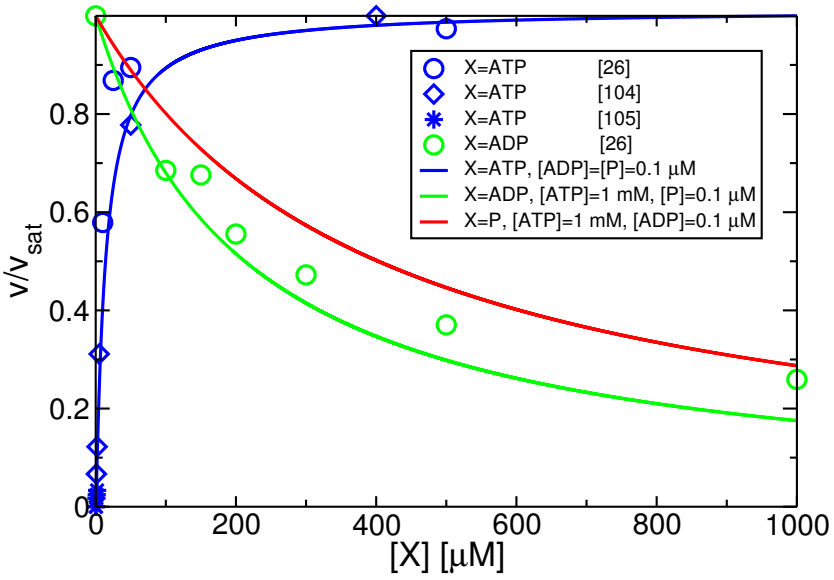

Figure 5.1 : Stepping velocity v/v_{sat} in units of the saturation velocity v_{sat} as a function of different nucleotide concentrations [X] as described in the inset. The experimental data are taken from Refs. [104, 105, 26]. The blue line shows the Michaelis-Menten-like increase in velocity with increasing [ATP], for [ADP]=[P]=0.1 μM, and agrees well with the experimental values measured by different groups (blue symbols). The green line represents the dependence on [ADP] at saturating concentration of ATP, [ATP]=1mM, and low phosphate concentration, [P]=0.1 μM. An increasing [ADP] concentration reduces the stepping velocity, since the flux of the reverse dicycle $\mathcal{F}^-$ increases and, thus reduces the dicycle excess flux $\Delta J(\mathcal{F}^+)$ as described by Eq. (2.21). We have rescaled the velocity by the saturating velocity because different experimental groups have reported different saturation velocities v_{sat}. Indeed, the myosin V construct studied in Ref. [26] was found to exhibit the saturating velocity $v_{sat} = 550$ nm/s, a value considerably higher than the value $v_{sat} = 450$ nm/s measured by other groups [20, 44, 104, 45, 53].

	Experiment	Forward cycle $\mathcal{F}$
v_{sat}	400-500 nm/s [20, 44, 104, 45, 53]	412 nm/s
K_m	12 μM [44]	10.8 μM

Table 5.1: Comparison of saturating velocity v_{sat} and Michaelis constant K_M as determined experimentally in Refs. [20, 44, 104, 45, 53] and calculated via Eq. (5.2) for the reduced uni-cycle network that consists only of the forward cycle $\mathcal{F}$ in Fig. 4.2.

present in experiments without being monitored. The influence of varying this minimal value to up to 1 μM is neglibible, see App. B. As can be inferred from Fig. 5.1, the calculated velocity dependence on [ATP] is in good agreement with the data. Moreover, our model captures the inhibiting effect of ADP on the stepping velocity, as measured in Ref. [26]. Increasing the P concentration, with saturating [ATP] and low [ADP], inhibits the stepping velocity in a way that is comparable to the effect of ADP. This inhibition, however, is leveled out for a higher value of the ATP release rate, which has been fixed to that of myosin II due to lack of experimental information. Increasing the ATP release rate leads of a decrease of the P binding rate as a consequence of the balance condition (4.6), and thus to a weakening of the inhibiting effect on the velocity.

5.2 Motor velocity and step ratio in the presence of load

We now address the dependence of the motor's stepping velocity on force F, where we distinguish two force regimes, below and above the stall force F_s. For assisting forces and resisting forces that do not exceed F_s, the behavior of myosin V qualitatively agrees with the behavior of kinesin [106]. The motor velocity is rather insensitive to assisting forces and does not significantly change compared to the case of zero force [45, 46]. For superstall resisting forces, the step velocity turns out to be essentially independent of the concentration of ATP. Data for the motor velocity as obtained by several experimental groups is shown in Fig. 5.2, where we compare experimental findings with the results of our model calculations. In the network description considered here, the velocity is governed by the competition between the mechanical slip or ratcheting cycle $\mathcal{M}$ and the chemomechanical forward cycle $\mathcal{F}$. This competition is strongly influenced by the binding rate of ATP. It can be understood by inspection of the branching points of the network, corresponding to the states 2 and 5 in Fig. 4.2. For the chemomechanical cycle $\mathcal{F}$ to be dominant, the transition rates ω_{25} and ω_{26} branching off to cycle $\mathcal{M}$ in state 2 have to be small compared to the rates within $\mathcal{F}$. Since the ATP binding rate ω_{23} is large for saturating [ATP], the dicycle $\mathcal{F}^+$ is very robust for large [ATP]. Moreover, the

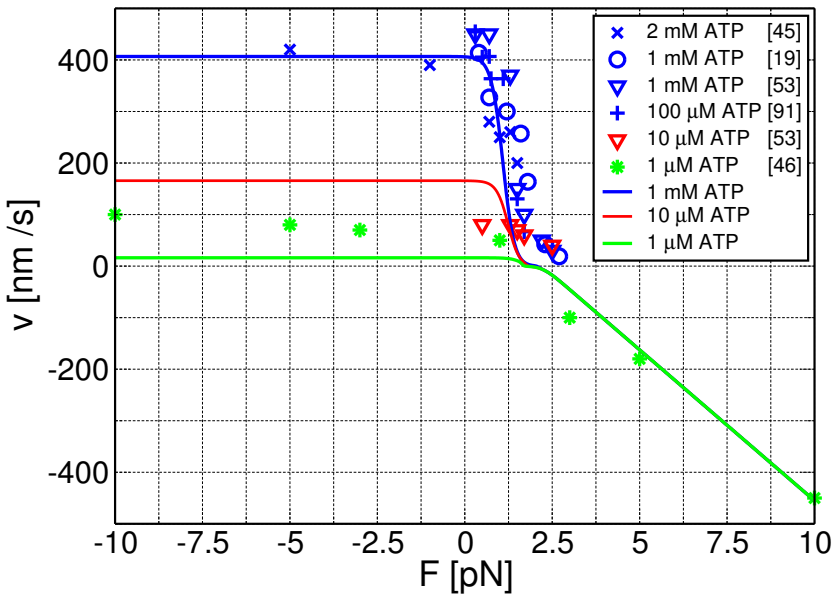

Figure 5.2 : Stepping velocity v as a function of external load force F as calculated from the complete network in Fig. 4.2. We use the sign convention that positive values of F correspond to resisting forces. The full lines represent our theoretical results, the symbols correspond to the experimental data as obtained by several groups [20, 45, 46, 53, 91]. These data were obtained for [ATP]$\geq$ 100 μM (blue symbols), [ATP]= 10 μM (red triangles), and [ATP]= 1 μM (green asterisks). The green, blue, and red lines describe the theoretical results for 1, 10, and 1000 μM ATP, respectively, with [ADP]=[P]=0.1 μM. The theoretical value of the stall force is $F_s \simeq 2$ pN with a weak dependence on [ATP]. This value lies within the range $-1.6\,\mathrm{pN} \lesssim F_s \lesssim 2.5\,\mathrm{pN}$ as found experimentally. For forces $F < F_s$, the motor velocity depends on [ATP], while it becomes independent of [ATP] for $F \gg F_s$, in agreement with the measurements in Ref. [46].

dissipative cycle $\mathcal{E}$ supports this effect: For large [ATP] $\geq$ 15 μM, the rapid rates of ATP binding and P release, $\hat{\kappa}_{56}$[ATP] and κ_{62}, strongly drive the system towards $\mathcal{F}^+$, while the considerably slower rate κ_{25} of ADP dissociation leads from state 2 towards $\mathcal{M}$.

In state 5, the mechanical stepping rates $\omega_{55'}$ for the strongly bound state EE compete with ATP binding. This suggests that the ATP binding rate ω_{56} should decrease with an increasing load force opposing the natural stepping direction of the motor. For switching between the two cycles $\mathcal{F}$ and $\mathcal{M}$, a minimal requirement is that the rates of ATP and ADP binding, ω_{56} and ω_{52}, in the enzymatic slip cycle $\mathcal{E}$ vanish in the limit of large resisting forces. This requirement is fulfilled by the force dependence as given by (4.25) with $F' = 1.6\,\mathrm{pN}$ and $\chi_{56} = \chi_{52} = 4$ as mentioned before. In this way, the other chemical rates need not depend on force, and we set $\chi_{ij} = 0$ for these, as summarized in Table 5.2. The force parametrization of the ADP binding rate takes two experimental observations into account. On the one hand, a decrease of the binding rate for single-headed constructs of Myosin V has been observed as a function of external load [93], but it has been argued, on the other hand, that in double-headed molecules, internal strain weakens this effect for forces up to the stall force [54] which has been incorporated into the parametrization (4.25) via the force scale F'. For forces above stall, i.e., $F > F_s$, the occupation probability in the ratchet cycle rises, and the velocity is given by

$$v \backsimeq \ell \Delta J^{st}_{55'}, \tag{5.3}$$

while for $F < F_s$, we have

$$v \backsimeq \ell \Delta J^{st}_{34'}. \tag{5.4}$$

Fig. 5.2 shows calculations for three different concentrations of ATP, i.e. , for [ATP]=1, 100, and 1000 μM with the concentrations of both ADP and P again fixed to $0.1\mu M$. As for the case of vanishing load force, the velocity depends, up to the stall force, on the concentration of ATP. For superstall forces, this behaviour changes, and the velocity becomes independent of the ATP concentration. For superstall forces, the ratchet or mechanical slip cycle $\mathcal{M}$ determines the behaviour of the step velocity. The velocity increases roughly linearly with force, which reflects the fact that the mechanical transition rates $\omega_{55'}$ and $\omega_{5'5}$, given by Eq. (4.19) and (4.20) are in the regime where the external force exceeds the barrier for performing a step in the EE state. The height of the potential barrier, U_{ba}, and the effective diffusion constant D, are found to be $U_{\mathrm{ba}} = 20\ k_{\mathrm{B}}T$ and $D = 4.7 \cdot 10^2\ (\mathrm{nm})^2/\mathrm{s}$. The parameters that we used for the force dependences are summarized in Table 5.2. A detailed view of the ratchet behaviour is shown in Fig. 5.3, which compares our results with the data of [46]. The step velocity is shown as a function of [ATP] for $F = \pm\ 5$ and $F = \pm 10$ pN. For assisting forces, $F = -5$ and -10 pN, the motor velocity is similar to the force-free case, while the ratchet behaviour is reproduced

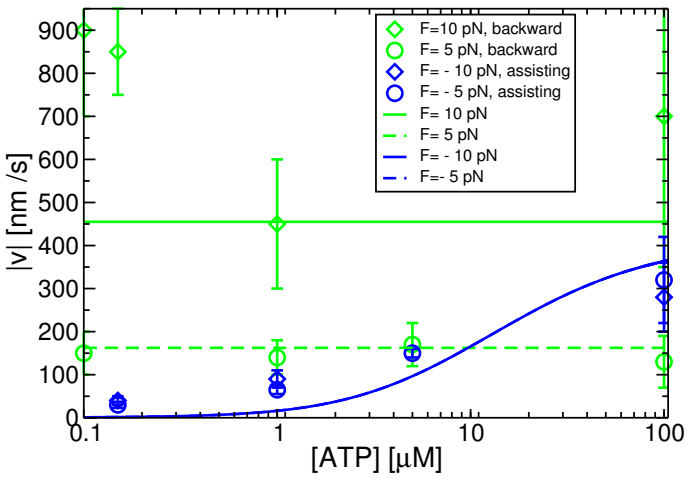

Figure 5.3 : Ratcheting behaviour as measured in [46] (symbols) compared to the theoretical results (lines). The figure shows the absolute value of the motor velocity $|v|$, as a function of [ATP] for superstall forces $F = \pm 5$ and ± 10 pN. The blue symbols and lines correspond to assisting loads, and the green ones to backward loads. The circles are for $F = \pm 5$pN, diamonds for $F = \pm 10$ pN. For backward loads, our theory leads to velocities that do not depend on [ATP]. For 5 pN backward load, the velocity (green dashed line) is in good agreement with the data, while for 10 pN pull, the theoretical velocity is lower than the experimental one. In the case of forward forces, the theoretical velocity matches the data qualitatively. Note that the blue dashed and the solid line are identical. For very low values of [ATP], the calculated velocity is underestimated, which might be due to the fact that [46] report, even in the absence of an external load, considerably higher stepping velocities at low [ATP] compared to other groups [104, 105].

by our model for resisting forces as given by $F = 5$ and 10 pN.

For further extraction of motor parameters, we use the ratio of forward to backward steps, as measured in [91] and shown in Fig. 5.4. The average step ratio q which is defined by the number of forward over the number of backward steps, can be calculated from the network theory via

$$q = \frac{P_3^{st}\omega_{34'} + P_5^{st}\omega_{55'}}{P_{4'}^{st}\omega_{4'3} + P_{5'}^{st}\omega_{5'5}}. \tag{5.5}$$

For the network consisting of the forward cycle $\mathcal{F}$ only and $F < F_s$, the ratio of forward

Force dependence	Transition rate ω_{ij}	Parameter	Value
Fueled stepping	$\omega_{34'},\ \omega_{4'3}$	θ	0.65
Forced stepping	$\omega_{55'},\ \omega_{5'5}$	U_{ba}	20 $k_{\mathrm{B}}T$
		D	$4.7 \cdot 10^2$ nm^2/s
ATP binding and release, $\mathcal{F}$	$\omega_{23},\ \omega_{32}$	$\chi_{23},\ \chi_{32}$	0
ATP binding, $\mathcal{E}$	ω_{56}	$\chi_{56},\ F'$	4, 1.6 pN
ATP release, $\mathcal{E}$	ω_{65}	χ_{65}	0
ADP binding and release, $\mathcal{F}$	$\omega_{12},\ \omega_{21}$	$\chi_{12},\ \chi_{21}$	0
ADP binding, $\mathcal{E}$	ω_{52}	χ_{52}, F'	4, 1.6 pN
ADP release, $\mathcal{E}$	ω_{25}	χ_{25}	0
P binding and release, $\mathcal{F}$	$\omega_{14},\ \omega_{41}$	$\chi_{14},\ \chi_{41}$	0
P binding and release, $\mathcal{E}$	$\omega_{26},\ \omega_{62}$	$\chi_{26},\ \chi_{62}$	0

Table 5.2: Parameters for the force depencence of the mechanical transitions and the ATP binding and release rate. The corresponding functions are specified in the main article.

over backward steps reduces to

$$q = \frac{P_3^{st}\omega_{34'}}{P_{4'}^{st}\omega_{4'3}} \approx 1 + \frac{\omega_{41}}{\omega_{4'3}} \tag{5.6}$$

in the limit of small [P] and [ADP], and using $\kappa_{3'4} \gg \kappa_{4'3}$. Note that, in the case of a single chemomechanical cycle, the stall force is reached only when the hydrolysis rate vanishes, i. e., the motor's chemical action is inhibited. This feature is a shortcoming of all uni-cycle models as first pointed out in [67]. Keeping in mind that the step ratio given by Eq. (5.6) holds for forces well below stall, we use it to determine the backward stepping rate for $F = 0$ to be $\kappa_{4'3} = 0.65\ \mathrm{s}^{-1}$. Moreover, using the exponential force dependence of $\Phi_{4'3}(F)$ as given by Eq. (4.13), we obtain the parameter value $\theta = 0.65$. The transition rates κ_{ij} and $\hat{\kappa}_{ij}$ that have been determined experimentally and through our calculations as well as those obtained from the balance conditions are summarized in Table 5.3.

5.3 Run length

To determine the run length of the motor, we take the DD state as the most probable state for detachment, because the motor spends most of its dwell time between two subsequent steps in this state. The probability of detachment is then given by the probability to be in the state DD, P_1, times an unbinding rate ω_u, which leads to the

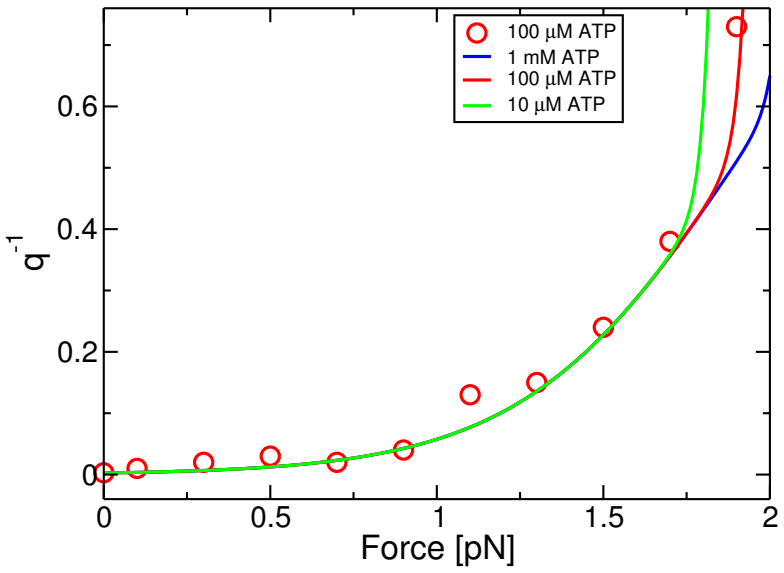

Figure 5.4 : Inverse step ratio q^{-1} of backward to forward steps as a function of load force F. The red, green, and blue lines were calculated using Eq. (5.5) for [ATP]=10, 100, and 1000 μM, respectively, with constant [ADP]=[P]=0.1 μM. For resisting forces that do not exceed F_s, the step ratio is in good agreement with the experimental data (red circles) as obtained in Ref. [91]. Note that this ratio is virtually independent of [ATP] for forces up to 1.6 pN.

run length

$$\Delta x = \frac{v}{P_1 \omega_u}. \tag{5.7}$$

Fig. 5.5 shows the runlength as a function of the nucleotide concentration with an unbinding rate $\omega_u = 0.4\ \mathrm{s}^{-1}$. In [26], the experimentally determined run length does not significantly change with increasing the concentration of ATP. In our theory, the run length increases strongly for small [ATP] and then saturates above [ATP] $\simeq 40\,\mu$M. In contrast, the data in [26] show a monotonic decrease in run length with increasing ADP concentration, which is correctly reproduced by our calculation, see Fig. 5.5. These results have been obtained without the use of any fitting parameter except for the unbinding rate ω_u. Since the motor state with bound ATP is more weakly bound to the filament, one would intuitively expect that unbinding occurs primarily from the states TD and DT. These latter states have, however, a relative low occupation probability, and unbinding from these states does not lead to a run length that decreases with

Rate	$\kappa_{ij},\ \hat{\kappa}_{ij}$	Value	Ref.
ATP binding$^{(\star)}$	$\hat{\kappa}_{23},\ \hat{\kappa}_{56}$	$0.9\ (\mu M\mathrm{s})^{-1}$	[48]
ATP release$^{(\star)}$	$\kappa_{32},\ \kappa_{65}$	$2 \cdot 10^{-5}\ \mathrm{s}^{-1}$	[103]
ADP binding$^{(\star)}$	$\hat{\kappa}_{21},\ \hat{\kappa}_{52}$	$4.5\ (\mu M\mathrm{s})^{-1}$	[44]
ADP release$^{(\star)}$	κ_{12}	$12\ \mathrm{s}^{-1}$	[48]
ADP release$^{(\ddagger)}$	κ_{25}	$1.2\ \mathrm{s}^{-1}$	-
P binding$^{(\dagger)}$	$\hat{\kappa}_{14}$	$0.65\ (\mu M\mathrm{s})^{-1}$	-
	$\hat{\kappa}_{26}$	$6 \cdot 10^{-7}\ (\mu M\mathrm{s})^{-1}$	-
P release$^{(\star)}$	$\kappa_{41},\ \kappa_{62}$	$250\ \mathrm{s}^{-1}$	[48]
Step	$\kappa_{34'}$ $^{(\star\star)}$	$7000\ \mathrm{s}^{-1}$	[96]
	$\kappa_{4'3}$ $^{(\ddagger)}$	$0.65\ \mathrm{s}^{-1}$	-
	$\kappa_{55'}$ $^{(\ddagger)}$, $\kappa_{5'5}$ $^{(\ddagger)}$	$1.5 \cdot 10^{-8}\ \mathrm{s}^{-1}$	-

Table 5.3: Transition rates for the motor network displayed in Fig. 4.2 for $F = 0$, i.e., in the absence of external load. The values have been obtained from experimental data ($\star$), from simulations ($\star\star$), the balance conditions (†), and by comparison of our calculations with the experimental data (‡). The experimental values in Refs. [48] and [44] have been obtained for monomeric and dimeric myosin V, respectively. A significant discrepancy is found between these two myosins for the binding rate of ADP, which was estimated to be $10 - 12\ (\mu M\mathrm{s})^{-1}$ for monomeric myosin V. In Ref. [96], the value for the stepping rate is referred to as the tethered diffusion rate.

increasing ADP concentration as in Fig. 5.5. This unbinding rate is at the lower bound of experimental values reported for single-headed myosin V with and without external load, 1.5 - 20 s^{-1} [101, 55]. For dimeric myosin, a dissociation rate of 0.004 s^{-1} has been reported [48]. For substall forces, we find that in the limit of low concentrations of ADP and P, the run length does not depend on force, which is in agreement with experimental observations [45].

5.4 Aspects of chemomechanical coupling

To characterize the chemomechanical coupling of the motor, let us introduce quantities that address the relationship of chemical and mechanical motor properties. The motor's chemical activity is reflected by the hydrolysis rate h. It is given by the flux through the transitions of the network that involve ATP hydrolysis, $|41\rangle$ and $|62\rangle$,

$$h = \Delta J^{\mathrm{st}}_{41} + \Delta J^{\mathrm{st}}_{62}. \tag{5.8}$$

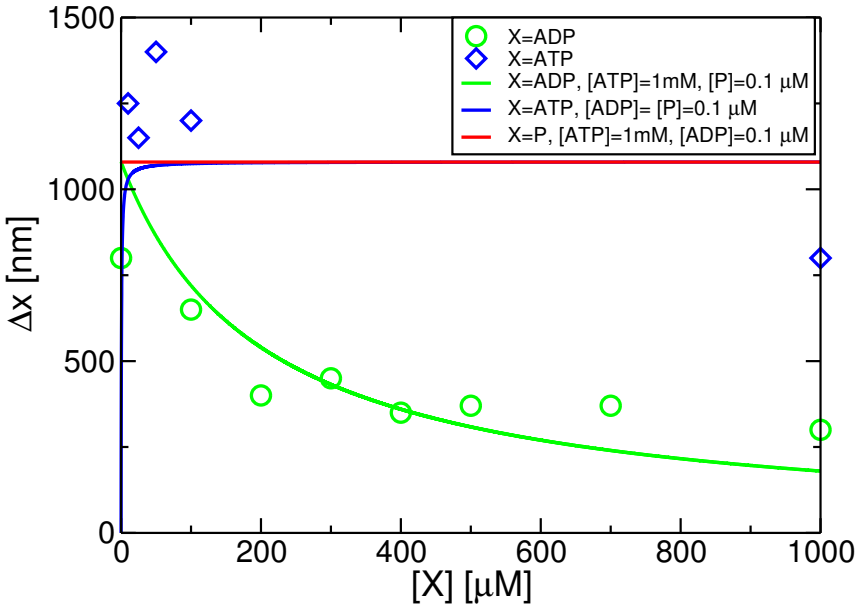

Figure 5.5 : Run length Δx as a function of different nucleotide concentrations [X] as described in the inset. The solid curves were calculated using Equ. (5.7), the symbols represent experimental data from Ref. [26].

As, in our network, the cycles $\mathcal{F}$, $\mathcal{E}$ and $\mathcal{M}$ solely share edges and do not have common transitions, the flux through two edges that belong to the same cycle is identical. Thus, we have $\Delta J^{\rm st}_{41} = \Delta J^{\rm st}_{34'}$, and comparison with $v = \Delta J^{\rm st}_{34'} + \Delta J^{\rm st}_{55'}$ leads, in the case that the fluxes in the cycles $\mathcal{E}$ and $\mathcal{M}$ can be neglected, to a hydrolysis rate that is proportional to the step velocity, $v \simeq h$. This can be easily seen by inspection of the cycle $\mathcal{F}$, where, on average, every forward step leads to the hydrolysis of an ATP molecule. To compare the hydrolysis rate to all steps irrespective of the direction of motion, let us define the total number of steps, $n^{\rm f+b}$, given by

$$n^{\rm f+b} = n^{\rm f} + n^{\rm b} = P_3\omega_{34'} + P_4\omega_{4'3} + P_5\omega_{55'} + P_{5'}\omega_{5'5}. \tag{5.9}$$

It is a measure for the mobility of the motor and illustrates, for instance, whether the application of an external load leads to a decreased velocity through the occurrence of backsteps or the reduction of forward steps. The coupling parameter

$$\lambda = \frac{h}{n^{\rm f+b}} \tag{5.10}$$

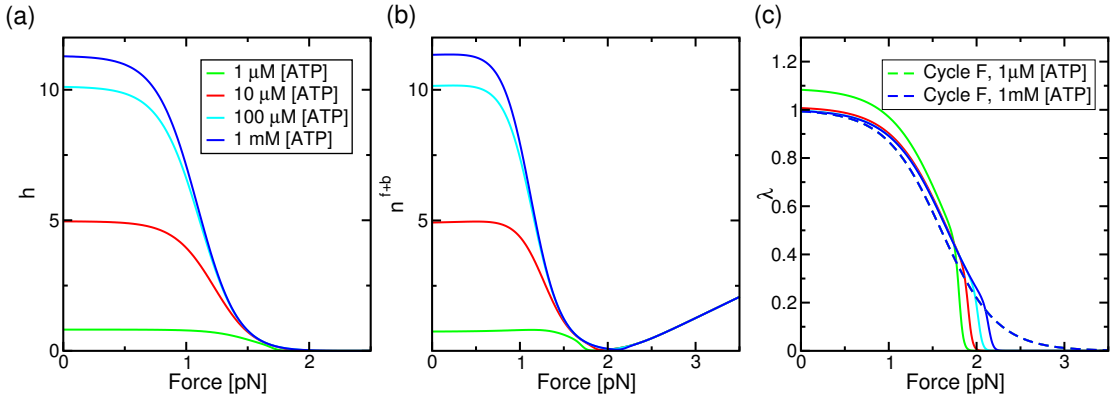

Figure 5.6 : Characterization of the chemomechanical coupling for the network as a function of external load, for different concentrations of ATP in the range of 1-1000 μM. (a) The hydrolysis rate h exhibits, for forces up to F_s, the same qualitative behaviour as the stepping velocity. It rises with increasing [ATP] and decays to zero with an increasing resisting force F. (b) Total number of steps, n^{f+b}, up to F_s, follows the same pattern. It almost vanishes for the stall force, and rises linearly for $F > F_s$ as a sign of forced backward stepping. (c) The coupling parameter $\lambda = h/n^{f+b}$ shows the relationship between hydrolyzed ATP molecules and the total number of steps. For $F = 0$ and [ATP]=1μM, $\lambda \sim 1.1$ as a sign of deviations from tight coupling. For comparison, the coupling parameter for a single cycle $\mathcal{F}$ is shown as a dashed line. It is $\lambda = 1$ for $F = 0$ for all values of [ATP]. For the single cycle, the coupling parameter λ does not depend on [ATP].

relates the hydrolysis rate h to the total number of steps, $n^{\mathrm{f+b}}$. As a consequence, $\lambda = 1$ for the case of tight coupling where every hydrolysis of an ATP molecule actually leads to a step. The influence of dissipative or slip cycles results in $\lambda > 1$. For $\lambda < 1$, there are more steps than hydrolyzed molecules, a situation given when the motor steps by means of a mechanical cycle.

Fig. 5.6 shows the hydrolysis rate h, the total step number $n^{\mathrm{f+b}}$ and the coupling λ of our network as a function of the external force for different concentrations of ATP. For forces up to the stall force, F_s, the qualitative behaviour of both the hydrolysis rate h and the total number of steps n^{f+b} agrees with the velocity v, see panels (a) and (b). For the regime where the external force exceeds stall, $F > F_s$, the hydrolysis rate decays to zero, while the n^{f+b} rises linearly with increasing force. For $F < F_s$, the hydrolysis and the step number are almost identical with the results obtained from the network given by the cycle $\mathcal{F}$. A notable difference occurs in the coupling parameter λ. It is shown in Fig. 5.6 (c), where λ for the network given by the single cycle $\mathcal{F}$ is shown for comparison.

First, the existence of the mechanical cycle $\mathcal{M}$ leads, for small concentrations of ATP, to deviations from tight coupling. Second, the coupling for the complete network decreases more rapidly than the one for $\mathcal{F}$.

The decay of λ in the complete network depends on the parameters that govern the decay of the force function $\Phi_{56}(F)$ and $\Phi_{52}(F)$ for ATP and ADP binding, χ_{56}, χ_{52} and F'. In our calculations, we use $\chi_{56} = \chi_{52} = 4$ and $F' = 1.6$ pN. The variation of these parameters results in slight changes of λ in the regime of F_s. For values of χ_{56} down to $\simeq 1$, the decay of λ and the splitting into is shifted towards higher values of F in an interval of 0.5 pN. For $\chi_{56} < 1$, the superstall step velocity turns [ATP]-dependent. For $F' > 1.6$, the deviations of λ with respect to the single cycle $\mathcal{F}$ set in at higher forces.

The motor efficiency η is a quantity that relates the chemical to the mechanical energy. In the context of a single motor cycle, it is defined as

$$\eta = \frac{Fv}{\Delta\mu}. \tag{5.11}$$

This definition is reasonable for the case where $v \simeq h$, which is strictly fulfilled for a single network cycle only. For networks that contain more than one cycle, can thus define an efficiency that is rescaled by the hydrolysis rate, h, as

$$\eta^h = \frac{Fv}{\Delta\mu h}. \tag{5.12}$$

Fig. 5.7 shows the efficiencies η and η^h as a function of load force, for different values of [ATP]. Both of them exhibit a maximum for a value of $F \neq 0$, which means that the motor has a region of optimal performance that is adjusted to the case of a small resisting load. This property is certainly useful in a cellular environment, where hindrance of the motor's activity is probably a more rule than an exception. The location of the maxima, however, is different, as η reaches is maximum for a value of 1 pN where a rapid decay of the velocity sets in, while the maximum of η^h is located close to the stall force F_s. This is not surprising as in the regime where the system's behaviour is close to that of a single cycle $\mathcal{F}$ only, η^h is rising linearly, because of $v \sim h$, and, as $\Delta\mu$ is fixed through the ATP concentration, the quantity reflects the rising resisting force F. For values of $F > F_s$, the efficiencies turn negative. We do not restrict η to positive values because its turn towards negative values is a sign for the motor's change in direction. The definition of η^h seems reasonable only as long as $\eta^h > 0$, because the hydrolysis rate h decays to zero as F increases and η^h turns singular.

The average quantities discussed here, like the velocity v and the hydrolysis rate h of the motor, depend, in general, on the chemical potential $\Delta\mu$ defined by 4.5 through the product concentrations [ATP], [ADP] and [P] , and the load force F. Let us characterize the balance between the chemical energy $\Delta\mu$ and the external load F specified by the

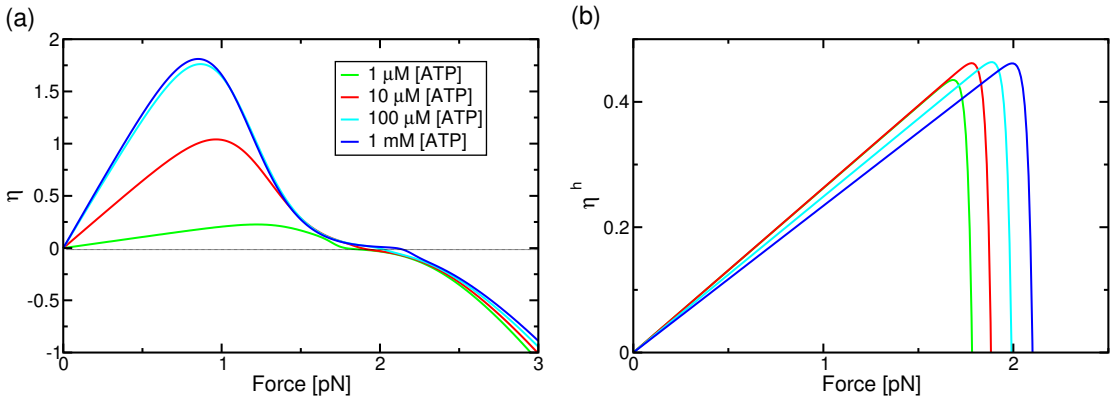

Figure 5.7 : Efficiency η (a) and rescaled efficiency η^h (b) as a function of external force, for [ATP]=1, 10, 100, and 1000μM. (a) The efficiency η exhibits a maximum that shifts towards smaller values of the resisting force F with increasing [ATP]. This is related to the fact that the maximal efficiency is reached before rapid decay of the step velocity sets in. The dashed line separates the negative values for η that are a notion of forced backward stepping. (b) The rescaled efficiency is constant in a regime of force where the velocity is tightly coupled to the hydrolysis rate. As the stall force F_s is approached, rapidly decays to zero as F_s is reached. Note that, as the concentration of ATP rises, there is a shift of the force where $\eta^h = 0$ towards higher values, which corresponds to a variation in F_s with [ATP].

stall condition, i. e., vanishing velocity, $v = 0$. For a single cycle, the relationship between $\Delta\mu$ and F is linear, which can be seen from inspection of $v = 0$. We briefly demonstrate this for the cycle $\mathcal{F}$, where the vanishing velocity leads to

$$v = \ell \Delta J_{34'} = 0, \tag{5.13}$$

which is equal to the condition

$$\omega_{12}\omega_{23}\omega_{34}\omega_{41} = \omega_{21}\omega_{32}\omega_{43}\omega_{14}. \tag{5.14}$$

Using $\omega_{ij} = \omega_{ij,0}\Phi_{ij}(F)$ and rearranging Eq. 5.14 leads to

$$\frac{\Phi_{34}}{\Phi_{43}} = \frac{\kappa_{21}\kappa_{32}\kappa_{43}\kappa_{14}}{\kappa_{12}\kappa_{23}\kappa_{34}\kappa_{41}} \frac{[\mathrm{ADP}][\mathrm{P}]}{[\mathrm{ATP}]} \frac{\Phi_{21}\Phi_{32}\Phi_{14}}{\Phi_{12}\Phi_{23}\Phi_{41}} \tag{5.15}$$

By using the balance conditions 4.6 and 4.7, this results in

$$\exp\left(\frac{\ell}{k_{\mathrm{B}}T}F\right) = K_{\mathrm{eq}}\frac{[\mathrm{ATP}]}{[\mathrm{ADP}][\mathrm{P}]} = \exp\left(\frac{\Delta\mu}{k_{\mathrm{B}}T}\right) \tag{5.16}$$

From the latter equality, one can see that $\ell F = \Delta\mu$, as shown in Fig. 5.8 (dashed line). In previous work, it has been shown that the presence of several chemomechanical cycles has an impact on the relationship between these two quantities [73]. As a consequence of

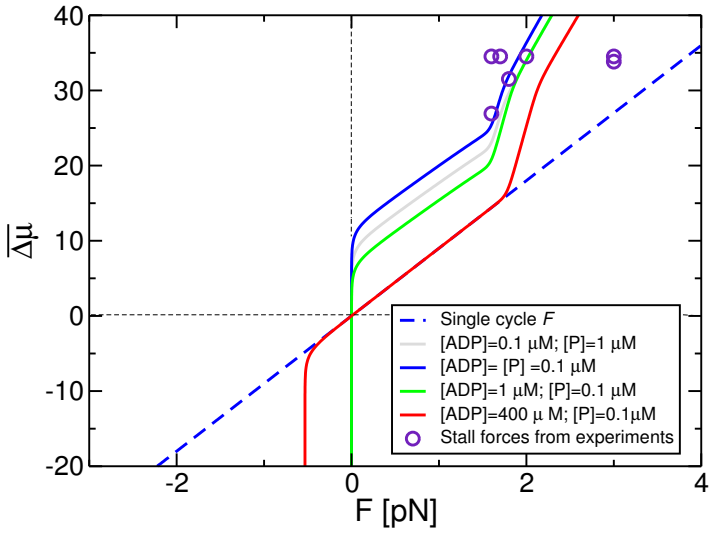

Figure 5.8 : Rescaled chemical potential $\overline{\Delta\mu}$ as a function of external force F for a vanishing velocity, $v = 0$. The solid lines correspond to the complete network, and the dashed line shows the relation 5.16 for a network given by the cycle $\mathcal{F}$. The stall force data determined by different groups [20, 44, 53, 45, 46, 47, 91], are shown as circles. The influence of the cycles $\mathcal{E}$ and $\mathcal{M}$ leads to a decoupling of $\overline{\Delta\mu}$ and F, for small amounts of [ADP] and [P], as shown by the blue, green, and grey lines. Here, for small values of $\overline{\Delta\mu}$, the stall force is zero irrespective of the chemical potential. As [ADP] is increased to 400 μM (red line), the behaviour agrees with the result for a single cycle in the regime of $-0.5 < F < 2$pN. For $F \sim 2$ pN, a regime with increased slope of the curve is reached, which, in turn, leads to a smaller variation of F_{s} in the range of $\overline{\Delta\mu} > 15$ than for the single cycle. Our results lie within the range of the experimental data.

5.16, the stall force F_{s} in a single cycle must vanish as $\Delta\mu$ tends to zero. This is not the case for kinesin, and a model of several chemomechanical cycles leads to a regime where

F_s is independent of $\Delta\mu$, see [72, 73]. As discussed in Appendix B, a clear conclusion about the relationship between $\Delta\mu$ and F based on the data can not be drawn. The model thus contains the single cycle $\mathcal{F}$ that is active for $F \leq F_s$ without the addition of pathways that would couple, for instance, a backward step and hydrolysis in one cycle. Let us turn to the influence of the of the full network, that includes the enzymatic slip cycle $\mathcal{E}$ and the mechanical cycle $\mathcal{M}$ by evaluation of the relation between $\Delta\mu$ and F for $v = 0$, shown in Fig. 5.8. The implicit relation given by the condition $v = 0$ can not be solved analytically, and we thus present a numerical relation here. Fig. 5.8 shows the rescaled chemical potential $\overline{\Delta\mu} = \frac{\Delta\mu}{k_B T}$ as a function of an external load force F for different values of [ADP] and [P], together with experimental data for the stall forces reported by several groups [20, 44, 53, 45, 46, 47, 91], as specified in more detail in App. B. For small resisting forces up to $\simeq 1.5$ pN, the relation is almost linear. For the different concentrations, there is an offset for $F = 0$, i. e., the curve rises rapidly to a minimal value of $\Delta\mu$ before the increase with force sets in. This feature arises from the dissipative cycle $\mathcal{E}$ and is a notion from the deviations from tight coupling, as also seen for the coupling parameter λ. With low concentrations of [ADP] and [P] (blue line), and for forces very close to zero, $F \simeq 0$, the chemical potential rises rapidly such that the motor can be chemically active in the absence of force, which is not the case for tight coupling given by the single cycle $\mathcal{F}$ (blue dashed line). With rising [ADP] and [P] (green, grey and red line), the rise of $\Delta\mu$ and thus the activity of the cycle $\mathcal{E}$ is suppressed. For resisting forces that exceed 1.5 pN, the behaviour of the full network differs considerably from the single cycle $\mathcal{F}$. For all concentrations, the curves enter a regime of an increased slope, which leads to a smaller variation of the corresponding stall forces with increasing $\Delta\mu$ in contrast to the single cycle. This observation is in agreement with the experimental data.

6 Dwell time distributions

The dwell times governing the mechanical displacement between two successive steps of myosin V have been determined experimentally for different nucleotide concentrations and external load forces [44, 45]. In this chapter, we calculate them using the formalism of Markov chains with absorbing boundaries based on a simple scheme related to the network cycle $\mathcal{F}$. It is valid for the motor motion for forces that do not exceed stall, $F < F_s$. For $F > F_s$, the dwell distribution is calculated using the mechanic step cycle $\mathcal{M}$. A comparison with the complete network allows to quantify the gating effect of the motor. In addition, we are able to observe features arising from different *conditional* or co-steps of the motor that agree with results from complex numerical simulations for single-headed myosin V constructs [77]. They contain direct information about the motor's backsteps.

6.1 Reduced network

For the calculation of dwell time distributions that separate two steps of the motor, let us recall the chemomechanical network of myosin V, as shown in Fig. 6.1 (a). A forward step starting at site x corresponds to a positive displacement towards the site $x + \ell$, and a backward step ends at site $x - \ell$, respectively, and the motor can undergo a set of chemical transitions at each location x_i. To distinguish more clearly between forward and backward steps, a state i will be indicated by i'', i, and i' corresponding to its location at sites $x - \ell$, x, and $x + \ell$, respectively. In this way, a transition $|ij'\rangle$ between two states i and j involves a forward step, while a transition $|ij''\rangle$ corresponds to a backward step. Prior to discussing a reduced version of the network shown in Fig. 6.1 (b), let us outline the arguments for the separation of the network cycles in different regimes of force.

Both the chemomecanical cycle $\mathcal{F}$ and the mechanical cycle $\mathcal{M}$ contain mechanical transitions that connect the states DT $\rightleftharpoons$ DT and EE $\rightleftharpoons$ EE. As discussed in chapter 5, stepping arises predominantly by means of the forward cycle $\mathcal{F}$ in the absence of an external load, and governs the motor's motion for forces below the stall force of the motor, $F < F_s$. For high backward forces, $F > F_s$, stepping takes place by means of the mechanical cycle $\mathcal{M}$.

In this chapter, we separate the network into two subsets and consider each of them in the corresponding regime of external load. This separation is justified in a regime of

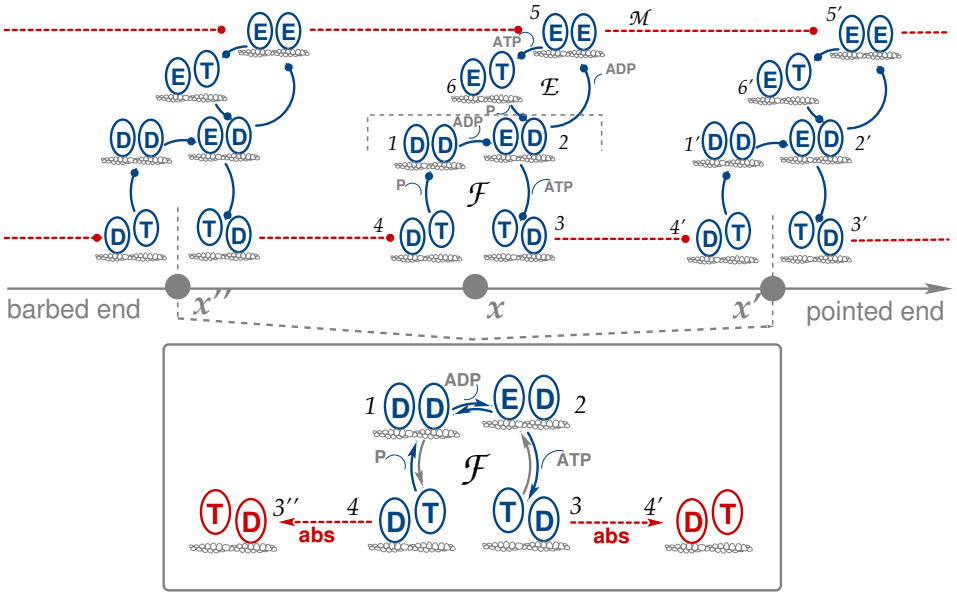

Figure 6.1 : (a) Original form of the network with dots pointing towards the direction of forward stepping or ATP hydrolysis. (b) Network with two absorbing states (red), constructed from the original network consisting of one copy of the chemomechanical cycle $\mathcal{F}$, with absorption into the two neighbouring states $3''$ and $4'$. The arrows indicate the direction of the transition, and transitions with rates $\simeq 0$ are shown in grey. A walk can start in state 3 or 4, which corresponds to a completed backward and a completed forward step, and can be absorbed in either of the two states $3''$ and $4'$. The dwell times separating two steps are thus governed by the sub-processes $44'$, $33''$, $43''$ and $34'$, that correspond to two successive forward steps, two successive backward steps, a backward after a forward step and vice versa.

external load where the cumulative transition probability for a given cycle is $\simeq 1$. Fig. 6.2 shows the cumulative occupation probability in the cycles $\mathcal{F}$ and $\mathcal{M}$, $P^{\rm st}_{\mathcal{F}} = \sum_{i\in\mathcal{F}} P^{\rm st}_i$ and $P^{\rm st}_{\mathcal{M}} = P^{\rm st}_{5'}$, as a function of an external load force F, with a saturating concentration of ATP and limiting concentration of ADP, and P, [ADP]=[P]=0.1 μM. Note that $P^{\rm st}_{\mathcal{F}}$ and $P^{\rm st}_{\mathcal{M}}$ only weakly depend on nucleotide concentrations and the regime of intermediate forces is valid for all concentrations considered in this work. Here, $P^{\rm st}_i$ is the steady state probability of the network shown in Fig. 6.1 (a). For forces below the stall force, $F < F_{\rm s}$, we have $P^{\rm st}_{\mathcal{F}} > P^{\rm st}_{\mathcal{M}}$, and for $F > F_{\rm s}$, the situation is reversed, $P^{\rm st}_{\mathcal{F}} < P^{\rm st}_{\mathcal{M}}$. In an intermediate regime of $F_{\rm s} \pm 0.2$ pN, both cycles are active, while for forces that do not lie withing this range, either one of the cycles completely governs the system. For assisting forces and forces that do not exceed the stall force, $F < F_{\rm s}$, the chemomechanical cycle $\mathcal{F}$ governs the stepping process, while for high resisting forces $F \gg F_{\rm s}$, the forced stepping takes place by means of the mechanic cycle $\mathcal{M}$. This separation of network

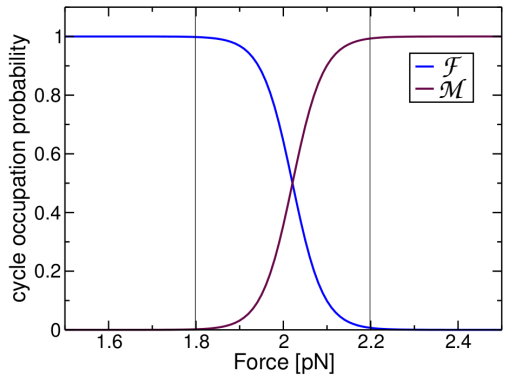

Figure 6.2 : Occupation probabilities $P^{\rm st}_{\mathcal{F}}$ and $P^{\rm st}_{\mathcal{M}}$ of the network cycles $\mathcal{F}$ and $\mathcal{M}$ for [ATP]=2 mM and [ADP]=[P]=0.1 μM. The chemomechanical cycle $\mathcal{F}$ dominates for forces below and the mechanical cycle $\mathcal{M}$ for forces above the stall force, $F_{\rm s} = 2$ pN. In a transition regime of $1.8 \leq F \leq 2.2$ pN, indicated by the horizontal lines, both cycles influence the system, while only one cycle is active for forces that are outside of this range.

cycles allows for determination of the networks with absorbing states related to the cycles $\mathcal{F}$ and $\mathcal{M}$. They correspond to the different trajectories between states of the motor that are *directly* connected to a mechanical transition in the two network cycles. One consists of the states that belong to the chemomechanical cycle $\mathcal{F}$, with the neighbouring states $3''$ and $4'$ being absorbing, as shown in Fig. 6.1 (b), and the other one is given by state 5, with the neighbouring states $5''$ and $5'$.

The dwell times between successive steps can arise from two different trajectories on

these networks. The dwell time of the motor starts just after a step has been completed, i. e., it has an initial state that is directly linked to a mechanical transition. One possible starting state for a dwell trajectory is DT, as it is reached directly after a forward step. Starting from this state, the subsequent possible mechanical displacements that can be observed are given by either a direct backward step through the transition $|43''\rangle$ or the trajectory $|41234'\rangle$ that leads to a forward step. Likewise, the pathways including a mechanical transition when starting in the state TD are given by either a direct forward step $|34'\rangle$ or a backward step following the trajectory $|32143''\rangle$. For the state EE as an initial state, there are always two possibilities of a direct mechanical transition, in either a backward $|55''\rangle$ or a forward direction $|55'\rangle$.

The dwell time between two neighbouring sites x and $x \pm \ell$ is thus governed by the distribution for completing a step after starting in either of the states 3 or 4 and ending up in either $3''$ or $4'$ for forces $F < F_{\mathrm{s}}$, and for starting in 5 and ending up in $5'$ or $5''$ for high resisting forces, respectively. A Markov process corresponding to the absorbing network in Fig. 6.1 (b) can now start in state 4 and sojourn a time τ_i in every state i, until it eventually reaches state $4'$, where it is being absorbed after taking a forward step. The distribution of dwell times between two successive forward steps is then given by the probability distribution for a random walk that starts in state 4 and is absorbed in state $4'$. Correspondingly, two successive backward steps are given by a walk starting in 3 and ending up in $3''$.

We use the network in Fig. 6.1 (b) as well as the one that consists of the state EE with two absorbing states to test for the agreement with experimentally determined dwell time distributions. The advantage of the network related to the cycle $\mathcal{F}$ is that it contains only the parameter θ for the force dependence of the step rate. For the full version of the network, we determine the distribution of dwell times from a simulation using the Gillespie algorithm [107]. The details of the simulation are given in App. C. In the next section, we will discuss the conditional distributions of dwell times associated with the reduced network.

6.2 Conditional dwell time distributions

The overall dwell time distribution consists of several distributions arising from different pathways that describe the conditional steps of the motor. The four possible walks for the network shown in Fig. 6.1 refer to transitions connecting two subsequent forward or backward steps, $|34'\rangle$ and $|43''\rangle$, or a backward following a forward step and vice versa, $|33''\rangle$ and $|44'\rangle$.

The transition rates ω_{ij} that occur in the reduced network shown in Fig. 6.1 are partly accessible to experiment, or fixed by balance conditions that, as a consequence of the laws of thermodynamics, emerge for every cycle of the chemomechanical network, as discussed in section 2.4. Inspection of Table 5.3 shows that in the chemomechanical

Absorbing network rates	ω_{ij}	Value	Ref.
ATP binding$^{(\star)}$	ω_{23}	$0.9{\cdot}[\mathrm{ATP}](\mu M\mathrm{s})^{-1}$	[108]
ATP release$^{(\dagger)}$	ω_{32}	0	-
ADP binding$^{(\star)}$	ω_{21}	$4.5{\cdot}[\mathrm{ADP}](\mu M\mathrm{s})^{-1}$	[44]
ADP release$^{(\star)}$	ω_{12}	$12\ \mathrm{s}^{-1}$	[48]
P binding$^{(\dagger)}$	ω_{14}	0	-
P release$^{(\star)}$	$\omega_{41},\ \omega_{62}$	$250\ \mathrm{s}^{-1}$	[48]
Step	$\omega_{34'}$ $^{(\star\star)}$	$7000\exp(-0.65\frac{\ell}{k_\mathrm{B}T}F)\ \mathrm{s}^{-1}$	[96]
	$\omega_{43''}$ $^{(\ddagger)}$	$0.65\exp(0.35\frac{\ell}{k_\mathrm{B}T}F)\ \mathrm{s}^{-1}$	-

Table 6.1: Transition rates ω_{ij} for the network with absorbing boundaries related to the cycle $\mathcal{F}$. The values for $F = 0$ have been obtained from experimental data ($\star$), from simulations ($\star\star$), balance conditions ($\dagger$), and the calculations discussed in chapter 4 ($\ddagger$). For the stepping rates, we use the force dependence obtained in 4.

cycle $\mathcal{F}$, the rates for ATP dissociation and P binding in the case of [P]$\simeq 0$, are very small, $\omega_{23} \simeq \omega_{14} \simeq 0$. The absence of phosphate agrees with the experimental conditions for the data used here [45]. For simplification, we set these rates to zero in our calculations. As a consequence, the possibility of two subsequent backward steps given by the transition $|33''\rangle$ vanishes. The transition rates which remain unchanged with respect to the complete network and occur in the absorbing network are summarized in Table 6.1 to illustrate that all chemical rates are taken from experiment, and the only force-dependent rates are the stepping rates $\omega_{34'}$ and $\omega_{43''}$.

The steady state probabilities, as given by Eq. 2.65 read, for the forward cycle $\mathcal{F}$,

$$P^{\mathrm{st}}_{44'} = \frac{\omega_{41}}{\omega_{41}+\omega_{43}} \tag{6.1}$$

$$P^{\mathrm{st}}_{34'} = 1 \tag{6.2}$$

$$P^{\mathrm{st}}_{43''} = \frac{\omega_{43}}{\omega_{41}+\omega_{43}} \tag{6.3}$$

$$P^{\mathrm{st}}_{33''} = 0. \tag{6.4}$$

They can be used to define a new Markov chain that refers to the sequence of forward and backward steps, as carried out explicitly in [76]. The latter process has a steady state that refers to the probability of taking a forward or a backward step, respectively,

which is given by the probabilities

$$\pi_f^{\rm st} = \frac{P_{34'}^{\rm st}}{P_{34'}^{\rm st} + P_{43''}^{\rm st}} \tag{6.5}$$

$$\pi_b^{\rm st} = \frac{P_{43''}^{\rm st}}{P_{34'}^{\rm st} + P_{43''}^{\rm st}}. \tag{6.6}$$

As shown in [76], average quantities of the motor like the ratio of forward and backward steps

$$q = \frac{\pi_f^{\rm st}}{\pi_b^{\rm st}} = \frac{\omega_{41} + \omega_{43}}{\omega_{43}} \tag{6.7}$$

can be expressed using these probabilities. With the use of Eqs. 2.64 and 2.65, the dwell time distributions for the four co-steps can be explicitly calculated and compared to the experimental data in [44, 45].

The distributions for forward and backward steps, $\rho_f^{\rm abs}(t)$ and $\rho_b^{\rm abs}(t)$, read

$$\rho_f^{\rm abs}(t) = \dot{P}_{44'}(t) + q^{-1}\dot{P}_{34'}(t) \tag{6.8}$$

$$\rho_b^{\rm abs}(t) = q\dot{P}_{43''}(t) \tag{6.9}$$

with the overall distribution $\rho^{\rm abs}(t) = \rho_f^{\rm abs}(t) + \rho_b^{\rm abs}(t)$. The full analytical form of the distributions is given in App. D.

The dwell time distribution in itself is given by a sum of weighted exponentials with the eigenvalues λ_i as decay rates. The tail of the dwell time distribution thus is governed by the smallest eigenvalue $\lambda^{\rm min} = \min(\lambda_i)$ [61]. The eigenvalues for the network $\mathcal{F}$ read

$$\lambda_{1,2} = \frac{1}{2}\left(\omega_{12} + \omega_{21} + \omega_{23} \pm \sqrt{(-\omega_{12} - \omega_{21} - \omega_{23})^2 - 4\omega_{12}\omega_{23}}\right) \tag{6.10}$$

$$\lambda_3 = \omega_{34} \tag{6.11}$$

$$\lambda_4 = \omega_{41} + \omega_{43} \tag{6.12}$$

Let us outline those external conditions where the minimal eigenvalue can directly been assigned to a given chemical rate. In the case of [ADP]$\simeq 0$, the first two eigenvalues reduce to $\lambda_1 = \omega_{23}$ and $\lambda_2 = \omega_{12}$. The eigenvalues $\lambda_{1,2}$ do not depend on an external load force, while $\lambda_{3,4}$ contain force-dependent forward and backward stepping rates. For a resisting force $F > 0$, the decrease of the stepping rate will contribute to the tail of the distribution, once ω_{34} reaches the order of ω_{12} in the case of saturating ATP and a low concentration of ADP. For $F = 1.1$ pN, we have $\omega_{34} \approx \omega_{12}$, i. e., in this regime of force the forward stepping rate will turn limiting to the motor's motion.

6.3 Absence of load: the gating effect

Fig. 6.3 shows the total distribution of dwell times, $\rho^{\text{abs}}(t)$, for $F = 0$ and different nucleotide concentrations using the transition rates shown in Table 6.1 and the experimental data from [44]. In order to compare our results with the experimentally determined distributions reported in [44, 45], we have rescaled the experimental data such that the area covered by the histogram is normalized.

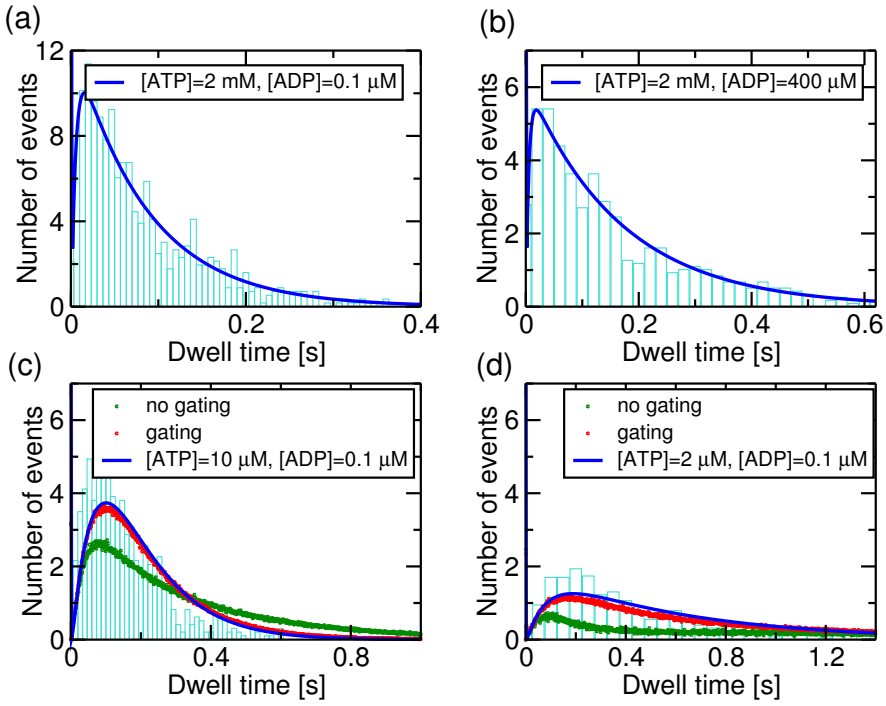

Figure 6.3 : Dwell time distributions calculated from the cycle $\mathcal{F}$ for different nucleotide concentrations shown as solid lines (blue), and the corresponding experimental data (cyan bars) taken from [45], with distributions and data normalized for comparison. If not indicated differently, experiments are performed in the absence of ADP and P, and in the calculations we set [ADP]=0.1 μM and [P]=0 μM (see text). (a) Dwell time distribution for saturating ATP concentration, [ATP]=2 mM. (b) For 400 μM of ADP and 2 mM of ATP, the distribution broadens and thus indicates the inhibiting effect of ADP on the stepping velocity. (c, d) Limiting amount of ATP, 10 and 2 μM. The symbols show simulated data without a gating (green dots) and gating with a 10-fold decelerated ADP release from the motor's leading head (red dots).

As the histogram shows the actual stepping events rather than a distribution, this procedure is justified if the histogram bins are sufficiently small, which is the case for

the data in [44, 45], where each histogram consists of more than one hundred events. For $F = 0$ and [ATP]=$2mM$, and [ADP]$\simeq 0$ (Fig. 6.3 a), our results are in good agreement with the data. We have $\lambda^{\min} = \omega_{12} = 12\text{s}^{-1}$, and the tail of the distribution thus reflects the rate of ADP release. With the addition of ADP, the distribution broadens significantly, which reflects the inhibiting effect of ADP on the motor's motion, a fact that is experimentally well established [108, 26, 53].

For a limiting amount of ATP (Fig. 6.3 c, d), the step velocity is, in case of the absence of [ADP] and $\omega_{34}/\omega_{43} \gg 1$, governed by the rate of ATP binding. Note that there is a minor discrepancy between the theoretical curve and the experimental values, that arises from the experimental uncertainty for the rate of ATP binding, ω_{23}. The rate constant $\hat{\kappa}_{23}$ $(\mu M\text{s})^{-1}$ used throughout this work has been determined in the presence of actin, i. e., for the actomyosin complex. Increasing this rate to 1.9 $(\mu M\text{s})^{-1}$, the one given in the absence of actin, i. e., for myosin only [48], leads to a better agreement of the distribution and the data. However, this rate would result in a Michaelis constant K_M that is contrary to the experimental value.

From comparison with simulations for the complete network, Fig. 6.1 (a), we can, in addition, quantify the gating effect. For low [ATP], the ATP binding transition $|23\rangle$ competes with the transition for ADP release from the front head, $|25\rangle$. Neglecting the gating effect by assuming equal rates of ADP release for both heads leads to discrepancies between the experimental data and the calculations (green dots). These vanish for a gating with $\xi = \omega_{12}/\omega_{25} \geq 10$ (red dots), which sets the upper level for the gating effect in agreement with the experimental observations [54, 92]. Let us point out here that all theoretical curves show a steep peak for dwell times ≤ 0.01 s, which is beyond the time resolution of the experimental setup and is barely seen in Fig. 6.3. These refer to rapid events and will be discussed in more detail in the context of an external force.

6.4 Presence of load: backward stepping

Let us consider the behaviour of the distributions subject to external load. For assisting forces, the motor's motion remains unaltered, while for resisting forces that exceed the stall force, it acts as a mechanical ratchet by means of forced stepping through the mechanical cycle $\mathcal{M}$. Fig. 6.4 shows the dwell distributions for different regimes of external load, for $F = -5$ and $F = 1$ pN, where the forward stepping cycle $\mathcal{F}$ governs the stepping behaviour, and $F = 5$ pN, where the mechanical cycle $\mathcal{M}$ is dominant to the motor's motion.

With the presence of an external load, the distributions change through the force-dependent forward and backward stepping rates ω_{34} and ω_{43} with the force factor $\theta = 0.65$. The eigenvalues $\lambda_{1,2}$ do not depend on an external load force, while $\lambda_{3,4}$ contain the stepping rates ω_{34} and ω_{43}. For a resisting force $F > 0$, the decrease of the stepping rate will contribute to the tail of the distribution, once ω_{34} reaches the order of ω_{12} in

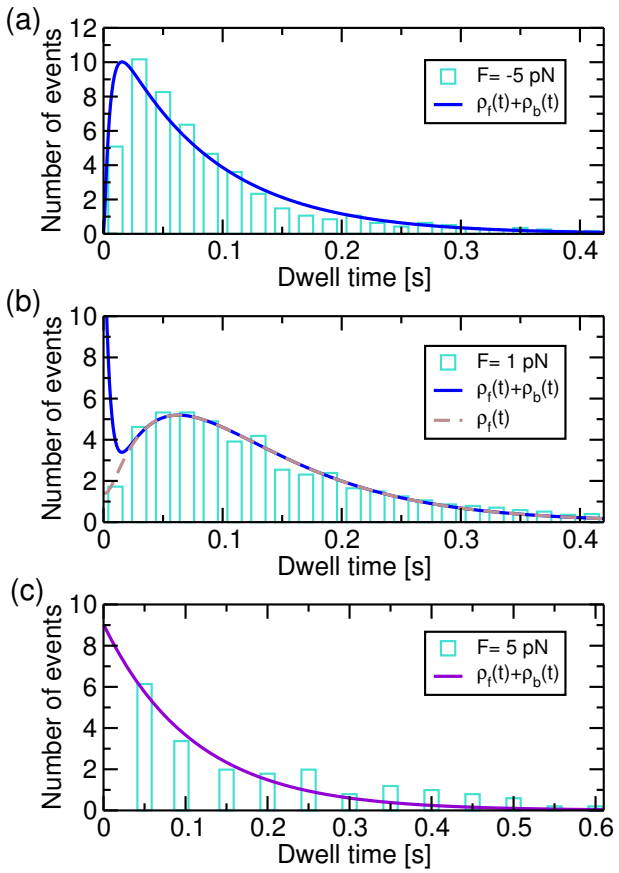

Figure 6.4 : Dwell time distributions for assisting, substall resisting and superstall load forces, $F = -5$ pN (a), $F = 1$ pN (b) and $F = 5$ pN (c) for 2 mM [ATP], 0.1 μM [ADP] and zero phosphate. The bars show the experimental data taken from [45], and the lines show the distributions obtained using the single network cycles $\mathcal{F}$ for $F \leq F_s$ (a and b, blue) and $\mathcal{M}$ for $F \geq F_s$ (c, magenta). As before, the data and the distributions have been normalized. (a) For $F = -5$ pN, the dwell distribution is virtually identical with the one for $F = 0$, indicating that an external assisting load does not alter the motor's chemomechanical stepping mechanism, and the distribution of dwell times is captured by the forward stepping cycle $\mathcal{F}$. (b) For $F = 1$ pN, the overall distribution of dwell times (solid line) shows a significant peak for dwell times up to 0.02 s, indicating the presence of backward steps. In the distribution of forward steps (dashed line), this peak is absent, and the distribution agrees with the data, which indicates that the experimental evaluation might lack events associated with backward steps. (c) For $F = 5$ pN, the distribution of dwell times follows a single exponential function (magenta line) as a result of the purely mechanical motion arising in the mechanical cycle $\mathcal{M}$. In the experiment, the result has been fitted with a single exponential decay, although a decay of the function for small dwell times and thus the existence of further limiting states can not be ruled out.

the case of saturating ATP and a low concentration of ADP.

For $F = -5$ pN (a), we find a good agreement between our results and the experimental data. This consolidates the fact that for assisting forces, the stepping behaviour is virtually unaltered with respect to $F = 0$, as discussed in [45]. All the theoretical curves show a steep decay of rapid events for short times ≤ 0.01 s, the time resolution of the experimental setup [45]. Yet, they occur in simulations for single-headed myosin V constructs [77]. These events turn to larger dwell times for with an increasing resisting force. For a force of $F = 1$ pN (b), they exceed the experimental resolution of 0.01 s (blue line). The maximum at short times stems from the distribution of backward steps, $\rho_b(t)$, and reflects the decrease of the forward stepping rate ω_{34}. The experimental data, however, agree with the distribution of forward steps, $\rho_f(t)$ (brown line). The amount of backward stepping events in [45] might have been insufficient to capture the behaviour of $\rho_b(t)$. On the other hand, these fast events directly refer to the forward stepping rate,

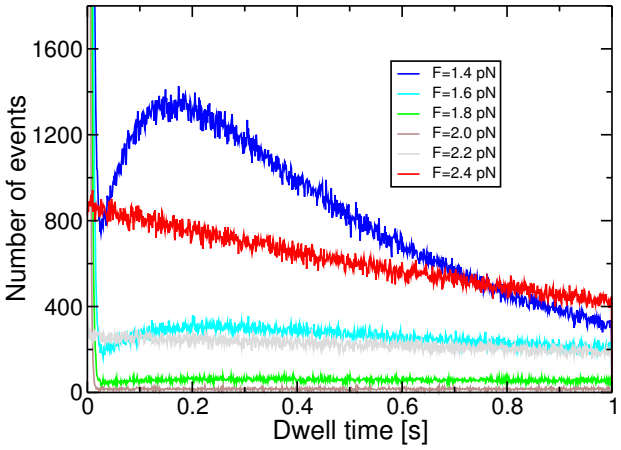

Figure 6.5 : Dwell time distributions for forces that cover the intermediate regime 1.8 pN $< F <$ 2.2 pN, in a range of $F = -1.4$ pN to $F = 2.4$ pN, in steps of 0.2 pN, simulated using the complete network from Fig. 4.2. The nucleotide conditions have been fixed to [ATP]=2 mM, [ADP]=[P]=0.1 μM. The shape of the distribution resembles, for 1.4 and 1.6 pN, the shape of the distributions for forces that are below these values. The distribution broadens as approaching a vanishing step velocity of the motor at the stall force $F_s \simeq 2$ pN, where the sharp peak of short events vanishes and turns into a single exponential distribution, whose slope rises with increasing the load force, as seen for $F = 2.2$ and $F = 2.4$ pN. Note that the simulation is based on $\approx 10^6$ events.

that might be affected by a more complex mechanism, like the reversal of the motor's

power stroke [55]. For high resisting forces, the mechanical cycle $\mathcal{M}$ is dominant to the motor's motion. The motor steps in a forced manner, and as the forward stepping rate $\omega_{55'} \simeq 0$ in this regime, the dwell time distribution reduces to an exponential distribution with the rate $\omega_{55''}$ for $F = 5$ pN, as shown in Fig. 6.4 (c). It agrees with the experimental data, although a decay of the distribution for short times and thus the existence of a 'hidden' state can not be ruled out.

In the regime of intermediate forces, the dwell time distributions are given by an overlap of the two cycles $\mathcal{F}$ and $\mathcal{M}$, as shown in Fig. 6.5. From the simulations, we find a smooth transition in a region of 0.2 pN around the stall force. This switching is a feature specific to our parametrization that exhibits a smooth transition restricted to a rather narrow regime of force, i.e., between $F = 2.0$ and $F = 2.2$ pN, where the peak of rapid events vanishes and the distribution turns into a single exponential function. With an increasing force up to the stall force F_{s}, the broadening of the distribution is a signature of the decaying step velocity, and its rise for $F > F_{\mathrm{s}}$ is a notion of its increase. To further characterize the switching between the two step cycles in more detail, it would be interesting to investigate the regime of this transition around the stall force in more detail. The observation of two distinct types of distributions would consolidate the network property that the ratchet behaviour of the motor is driven by a fundamentally different process than the usual enzymatic step cycle of the motor.

7 Summary and further perspectives

7.1 Chemical kinetics of myosin V

We have studied the stepping properties of the molecular motor myosin V as a function of nucleotide concentration and external load in a quantitative way. Using a relatively simple network, we have described the motor's motion for forces both below and above the stall force. A network description that includes one main catalytic cycle reproduces both the step velocity and the run length as a function of nucleotide concentration in quantitative agreement with experimental findings, as shown in Figs. 5.1 and 5.5. The latter result for the runlength does not depend on any fitting parameters except for the unbinding rate ω_u.

The motor's motion as a function of external load force is governed by the force dependence of the mechanical stepping rates below stall, whereas the chemical transition rates do not significantly depend on force in this regime. As can be infered from the ratio of forward to backward steps, see Fig. 5.4, the occurrence of backward steps at substall forces can be explained by an increasing ratio of the backward to forward stepping rate in the single step cycle $\mathcal{F}$ which arises from the decreasing probability of forward stepping. This motor property of myosin V differs from the corresponding one of kinesin, for which another chemomechanical cycle acts to increase the probability for backward steps.

For backward forces that exceed the stall force, our network description captures the ratcheting behaviour of the motor, as shown in Fig. 5.2. The forced backward stepping arises from the mechanical cycle $\mathcal{M}$ with step rates that have been derived using a discretized version of the Fokker-Planck-equation, see Eq. (4.19) and (4.20).

Switching the operation mode of the motor from the chemomechanical cycle $\mathcal{F}$ to the mechanical ratchet cycle $\mathcal{M}$ for large load forces F should be useful if myosin V and kinesin are attached to the same intracellular cargo particle as observed experimentally in [109] and considered theoretically in [110]. In these latter studies, the myosins and kinesins moved along the same filament. If the myosins are in contact with actin filaments whereas the kinesins move along microtubules as discussed, e. g., in [111], the switching from the chemomechanical cycle $\mathcal{F}$ to the mechanical ratchet cycle $\mathcal{M}$ allows the myosins to stay in touch with the actin filaments even if the kinesins pull in the opposite direction and generate forces of the order of their stall force, which is about 7 pN.

The competition between the chemomechanical cycle $\mathcal{F}$ and the mechanical cycle $\mathcal{M}$ essentially depends on the binding rates of ATP and ADP in the enzymatic cycle $\mathcal{E}$.

Both rates decrease for a high load force, while the other chemical rates need not depend on force. For substall forces, the force dependence of ADP binding and release as well as of ATP binding is believed to be weak for dimeric myosin V [54, 55, 101]. The decrease of the binding rates for superstall forces could arise from a deformation of the molecule. For this regime, an inhibition of the powerstroke of myosin V has been observed, which can lead to the decline of its catalytic function. A possible mechanism is provided by a partial closure of the nucleotide binding pocket of the leading head, when the motor molecule experiences superstall load forces. It remains to be seen if such a molecular mechanism can be corroborated by further experimental studies.

7.2 Dwell time distributions

We have calculated the dwell time distributions of the molecular motor myosin V by splitting our network description into single motor cycles that are dominant in different regimes of an external force. For a range of 0.2 pN around the stall force, an intermediate regime arises where both cycles compete with each other. For forces below this regime, the dwell time distributions can be determined using a network with two absorbing boundaries as shown in Fig. 6.1, and can be separated into the distributions of forward and backward steps. We quantify the intermediate regime using a Gillespie algorithm, and use the mechanical cycle $\mathcal{M}$ to determine the dwell times for forces that exceed stall.

For the distributions obtained for $F = 0$ and different nucleotide conditions, shown in Fig. 6.3, we find good agreement with the experimental data. In addition, we are able to quantify the gating effect that is thought to be the primary cause for the molecule's coordination of heads. At low concentrations of ATP, the simulation results for the complete network agree with the data as well as the analytical distribution for the cycle $\mathcal{F}$ choosing an ADP release rate from the leading head that is 1/10 of the value for the trailing head.

In the presence of load, we compare the data with the distributions arising from the cycles $\mathcal{F}$ and $\mathcal{M}$. For superstall forces, the distribution is governed by a single exponential decay, while it is multi-exponential for the cycle $\mathcal{F}$. All distributions calculated using the cycle $\mathcal{F}$ exhibit a peak that refers to fast events, which broadens in the presence of a resisting force. It can be associated with the distribution of backward steps, and has not been observed experimentally. For small resisting load forces, the experimental data agree with the distribution of forward steps rather than with the full distribution, which may be due to the lack of data for backward stepping, as indicated in Fig. 6.4. For the intermediate regime, we have used a simulation algorithm to examine the transition between the two cycles $\mathcal{F}$ and $\mathcal{M}$. We find that the transition regime is given by the overlap of the two distributions, which is a notion of effective switching between these cycles.

The simple chemomechanical model serves as an interpolation between the use of a simple two-state model, that cannot be a priori connected to experimental transition rates, and simulations that are based on very complex kinetic schemes, but rely on a number of fit parameters. We observe the same characteristic behaviour of the distribution of dwell times that has been calculated to fit distributions of single-headed myosin V, [77, 101], with a rapidly decaying peak for small dwell times, followed by a broader peak for intermediate dwell times. This reinforces the hypothesis that the behaviour of the stepping motor is based, for forces up to the stall force, on a single chemomechanical cycle, which is coordinated by the force-dependent release of ADP.

7.3 Power stroke and collective behaviour of molecular motors

In the past months, fundamental experimental progress has been achieved in characterizing the power stroke of myosin V. The influence of the lever arm on the ADP release rate from the trailing and the leading head through its strain-dependence has been investigated in [36]. The direct observation of the molecule's telemark configuration a few years ago [112] has been taken to a new level through video imaging using rapid atomic force microscopy, supporting a study of the force generation through conformational changes at the actin binding site that has been carried out with FRET [50]. It would be interesting to address, from a theoretical point of view, the question how this power stroke affects the stepping mechanism of the molecule, like, for instance, its substeps. These have been addressed in numerous experiments [53, 47, 54, 55, 56] but with different conclusions with respect to substep sizes. An instructive, albeit slightly outdated comment on the topic is given in [113]. In a study with exceptionally high resolution [47], the effect of [ATP] on three substeps of the myosin V has been observed, the first of which has a duration that depends on the concentration of ATP. This step is associated with a power stroke conformation of the motor: It is thought that upon binding of and ATP molecule, a conformational change is discussed to induce the prestroke position of the motor, and weaken the binding affinity of the trailing head. A theoretical analysis should certainly establish a connection of this step with the study of the power stroke and its reversal [55].

A further aspect that needs to be clarified is the detailed mechanism of a backward step, and how it is influenced by the power stroke and its eventual reversal. The mechanism of the forward step is given by a combination of the stroke and a diffusion [52, 96], but what is the nature of the mechanism that governs in backward step? Is it a direct reversal of the forward step or is it enabled only in the case the power stroke is inhibited? The quantitative discussion of these issues can lead to a better understanding of the details of the myosin's step in itself.

Finally, let us turn the focus from small, sub-step length scales, to those exceeding the motor's step size where the collective behaviour of molecular motors starts to play a role. An interesting feature that is specific to the myosin V is the ratcheting mechanism. What benefit could it have for the motor traffic of both single and interacting molecular motors? To elucidate the consequence of the ratcheting mechanism, it would be interesting to test tug-of-war scenarios between myosin V and VI, a motor moving into the opposite direction of the actin filament. A stochastic tug-of-war for motors that are attached to the same cargo, but move in different directions can result in directed transport, as demonstrated in [114]. Kinesin has a stall force of 7 pN and thus can exert load forces that are in the superstall regime of the myosin V. If both a kinesin and a myosin V motor are attached to the same cargo, the myosin's defensive modus operandi might ensure the molecule to remain bound to its track until it detaches from the cargo. This behaviour could thus help to improve the efficiency of cellular cargo transport without any external regulatory control.

7.4 The world outside the test tube

Because of recent development and refinement of experimental procedures, it is nowadays possible to track down molecular motors, in their natural environment, the cell. With quantum dots attached, myosin V has been observed inside HeLa cells and cells of the actin cortex at the level of single-molecule studies [115, 116, 117]. The cargo domain influences the structural state of myosin V [118], which raises the question how the motion of myosin V is regulated in the cellular environment by other factors than nucleotide concentrations and forces. Ca^{2+} is known to regulate the active state of myosin V, and it would thus be interesting to investigate aspects of motor trafficking as a function of the calcium level. Moreover, the motor is not alone: Myosin V has to maneuver through its cellular environment upon interaction with microtubules and kinesin, as investigated in [119, 120, 109, 110]. The motor's own tracks, actin filaments, are covered with numerous motors moving in both directions, and obstacles such as the Arp 2/3 junction. It remains an open question how the cell deals with coordination of these interacting machines to ensure a functioning and stable system of cargo transportation. Do collective transport phenomena such as traffic jams have a higher function in the cell? Kinesin traffic, for instance, has been proposed to affect the depolymerization of microtubules through accumulation at the filament's end [121]. Many aspects about the chemical surrounding in the living cell that determine the operational regime of molecular motors remain open. The ATP concentration might vary inside a cell, but it is unclear whether it can reach a sufficiently low level that is rate-limiting to the motor's motion, and what effect it could have in the cell to collectively slow down motors. In addition, little is known about how densely motors are packed on the filament. There is sparse quantitative information about filament and motor densities in living organisms, such that it is not possible to

specify how crowded the environment of the motors is, and at which level they interact for transport. Addressing these questions both experimentally and theoretically will help to better understand the fascinating structure of the complex transport system in the cell. In this way, molecular motors can broaden the insight into the matter that constitutes life.

A Spanning trees for the chemomechanical network

In this work, we deal with several copies of a given chemical network that are connected by mechanical transitions, see Fig. 4.2. A path completion in the network takes place along trajectories that either connect two identical copies of a chemical state or the chemical state in itself, which is due to the periodic boundary conditions used for the system. One of the network cycles, $\mathcal{M}$, solely consists of mechanical transitions and thus constitutes a pathway of identical forward and backward transitions with the stepping rates $\omega_{55'}$, $\omega_{5'5''}$... and $\omega_{5'5}$, $\omega_{5''5'}$..., respectively, related by the balance condition 4.11. The number of mechanical transitions given by the corresponding di-edges in this pathway is $2N$, where N is the number of copies used for the network.
The network's dynamics properties should clearly be independent of the number of copies used for the network description. In the following, we use a simple example to illustrate how to deal with varying the number of copies for a given network, a single copy of which contains a loop.

The stochastic process for a network with a loop, is, in contrast to discrete time Markov processes, not well defined in the theory of Markov processes in continuous time, which exclude a transition leading from a state back to itself, and the transition matrix of the system can not be given. An extension to two copies of the network splits the state the loop belongs to into distinct copies, i. e., formally different states, and the Markov process can be recovered. Using the graph-theoretical approach by Kirchhoff, the step velocity through the self-loop can still be determined, in case the construction of a spanning tree is understood as considering all edges pointing towards a certain node. A loop thus forms two spanning trees, given by its two di-edges, which implicitly incorporates a differentiation of the state, as an orientation of the loop defines a stepping direction.

In Fig. A.1 (a), a network is shown that consists of three chemical on one mechanical transition, represented by solid and dashed lines. Panels (b) and (c) show the extended version of the network that consists of two and three of its copies. Let us now illustrate that the total velocities calculated from these networks are identical. Let $\mathcal{A}$, $\mathcal{A}'$ and $\mathcal{A}''$ be the network cycles for the chemical transitions, and $\Omega_i^{\mathcal{A}}$ the measures for the spanning trees as defined in 2.5 for the network cycle *only*, while we use Ω_i for the full network. By definition, we have equal transition rates within the network cycles, $\omega_{ij} = \omega_{i'j'} = \omega_{i''j''}$, if

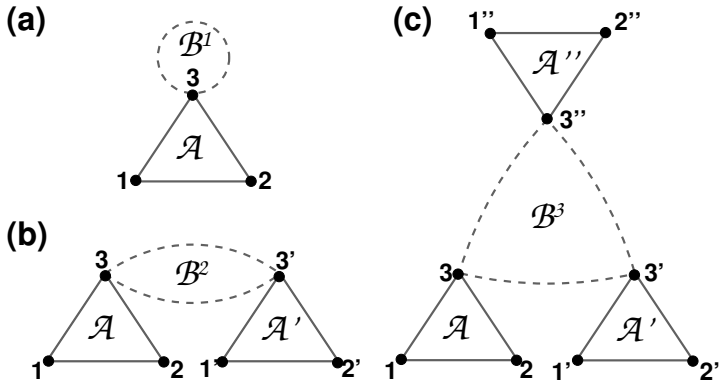

Figure A.1 : Illustration of network extension from one to three copies, with chemical transitions shown as solid and mechanical transitions as dashed lines. Each edge contains two directed transitions that are oriented with opposite directions to each other. (a) Network that consists of three states, with the third one having a loop that corresponds to a stepping transition. (b, c) Two and three copies of the same network, with $N = 2$ and $N = 3$, where the prime indicates a different spatial location. The transition rates in the new copies remain unchanged with respect to the original network. The cycles enclosed by chemical rates are denoted by $\mathcal{A}$, $\mathcal{A}'$ and $\mathcal{A}''$, while the mechanical transitions form the cycles $\mathcal{B}^N$, where $N = 1, 2, 3$.

follows that $\Omega_i^{\mathcal{A}} = \Omega_{i'}^{\mathcal{A}'} = \Omega_{i''}^{\mathcal{A}''}$. Now, let $\mathcal{B}^N$ be the cycle that is enclosed by mechanical transition, where $N = 1, 2, 3$ indicates the network with the corresponding number of copies. To distinguish between a forward and a backward step, we label the rates along the positive direction of $\mathcal{B}$ by an (f) and those along the negative direction by a (b). The stepping velocity in Fig. A.1 (a) is given by

$$v = \ell(\omega_{33}^f - \omega_{33}^b)\frac{\Omega_3}{\sum_i \Omega_i} = \ell(\omega_{33}^f - \omega_{33}^b)\frac{\Omega_3^{\mathcal{A}}}{\sum_i \Omega_i^{\mathcal{A}}}. \tag{A.1}$$

The latter equality holds because we have

$$\Omega_3 = \Omega_3^{\mathcal{A}}(\omega_{33}^f + \omega_{33}^b) \tag{A.2}$$

and

$$\sum_i \Omega_i = \sum_i \Omega_i^{\mathcal{A}}(\omega_{33}^f + \omega_{33}^b). \tag{A.3}$$

The loop that forms the cycle $\mathcal{B}^1$ is an artificial projection of the displacement onto a single site, but works for calculations because of assigning an oriented displacement

to the mechanical transitions. To investigate two copies of the network, $N = 2$, the chemical states are repeated and assigned a spatial position that corresponds to x and $x' = x + \ell$, separated by one mechanical transition. To close the structure periodically, a second mechanical transition with the stepping oriented in the opposite direction has to be included to ensure successive forward or backward stepping. These two transitions form the cycle $\mathcal{B}^2$. The velocity for the network with $N = 2$ is now given by the flux through both of the mechanical transitions,

$$v = \ell \left(\omega^f_{33'} \Omega_{3'} - \omega^b_{3'3} \Omega_3 - \omega^b_{33'} \Omega_{3'} + \omega^f_{3'3} \Omega_3 \right) \frac{1}{\sum_j \Omega_j}. \tag{A.4}$$

Here, the index j runs through all states of the network, $j = 1, ..3, 1'...3'$. This expression can be again simplified by explicit calculation of the Ω_j, which, for the states 3 and 3', are given by

$$\Omega_{3'} = \Omega_3^{\mathcal{A}} \cdot \Omega_3^{\mathcal{A}'} \cdot (\omega^b_{33'} + \omega^f_{33'}) \tag{A.5}$$

and

$$\Omega_3 = \Omega_3^{\mathcal{A}'} \cdot \Omega_3^{\mathcal{A}} \cdot (\omega^b_{3'3} + \omega^f_{3'3}). \tag{A.6}$$

The sum over all states of the network, consequently, reads

$$\sum_i \Omega_i \;=\; \Omega_3^{\mathcal{A}'} (\omega^b_{3'3} + \omega^f_{3'3}) \left(\sum_i \Omega_i^{\mathcal{A}} \right) + \Omega_3^{\mathcal{A}} (\omega^b_{33'} + \omega^f_{33'}) \left(\sum_{i'} \Omega_{i'}^{\mathcal{A}'} \right). \tag{A.7}$$

As $\omega^f_{33'} = \omega^f_{3'3}$ and $\omega^b_{33'} = \omega^b_{3'3}$ in accordance with the definition from the network extension, the velocity yields

$$v = 2\ell(\omega^b_{33'} + \omega^f_{33'})(\Omega_3^{\mathcal{A}})^2 \frac{1}{2\Omega_3^{\mathcal{A}} \sum_i \Omega_i^{\mathcal{A}}} = \ell(\omega^f_{33} - \omega^b_{33}) \frac{\Omega_3^{\mathcal{A}}}{\sum_i \Omega_i^{\mathcal{A}}}. \tag{A.8}$$

The extension to the network with $N = 3$ is straightforward. As the expressions are somewhat lengthy, we omit the calculation here and conclude with pointing out that the orientation of the stepping transition, is, in contrast to the case where $N = 1, 2$ implemented in the network through the order of the states $|33'3''\rangle$.

The smallest network that can be given for the Myosin V stepping behaviour includes a self-loop, as shown in Fig. A.2 (a). In our definition, stepping through a di-edge that corresponds to a forward transition is equivalent to the transition $|55'\rangle$, and likewise, $|5'5\rangle$ refers to a backward transition. In this way, a cycling velocity through this transition can be determined by running through the loop. As can be seen in the previous calculation,

that the steady state given by $\Omega_i \sum_i \Omega_i$ of the underlying Markov process does not depend on the rates given by the loop, and the stepping velocity given by the cycle $\mathcal{M}$ is given by their difference, $v \sim \omega_{55'} - \omega_{5'5}$. In the case of zero force, we have $\omega_{55'} = \omega_{5'5}$, and the purely mechanical step cycle $\mathcal{M}$ does not contribute to the total stepping velocity; it corresponds to a diffusion process. The network used throughout this work has been

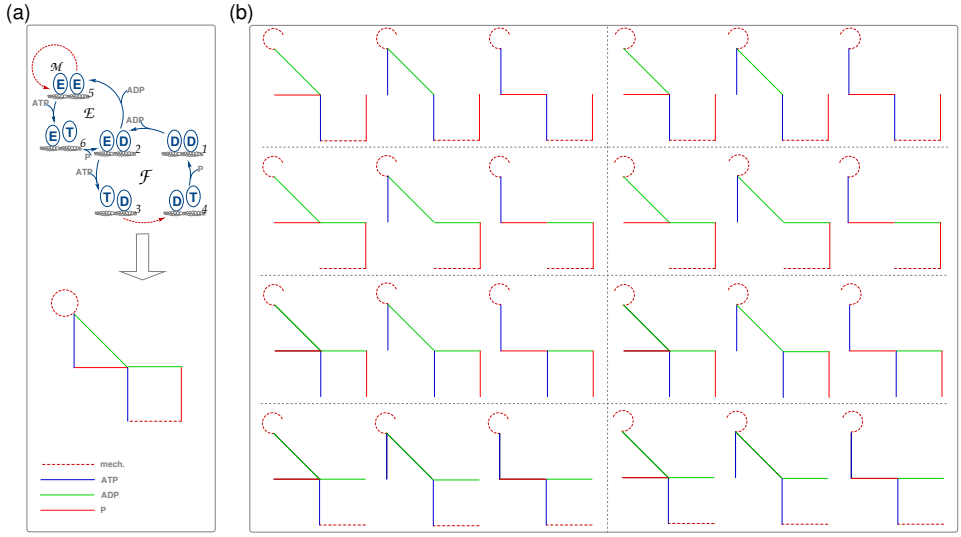

Figure A.2 : Single copy of the network with three cycles $\mathcal{F}$, $\mathcal{E}$ and $\mathcal{M}$ (a) and the corresponding set of spanning trees (b). (a) The full representation of the network is shown in the upper panel, with the corresponding graph in the lower panel. Its edges are color-coded such that the dashed, dark red lines correspond to mechanical transitions, ATP binding and release rates are shown in blue, and green and light red stand for ADP and P, respectively. (b) The spanning trees consist of all possible combinations of spanning trees for the single cycles $\mathcal{F}$, $\mathcal{E}$ and $\mathcal{M}$. Going from left to right, all spanning trees for a fixed part of $\mathcal{F}$ are shown. Note that the edge that forms the mechanical cycle $\mathcal{M}$ results in two distinct spanning trees as both di-edges point towards the rest of the graph independently. These sets are separated by the vertical grey line. Going from top to bottom, the four spanning trees of trees of $\mathcal{F}$ are passed through.

extended to contain three identical copies of a set of chemical states, as shown in Fig. 4.2. To keep the amount of spanning trees manageable, we show them for a single copy of the network. The Ω_i to obtain the corresponding steady state probability distribution,

$P_i^{\text{st}} = \Omega_i \sum_i \Omega_i$, read

$$
\begin{aligned}
\Omega_1 &= (\omega_{32}\omega_{21}(\omega_{43}+\omega_{41}) + \omega_{34}\omega_{41}(\omega_{21}+\omega_{23}))(\omega_{52}\omega_{62}+\omega_{56}\omega_{62}+\omega_{65}\omega_{52})(\omega_{55'}+\omega_{5'5}) \\
\Omega_2 &= (\omega_{43}\omega_{32}(\omega_{12}+\omega_{14}) + \omega_{41}\omega_{12}(\omega_{34}+\omega_{32}))(\omega_{52}\omega_{62}+\omega_{56}\omega_{62}+\omega_{65}\omega_{52})(\omega_{55'}+\omega_{5'5}) \\
\Omega_3 &= (\omega_{12}\omega_{23}(\omega_{43}+\omega_{41}) + \omega_{14}\omega_{43}(\omega_{21}+\omega_{23}))(\omega_{52}\omega_{62}+\omega_{56}\omega_{62}+\omega_{65}\omega_{52})(\omega_{55'}+\omega_{5'5}) \\
\Omega_4 &= (\omega_{23}\omega_{34}(\omega_{12}+\omega_{14}) + \omega_{21}\omega_{14}(\omega_{34}+\omega_{32}))(\omega_{52}\omega_{62}+\omega_{56}\omega_{62}+\omega_{65}\omega_{52})(\omega_{55'}+\omega_{5'5}) \\
\Omega_5 &= (\omega_{43}\omega_{32}(\omega_{12}+\omega_{14}) + \omega_{41}\omega_{12}(\omega_{34}+\omega_{32}))(\omega_{62}\omega_{25}+\omega_{26}\omega_{65}+\omega_{65}\omega_{26})(\omega_{55'}+\omega_{5'5}) \\
\Omega_6 &= (\omega_{43}\omega_{32}(\omega_{12}+\omega_{14}) + \omega_{41}\omega_{12}(\omega_{34}+\omega_{32}))(\omega_{52}\omega_{26}+\omega_{56}\omega_{26}+\omega_{25}\omega_{56})(\omega_{55'}+\omega_{5'5}),
\end{aligned}
$$

with the normalization factor $\sum_i \Omega_i$. As each Ω_i contains the factor $(\omega_{55'} + \omega_{5'5})$, one can easily see that $\Omega_i / \sum_i \Omega_i$ does not depend on ($\omega_{55'}$, and $\omega_{5'5}$).

B Network properties and additional experimental information

In this section, the basic ideas leading to our minimal model are discussed in more detail with respect to experimental findings that lead to qualitative insight rather than numerical input to the network. In our description, the existence of additional pathways is not ruled out a priori, and here, some arguments how omitted pathways are effectively incorporated, or do not change general properties of the results considered here, are given. We proceed with summarizing the experimental results that address the force dependence of chemical transition rates. Finally, we review additional experimental control parameters that could be included into the network.

B.1 Additional pathways and properties of F_s

As has been pointed out in chapter 5.4, a single chemomechanical network cycle has the inherent property that the stall force tends to zero as the energy supply to the motor is decreased, i. e., a vanishing hydrolysis rate h forces the stall force F_s to vanish because of the linear relationship between hydrolysis rate and motor motion. This property has been discussed in section 5.4. In the limit of a network that consists of the single cycle $\mathcal{F}$ only, one has thus to keep in mind that it has this property, although it need not necessarily be true for the real system. In the experimental community, it is generally assumed that the stall force does not depend on the supply of chemical energy, but a summary of experimental data of the stall forces measured for myosin V does not lead to a clear conclusion. The experimental values for the stall force of myosin V, that have been carried out under different experimental conditions, are shown in Fig. B.1 (a). Two groups, Mehta and Uemura, [20, 53] report a rather large stall force around 3 pN. Both of these do not use a feedback clamp, which means that the motor works steps against an increasing force until it either halts or detaches after several steps. There is no clear distinguishment between stall and detachment force. Furthermore, the group of Kad [91] refers to a "force prior to detachment" rather than a stall force. We point out here that the experiments carried out by the Rief group [45, 46] report rather low stall forces, $F_s \simeq 1.6$ pN, but, as a contrast, measure stepping velocities for a limiting amount of ATP, [ATP]=1 μM that typically are considerably higher, $v \simeq 100$ nm/s, than these determined by other groups [104, 105], where $v = 10 - 30$ nm/s. When considering these

stall forces as a function of the corresponding ATP concentrations given in terms of the chemical potential $\Delta\bar{\mu}$, one can, in principle, get an information about the functional relationship between F_s and $\Delta\bar{\mu}$. As can be infered from Fig. B.1 (b), the spread of the data does not allow for a clear conclusion. To calculate the chemical potential $\Delta\bar{\mu}$, one has to fix the concentrations of [ADP] and [P]. We show the potential for two different limiting concentrations that are above our threshold value of $0.1\mu M$, [ADP]=[P]=$0.5\mu M$ (red circles) and $1\mu M$ (cyan circles) to illustrate that the impact of this limiting value of the two concentrations does not influence the chemical potential significantly.

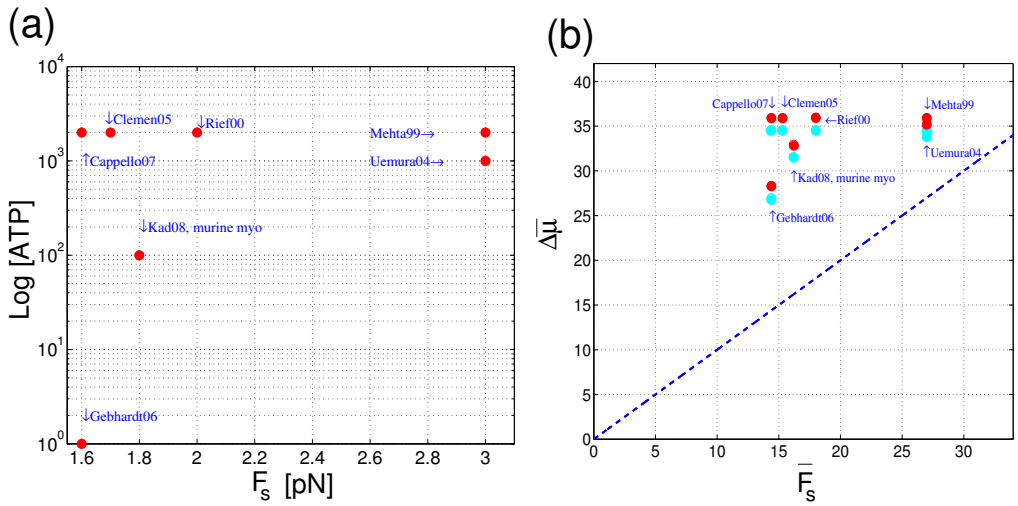

Figure B.1 : (a) Experimental values of the stall force F_s for different concentrations of [ATP], measured by different groups [20, 44, 53, 45, 46, 47, 91]. All constructs are from chick brain, except the one by Kad [91], which is murine, with actin filaments stemming from rabbits. (b) Stall force values in terms of the rescaled chemical potential $\Delta\bar{\mu} = \Delta\mu/k_BT$ and force $\bar{F} = \ell F/k_BT$. The concentrations of phosphate and ADP have not been reported for these experiments, and are typically assumed to be small. We use two values for [ADP] and [P], [ADP]=[P]=0.5 μM (red circles) and 1 μM (cyan circles). The solid line corresponds to vanishing velocity, $v = 0$, and hydrolysis rate, $h = 0$, as given by a single cycle $\mathcal{F}$. A conclusion about a variation of stall force with [ATP] concentration can not be drawn due to the spread in the data.

The existence of additional cycles that influence the motion of myosin V are thus not ruled out, but our network suggest that this influence might be small. In the regime of resisting forces up to the stall force F_s, two possible pathways are shown in Fig. B.2. The first cycle, shown in orange, involves a hydrolytic reaction upon backward stepping and introduced the state DE into the system, as reviewed in [99], while the green one involves the states TE and DE. These cycles contain the common backward stepping transition TD → DT along their direction of hydrolysis. What both cycles have in common is that

their preferred direction, indicated by arrows, involves ADP release from the molecule's leading head. This release rate, through gating, is slower than for the trailing head. But even if it were not, the influence of both cycles for small forces can not be distinguished from the main cycle $\mathcal{F}$ because all cycles share, in the backward direction, the same the rate-limiting step, namely the backward stepping transition. We have checked that,

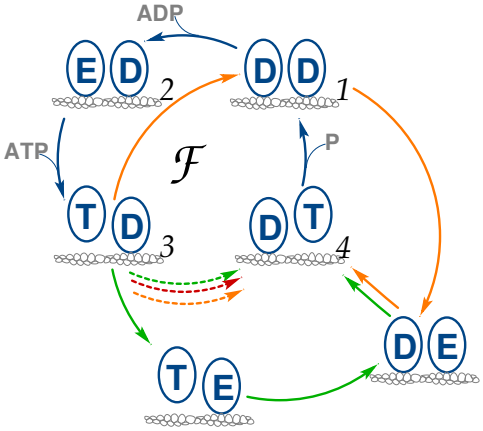

Figure B.2 : A network that consists of the chemomechanical cycle $\mathcal{F}$, with additional pathways for backward stepping, shown in orange and green. The orange pathway is based on the idea of reversing the symmetry of the motor's motion. The chemical pathway followed for the trailing head, that leads to a forward step, has an analogue for the leading head, connected with a backward step, given by the cycle DD → DE → DT → TD → DD. As discussed in the text, the existence of such a pathway can not be ruled out, but fits experimental data only with the use of additional parameters. The green cycle, given by the pathway TD → TE → DE → DT → TD is motivated by the idea to have a backward step connected to a hydrolysis that does not lead to slip cycles in the chemomechanical step cycle $\mathcal{F}$.

without further parametrization, the existence of these cycles, single and in combination, does not change our central qualitative results like the step ratio and the force-velocity relationship. While it would change the relation between $\Delta\bar{\mu}$ and $\bar{F}$, these changes occur for values of control parameters that are not accessed in typical experiments, like sub micro-molar concentrations of ATP. As the backward stepping rate, $\omega_{4'3}$, has been fixed through a fit to the experimental step ratio, its value can still capture effects of 'hidden' cycles.

A shortcoming of the orange cycle in Fig. B.2 is that it leads to inconsistency with experiment: The existence of a hydrolytic transition prior to a step leads, without further parametrization, to a decay in step velocity as a function of resisting load force that is more rapid than the one observed experimentally. Thus, our model enforces the assumption that weakening of the actin bond leads to rapid detachment of the trailing

head and that hydrolysis is supported with a head being attached to the filament. Taking the orange pathway into account would thus require a force dependent rate of hydrolysis that decreases for the leading head with a resisting force and, in the same time, increases for the trailing head. In the network presented here, such a parametrization is not necessary to explain the data up to the stall force. Moreover, the connection of these states with the mechanical cycle $\mathcal{M}$ would require the use of even more parameters.

In general, the force dependence of transition rates is an issue that is not trivial to treat both experimentally and theoretically. The functional changes in a complicated molecular complex like the myosin's binding pocket subject to a distorting force can not, at least not without limitations for the regime of force, be generalized into a simple physical framework, like Kramer's theory. Neither can they be determined experimentally in a straightforward manner because a direct observation would have to address an isolated chemical state, which usually is not feasible. Let us now briefly discuss the most important experimental findings about the force dependence of chemical transition rates.

B.2 The effect of load force on nucleotide binding

The rate of ADP binding and release as a function of load

To investigate the effect of gating, i. e., an accelerated rate of ADP release from the molecule's trailing head compared to the leading head, the response of single-headed Myosin V constructs to external load has been studied [101, 93]. Both binding and release of ADP are sensitive to load, and they change in an irregular way. In [93], the ATP binding rate decreases for both assisting and resisting forces, while ADP release is enhanced in the case of assisting forces and decreases for resisting forces, as shown in Fig. B.3. As the measurement contains both E and D states, these rates have been determined from a fit to a three state model of actomyosin binding and unbinding in [93]. Experiments carried out with double-headed Myosin, however, do not necessarily find this effect. It is thought that through intramolecular tension the molecule experiences different forces at the leading and the trailing head, when bound to the actin filament. An externally applied force acts in a backward direction on the leading head, while it is assisting for the trailing head. Thus, the ADP release is thought to be accelerated at the trailing head with respect to the leading head [90, 92]. Elasticity calculations in [95] show that the intramolecular tension can lead to internal forces up to $\simeq 2$ pN. Thus, a resisting external load would have to first overcome this tension prior to acting on the molecule. In [45], a significant force dependence of the ADP binding and release rates is ruled out for the double-headed motor for forces that do not exceed stall.

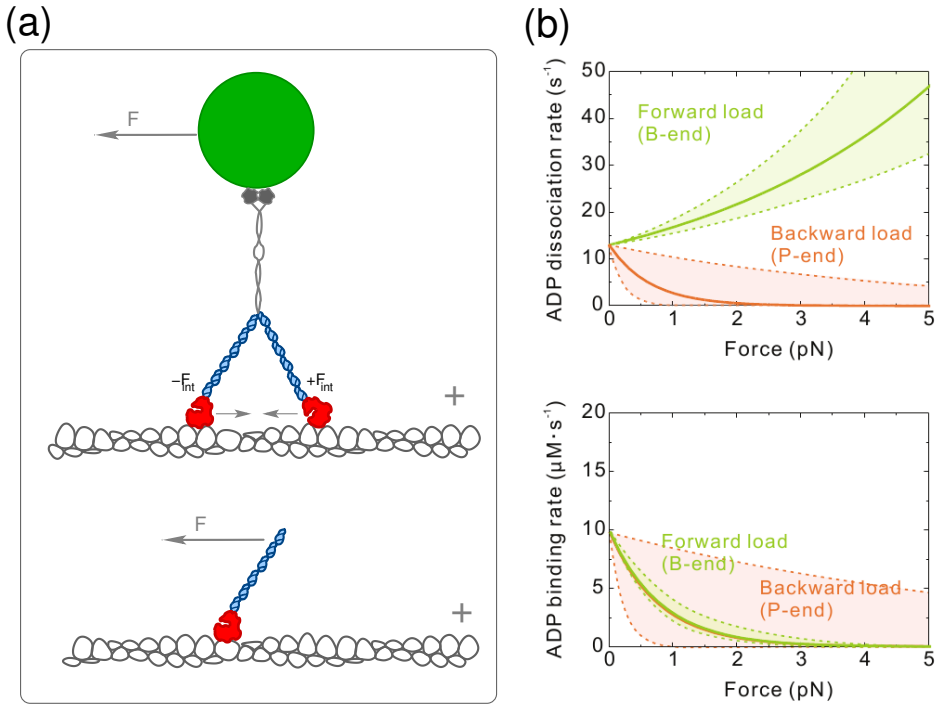

Figure B.3 : Forces acting on double - and single- headed myosin V constructs (a) and ADP dissociation and binding subject to an external force tested on a single-headed Myosin V construct, as measured in [93] (b). (a) The upper panel shows the external force applied to a cargo attached to the molecule, as well as internal forces that arise from intramolecular strain, F_{int}, acting in opposite directions on the leading and the trailing head, respectively. The exact impact of F on the heads is not resolved up to date. The lower panel indicates a force exerted onto a single head, with a direction that directly affects the motor head. (b) In the experiment [93], the green solid lines indicate an assisting force towards the barbed end of the actin filament (F<0 throughout this work), and backward loads towards the pointed end of the filament are shown in green. The dashed lines limiting the shaded areas sketch the uncertainty of the result. Upper panel, ADP dissociation rate. When pulled backwards (red line), the dissociation of ADP decreases exponentially, while it increases for assisting load. The value for $F = 0$ agrees with the findings in [48]. Lower panel, ADP binding rate. The rate of ADP binding decreases for both assisting and resisting forces. The figure is taken from [93].

The rate of ATP binding and release as a function of load

In [54, 55], the authors conclude that the ATP binding rate does only weakly depend on force for resisting forces up to 2 pN. In our calculations, the force dependence of the ATP binding rate sets in at forces that are in the range of the stall force F_s, for binding to an empty trailing head, where the leading head is empty. In [46], the step velocity for resisting forces that exceed the stall force does not significantly depend on [ATP]. The rate of ATP binding varies over two orders of magnitude with ATP concentration, being limiting to the step velocity for low [ATP]. In the network, a step velocity for superstall forces that does not depend on [ATP] is thus only feasible by *i)* a purely mechanical stepping cycle, $\mathcal{M}$, and *ii)* the decay of the ATP binding rate with force. In the network cycle $\mathcal{F}$, the nucleotide binding and release need not depend on force to maintain the ratchet behaviour which arises through the decrease of the binding rates of ATP and ADP in the enzymatic slip cycles $\mathcal{E}$.

The set of chemical rates that decay to zero with an external load is not unique. A forced stepping behaviour is characterized by a nonzero velocity in the mechanical cycle $\mathcal{M}$. To achieve this, a fraction of the rates competing with the cycle $\mathcal{M}$ need to decrease with resisting force. Formally, the requirement that $v \neq 0$ as $F \to \infty$ holds for different subsets of rates, e. g. P and ATP binding in the enzymatic cycle $\mathcal{E}$. The decay of chemical rates with an external load has to be in accordance with the balance conditions, which forces for introduction of unknown parameters into the system. It is thus certainly reasonable to restrict the decaying rates to a minimum. A strict mathematical analysis of how to achieve the limit of a nonvanishing velocity for large resisting forces is not feasible, because the asymptotic behaviour of the velocity with an increasing resisting force is determined by whether a chemical rate decays to zero, and how fast it does so or remains constant, and this information is not available for most of the chemical rates. The set of rates we have used for force-dependence, the binding of ATP and ADP in $\mathcal{E}$, leads to a mechanical ratchet that is both independent of [ATP] and [ADP], where the latter dependence in the regime of superstall forces has not been tested experimentally so far.

B.3 Experimental conditions

Biological experiments tend to be as diverse as life in itself. The attempt to explain experimental data demands for some care about the details of experimental conditions, because they may, in general, affect the results. Three major classes of experimental settings can be given as follows. First, there are measurements of double-headed and single-headed myosin V constructs, with the latter sometimes differing in the length of IQ motifs, i.e., the length of the lever arm [36, 37, 38, 39]. Second, the constructs stem from various organisms. The actin filaments typically are from the rabbit sceletal

muscle, while the myosin V is chick brain [45, 44, 20, 53, 46], and murine [91]. Third, the chemical environment in which the Myosin V has been tested may differ, e.g., there are different buffers, and different ionic strengths. Experiments with Myosin V are typically carried out at room temperature. To keep the ionic strength at constant level, different buffers are used, typically $\simeq 1\ mM$ EDTA, $\simeq 4\ mM$ $MgCl^2$, and the solution has a pH of 7.4 [26, 45]. KCl is a salt typically added to the experiments to mimick the chemical environment of the cell, it content varying from 25 -100 mM. In few experiments [91, 55], the salt conditions are controlled by using the physiological concentration of phosphate of up to $\simeq 40\ mM$, which is the ionic equivalent of ca. 92 mM KCl. The run length depends both on the KCl and phosphate concentration [26], and [55] find that [P] does not influence their findings about the myosin's power stroke significantly. The influence of [P] on the step ratio has been tested [91], but the vast majority of myosin experiments does not monitor [P] dependence as the corresponding concentrations are assumed to be small. The influence of Mg^{2+}, that, together with water, is involved in the hydrolysis of ATP, and Ca^{2+}, which influences the active and inactive state of the molecule and is known to bind to the molecule's lever has been investigated in [40, 41, 42].

C The Gillespie algorithm

The analytical calculations presented in this thesis have been crosschecked with simulations based on a Gillespie algorithm [107]. In addition, this algorithm has been used to calculate the distribution of dwell times for our network representation. In the following, we outline the structure of the algorithm along with an overview about the simulation parameters.

1. Set all rate constants for the transition rates ω_{ij}, and calculate the corresponding dwell times in each state, $\tau_i = 1/\sum_j \omega_{ij}$. Set an initial state. Note that the extraction of data can start only once the system has equilibrated to avoid influence from the starting state. Here, the initial state has been chosen as the DD state, because the occupation probability for this state in the stationary distribution is more than 90 %, and stationarity is reached after only a few steps. For the distribution of dwell times, one might want to circumvent the time for equilibration. This can be done by chosing an initial state with a probability according to the stationary distribution of network, as pointed out in [77]. Chose a simulation time. In our system, the simulation time has been set to perform $\simeq 10^6$ steps.

2. Set the system time to zero.

3. Initialize a jump from the present state i by drawing a random number n_r from the interval $[0, 1]$. Here, we have used a Mersenne Twister random number generator, which was initialized with the process ID to ensure that each realization of a run would differ. The probability to jump to a specific state i from state j is given by $\tau_i\omega_{ij}$, and the probabilities for all states branching off i are normalized.

4. Assign an interval of size $\tau_i\omega_{ij}$ in [0,1] to each state j connected to i and compare the intervals successively with the random number n_r. For reasons of speed, intervals should be sorted in order of decreasing size. If n_r lies within the interval, accept the move to the new state j, if it lies outside, reject it.

5. Draw a random number $t_j^{n_r}$ that is exponentially distributed with the average of the new state, τ_j. An exponentially distributed random number can be obtained by inverse transform sampling: An equally distributed random number n_r is drawn from the interval]0,1] and $t_j^{n_r}$ is determined as $t_j^{n_r} = -\ln(r)\tau_j$. Note that $n_r \neq 0$ is required in order to have a well-defined logarithm.

6. Update the time by adding the dwell time t^{n_r} to the system time.

7. Return to step 3 and repeat the procedure until the simulation time is reached.

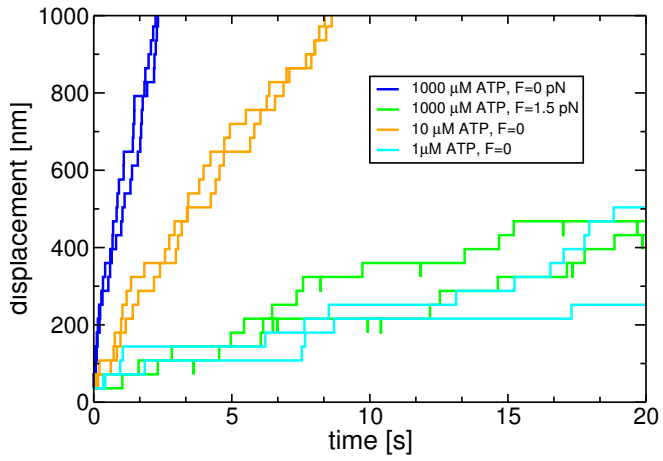

Figure C.1 : Stepping trajectories obtained with the Gillespie algorithm for different nucleotide concentrations and forces. The slope of the trajectory corresponds to the motor's velocity. Two different realizations are shown for each control parameter to indicate the variability of displacement. In the absence of force, $F = 0$, we first vary the ATP concentration. The blue lines are for a saturating concentration of ATP, while the cyan and orange lines are for limiting ATP concentration, [ATP]=10 μM and [ATP]=1 μM, respectively. The green line shows stepping for saturating ATP under a resisting force of 1.5 pN. One can clearly see that with decreasing [ATP], the dwell times of the motor rise, while in presence of an external load, backstepping events occur in addition.

The algorithm mimicks a stochastic process on a given network with $1...N$ states with specified transition rates ω_{ij} for going from state i to j. One can thus access all average quantities that have been obtained analytically, and additional information like higher moments of waiting times or cycle completions, as well as dwell time distributions that are outside the reach of an analytical solution. The stationary distribution of the process is extracted by monitoring the time the motor spends in each state j and averaging over *i)* a long run time or *ii)* many realizations such that the fraction of time spent in each state j with respect to all possible states $1...N$ can be determined. By recording the positions j the particle visits as a function of the stepping time, and recording each displacement, a stepping trajectory for the algorithm can be obtained, and the

corresponding distribution of dwell times is then given by a histogram of the times separating these events. Fig. C.1 shows different trajectories that have been obtained for our network, see Fig. 4.2 with different nucleotide concenrations with and without a resisting load. For each concenration, two trajectories are shown. The slope of the trajectories now corresponds to the stepping velocity of the motor, and the distance by which two realizations of a run are separated indicate the dispersion of the process.

D Explicit solutions of the dwell time distributions

We give the explicit solutions of the time-dependent derivatives of the network probabilities $P_{ij}(t)$ that determine dwell time distributions as given in chapter 6, as used in 6.8 and 6.9.

$$\begin{aligned}
\dot{P}_{44'}(t) &= \omega_{12}\omega_{23}\omega_{34}\omega_{41} \cdot \\
&\quad [-e^{-t\omega_{34}} \cdot B_1 \\
&\quad -e^{-t(\omega_{41}+\omega_{43})} \cdot B_2 \\
&\quad -e^{-\frac{1}{2}t(\omega_{12}+\omega_{21}+\omega_{23}+A)} \cdot \frac{B^{(+)}}{D} \\
&\quad +e^{-\frac{1}{2}t(\omega_{12}+\omega_{21}+\omega_{23}-A)} \cdot \frac{B^{(-)}}{D}] \qquad \text{(D.1)} \\
\dot{P}_{43''}(t) &= \omega_{43}e^{-t(\omega_{41}+\omega_{43})} \\
\dot{P}_{34'}(t) &= \omega_{34}e^{-t\omega_{34}}, \qquad \text{(D.2)}
\end{aligned}$$

with the coefficients

$$\begin{aligned}
A &= \sqrt{(\omega_{12}+\omega_{21})^2+\omega_{23}^2} \qquad \text{(D.3)} \\
B_1 &= \frac{1}{(\omega_{34}-\omega_{41}-\omega_{43})} \cdot \\
&\quad \frac{1}{(\omega_{12}(\omega_{23}-\omega_{34})+\omega_{34}(-\omega_{21}-\omega_{23}+\omega_{34}))} \\
B_2 &= \frac{1}{(-\omega_{34}+\omega_{41}+\omega_{43})} \cdot \\
&\quad \frac{1}{(\omega_{12}(\omega_{23}-\omega_{41}-\omega_{43})-(\omega_{21}+\omega_{23}-\omega_{41}-\omega_{43})(\omega_{41}+\omega_{43}))}
\end{aligned}$$

$$
\begin{aligned}
B^{(\pm)} &= -\omega_{12}^2 - \omega_{21}^2 - 2\omega_{21}\omega_{23} - \omega_{23}^2 + \\
&\quad \omega_{21}\omega_{34} + \omega_{23}\omega_{34} + \omega_{21}\omega_{41} + \omega_{23}\omega_{41} - \\
&\quad 2\omega_{34}\omega_{41} + \omega_{21}\omega_{43} + \omega_{23}\omega_{43} - 2\omega_{34}\omega_{43} + \\
&\quad \pm A(\omega_{21} + \omega_{23} - (\omega_{34} + \omega_{41} + \omega_{43})) + \\
&\quad \omega_{12}(-2\omega_{21} + \omega_{34} + \omega_{41} + \omega_{43} \pm A)) \\
D &= 2A(\omega_{12}(\omega_{23} - \omega_{34}) + \omega_{34}(-\omega_{21} - \omega_{23} + \omega_{34})) \\
&\quad (\omega_{12}(\omega_{23} - \omega_{41} - \omega_{43}) - (\omega_{21} + \omega_{23} - \omega_{41} - \omega_{43})(\omega_{41} + \omega_{43})).
\end{aligned}
\tag{D.4}
$$

E List of symbols

Latin symbols

$\mathbf{A}$	Adjacency matrix	p. 17
A_{ij}	Elements of an adjacency matrix	p. 17
$^{\text{abs}}$	Index for absorption	p. 29
$\mathcal{C}$	Cycle	p. 17
$\mathcal{C}_\nu^d$	Dicycle with orientation $d = \pm$	p. 21
$c_{ij,\nu}$	Index for the orientation of a cycle with respect to a related excess flux, with values 0, 1, -1	p. 21
^{d}	Orientation of a dicycle, $d = \pm$	p. 21
D	Diffusion constant	p. 22
D_m	Small scale diffusion coefficient in a chemical state m	p. 35
$^{\text{db}}$	Index for detailed balance	p. 23
$e(x, n \mid y, m)$	Exponential function that depends on the potential difference between chemical states n to m at locations x and y	p. 37
$^{\text{eq}}$	Index for equilibrium	
F	Component of the load force $\vec{F}$ that is parallel to the actin filament	p. 25
F‘	Force scale used in the force functions for chemical transitions	p. 52
F_{s}	Stall force of a molecular motor	p. 41
$\mathcal{G}$	Graph	p. 17
$g(t)$	Stochastic quantity influencing a potential $U(x)$	p. 34
h	Average hydrolysis rate of the motor in the steady state	
$I_m(x,t)$	Transition current density in a chemical state m	p. 34
$\mathbb{I}_{nm}$	n-by-m identity matrix	p. 32
J_{ij}^{st}	Steady state flux from state i to j	p. 17
$\Delta J^{\text{st}}(\mathcal{C}_\nu)$	Steady state excess flux on a cycle	p. 21
ΔJ^{eq}	Equilibrium flux for the states i and j	p. 23
ΔJ_{ij}	Local excess flux J between two states i and j	p. 17
$J_m(x,t)$	Lateral current in a chemical state m	p. 34
$J_{\text{tot}}(x,t)$	Total lateral current for all internal states	p. 36
k_{B}	Boltzmann’s constant	p. 24

ℓ	Step length of the motor	p. 22
ℓ_β	Step length of a step β	p. 26
ℓ_Ω	Localization length associated with $\Omega_{nm}(x)$	p. 36
l_i	Edge of a graph	p. 18
$n^{\mathrm{f+b}}$	Total number of motor steps	p. 63
$n_\alpha^\pm(\mathcal{C}_\nu^\pm))$	Number of binding (+) / release (-) of nucleotide species α per dicycle	p. 26
$n_\beta^{f,b}(\mathcal{C}_\nu^\pm))$	Number of forward (f) / backward (b) steps of type β per dicycle	p. 26
n_r	Equally distributed random number	p. 103
$\langle n_{\mathcal{C}^\pm}(t)\rangle$	Average number of cycle completions at time t	p. 22
$\langle n_{\mathcal{C}}(t)\rangle$	Average number of dicycle completions at time t	p. 22
$\mathbf{P}$	Matrix of solutions P_{ij} to the unrestricted master equation	p. 31
P_i^{eq}	Equilibrium probability for the motor to be in state i	
$P_i(t)$	Probability to find a motor in state i	p. 16
P_i^{st}	Steady state probability for the motor to be in state i	p. 17
$P_{ij}(t)$	Probability for a motor to dwell in state j given that it started in state i at $t = 0$	p. 28
$P_{ij\|k}$	Conditional probability for absorption with initial state i and absorbing state k	p. 30
$P_{ij,k}(t)$	Fraction of walks that start in i sojourn in j and are absorbed in k	p. 30
P_{ik}^{st}	Steady state probability for the motor to be absorbed in k given that it started in state i	p. 29
Pe	Peclet number	p. 23
$\Pr\{...\}$	Probability for an event to happen under the condition specified in $\{...\}$	p. 29
$P_m(x,t)$	Probability density for a chemical state m	
$P_{\mathrm{tot}}(x,t)$	Total probability density for all internal states	

$\mathbf{Q}$	Matrix constructed of eigenvectors of $\mathbf{T}$	p. 31
$\mathbf{Q^{-1}}$	Inverse of $\mathbf{Q}$	p. 31
$Q(\mathcal{C}_\nu^\pm)$	Thermal energy of a cycle $\mathcal{C}_\nu^\pm$	p. 25
r	Randomness parameter	p. 23
$_s$	Index for the different spanning trees associated with a graph	p. 18
$S(t)$	Entropy	p. 23
S^{i}	Internal entropy	p. 24
S^{e}	External entropy	p. 24
$\Delta S^{\mathrm{i}}(\mathcal{C}_\nu^\pm)$	Average entropy production during a dicycle completion	p. 24
t	Time	p. 16
t_i^{abs}	Time for absorption or dwell time when starting in a state i	p. 29
T	Temperature	p. 25
$\mathbf{T}$	Transfer matrix	
$\mathbf{T^0}$	Matrix that contains the absorbing states	p. 31
T_{ij}^0	Matrix that contains the absorbing states with entries ij	p. 31
$\mathcal{T}_s$	Spanning tree of a graph $\mathcal{G}$	p. 18
$\vec{\mathcal{T}}_s^i$	Directed or rooted spanning tree pointing towards a node i	p. 18
$U(\mathcal{C}_\nu^\pm)$	Internal energy of a cycle $\mathcal{C}_\nu^\pm$	p. 26
$U(x,t)$	Potential of molecular interaction that depends on a continous spatial coordinate x and time t	p. 34
$U(x)$	Time-independent potential of molecular interaction that depends on a continous spatial coordinate x	p. 34
$U_m(x)$	Potential of molecular interaction in a chemical state m	p. 35
v	Average stepping velocity of the motor in the steady state	p. 22
v_i	Vertex of a graph	p. 18
$V(x,t)$	External potential that depends on a continous spatial coordinate x and time t	p. 33
$V_m(x)$	Effective force potential of molecular interaction in a chemical state m	p. 35
$W(\mathcal{C}_\nu^\pm)$	Work connected to a cycle $\mathcal{C}_\nu^\pm$	p. 25
x	Continous, one-dimensional spatial coordinate	p. 34
x_k	Discrete position at with index k within a position x and $x+\ell$ on the filament	p. 36

$\langle 12..ij1\rangle$	Transitions for a network cycle without orientation	p. 21
$\|12...ij1\rangle$	Transitions for a network cycle along its +-direction	p. 21
$\|1ji...21\rangle$	Transitions for a network cycle along its −-direction	p. 21
$\|ij\rangle$	Transition from state i to state j	p. 21

Greek symbols

$\delta(x)$	Dirac's delta function	p. 36
ζ_{fr}	Friction coefficient	p. 33
ζ	Ratio of transition rates κ_{25}/κ_{12}	p. 50
η	Efficiency	p. 66
η^h	Efficiency rescaled with the hydrolysis rate	p. 66
θ	Parameter for the functions $\Phi_{ij}(F)$ of the stepping rates in the cycle $\mathcal{F}$	p. 48
κ_{ij}	Transition rate at $F = 0$ for nucleotide release and mechanical stepping	p. 46
$\hat{\kappa}_{ij}$	Transition rate at $F = 0$ for nucleotide binding	p. 46
κ_ν	Chord	p. 19
λ	Coupling parameter	p. 64
λ_0	Zero eigenvalue of matrix $\mathbf{T}$	p. 28
λ_i	i-th eigenvalue associated with matrix $\mathbf{T}$	p. 19
$\mathbf{\Lambda}$	Diagonal matrix with eigenvalues λ_i to $\mathbf{S}$ on the diagonal	p. 31
$\mu(\mathcal{C}_\nu^\pm)$	Chemical energy of a cycle $\mathcal{C}_\nu^\pm$	p. 26
μ_α	Chemical energy gained or released by binding or release of a nucleotide species α	p. 26
$\xi(t)$	Stochastic noise in the Langevin equation, white in our case	p. 33
$\rho_i^{\text{abs}}(t)$	Probability density for absorption with initial state i	p. 31
$\rho_{i\|k}^{\text{abs}}(t)$	Conditional probability density distribution to start in i and being absorbed in k	p. 30
$\sigma_{n_\mathcal{C}}^2(t)$	Variance associated with the completion of a network cycle	p. 22
$\tau_{\mathcal{C}^\pm}$	Mean time for a cycle completion in the cycle's direction $\pm$	p. 22
τ_i	Average dwell time in a state i	p. 29
$\tau_{i\|k}^{\text{abs}}(t)$	Conditional average absorption time to start in i and being absorbed in k	p. 31
$\Phi_{ij}(F)$	Function for the force dependent part of the transition rate ω_{ij} from state i to state j	p. 46
ω_{ij}	Transition rate from state i to state j	p. 17
χ_{ij}	Parameter for the functions $\Phi_{ij}(F)$ of the chemical transitions	p. 52
$\psi_i(t)$	Exponential distribution of waiting times in a state i	p. 29
$\omega_{nm}(x_k)$	Transition rate from chemical state n to m associated with location x_k	p. 36
Ω_i	Sum of all measures for a directed spanning trees $\vec{\mathcal{T}}_s^i$ for a given node i	p. 19
$\Omega(\vec{\mathcal{T}}_s^i)$	Measure for a directed spanning tree	p. 18
$\Omega_{nm}(x)$	Transition rate functions for transition from state n to state m	p. 36

Abbreviations

ADP	Adenosine diphosphate	p. 10
[ADP]	ADP concentration	p. 47
ATP	Adenosine triphosphate	p. 3
[ATP]	ATP concentration	p. 47
D	Chemical state with bound ADP	p. 16
DNA	Deoxyribonucleic acid	p. 5
E	Empty state	p. 16
FPE	Fokker-Planck equation	p. 34
FRET	Fluorescence Resonance Energy Transfer	p.10
GTP	Guanosine triphosphate	p. 7
IQ	Calmodulin binding sequence of amino acids	p. 9
MD	Molecular Dynamics (simulations)	p. 10
P	Phosphate	p. 15
T	Chemical state with bound ATP	p. 16
Θ	Chemical state with bound ADP*P	p. 16
[P]	Phosphate concentration	p. 47
RNA	Ribonucleic acid	p. 7

Bibliography

[1] B. Alberts. Molecular Biology of the Cell. Garland, 4th edition, 2002.

[2] G. Michal. Biochemical pathways. Spektrum, 1999.

[3] Poster of metabolic pathways. http://www.sigmaaldrich.com.

[4] M. G. L. Heuvel and C. Dekker. Motor proteins at work for nanotechnology. Science, 317:333, 2007.

[5] U. Seifert. Fluctuation theorem for a single enzym or molecular motor. Europhysics Letters, 70:36, 2005.

[6] A. Lau, D. Lacoste, and K. Mallick. Nonequilibrium fluctuations and mechanochemical couplings of a molecular motor. Physical Review Letters, 99:158102, 2007.

[7] S. Liepelt and R. Lipowsky. Operation modes of the molecular motor kinesin. Physical Review E, 79:011917, 2009.

[8] S. Liepelt and R. Lipowsky. Impact of slip cycles on the operation modes and efficiency of molecular motors. Journal of Statistical Physics, 141:1, 2010.

[9] T. Schmiedl and U. Seifert. Efficiency of molecular motors at maximum power. Europhysics Letters, 83:30005, 2008.

[10] J. Howard. Mechanics of Motor Proteins and the Cytoskeleton. Sinauer Associates, 2001.

[11] R. Lipowsky, S. Liepelt, and A. Valleriani. Energy conversion by molecular motors coupled to nucleotide hydrolysis. Journal of Statistical Physics, 135:951, 2009.

[12] R. Lipowsky, J. Beeg, R. Dimova, S. Klumpp, S. Liepelt, and M. J. I. Müller. Active bio-systems: from single motor molecules to cooperative cargo transport. Biophysics reviews and letters, 4:77, 2009.

[13] R. Lipowsky and S. Klumpp. Life is motion: multiscale motility of molecular motors. Physica A: Statistical Mechanics and its Applications, 352:53, 2005.

[14] P. Reimann. Brownian motors: noisy transport far from equilibrium. Physics Reports, 361:57, 2002.

[15] F. Jülicher, A. Ajdari, and J. Prost. Modeling molecular motors. Reviews of Modern Physics, 69:1269, 1997.

[16] R. Dean Astumian. Thermodynamics and kinetics of a brownian motor. Science, 276:117, 1997.

[17] V. Bierbaum and R. Lipowsky. Chemomechanical network cycles of the molecular motor myosin V. Biophysical Journal, 100:1747, 2011.

[18] V. Bierbaum and R. Lipowsky. Dwell time distributions for myosin v. In preparation.

[19] Y. Goda. Along memory lane. Nature News and Views, 456:590, 2008.

[20] A. D. Mehta, R. S. Rock, M. Rief, J. A. Spudich, M. S. Mooseker, and R. E. Cheney. Myosin-V is a processive actin-based motor. Nature, 400:590, 1999.

[21] T. Sakamoto, M. R. Webb, E. Forgacs, and H. D. White. Direct observation of processive movement by individual myosin V molecules. Biochemical and Biophysical Research Communications, 272:586, 2000.

[22] Z. Wang, J. G. Edwards, N. Riley, W. D. Provance Jr., R. Karcher, X.-D. Li, I. G. Davison, M. Ikebe, J. A. Mercer, J. A. Kauer, and M. D. Ehlers. Myosin Vb mobilizes recycling endosomes and AMPA receptors for postsynaptic plasticity. Cell, 135:535, 2008.

[23] S. Correia, S. Bassani, T. C. Brown, F.-M. Lise, D. M. Backos, A. El-Husseini, M. Passafaro, and J. S. Estaban. Motor protein–dependent transport of AMPA receptors into spines during long-term potentiation. Nature Neuroscience, 11:457, 2008.

[24] J. A. Spudich. The myosin swinging cross-bridge model. Nature Reviews Molecular Cell Biology, 2:387, 2001.

[25] L. Liu, D. W. Taylor, E. B. Krementsova, K. M. Trybus, and K. A. Taylor. Three-dimensional structure of the myosin v inhibited state by cryoelectron tomography. Nature, 442:208, 2006.

[26] J. E. Baker, E. B. Krementsova, G. G. Kennedy, A. Armstrong, K. M. Trybus, and D. M. Warshaw. Myosin V processivity: Multiple kinetic pathways for head-to-head coordination. Proceedings of the National Academy of Sciences of the United States of America, 101:5542, 2004.

[27] N. Kodera, D. Yamamoto, R. Ishikawa, and T. Ando. Video imaging of walking myosin V by high-speed atomic force microscopy. Nature, 468:72, 2010.

[28] M. A. Titus. Motor proteins: Myosin V - the multi-purpose transport motor. Curr. Biol., 7:R301, 1997.

[29] S Reck-Peterson. Class V myosins. Biochimica et Biophysica Acta - Molecular cell research, 1496:36, 2000.

[30] A. D. Mehta. Myosin learns to walk. Journal of Cell Science, 114:1981, 2001.

[31] M. J. Tyska and M. S. Mooseker. Myosin-v motility: these levers were made for walking. Trends in Cell Biology, 13:447, 2003.

[32] R. D. Vale. Myosin V motor proteins: marching stepwise towards a mechanism . Journal of Cell Biology, 163:445, 2003.

[33] J. E. Molloy and C. Veigel. Myosin motors walk the walk. Science, 300:2045, 2003.

[34] J. R. Sellers and C. Veigel. Walking with myosin V. Current Opinion in Cell Biology, 18:68, 2006.

[35] A. Vilfan. Five models for myosin v. Frontiers in Bioscience, 14:2269, 2009.

[36] O. Oke, S. Burgess, E. Forgacs, P. Knight, T. Sakamoto, and J. Sellers. Influence of lever structure on myosin 5a walking. Proceedings of the National Academy of Sciences of the United States of America, 107:2509, 2010.

[37] J. R. Moore, E. B. Krementsova, K. M. Trybus, and D. M. Warshaw. Does the myosin V neck region act as a lever? Journal of Muscle Research and Cell Motility, 25:29, 2004.

[38] T. J. Purcell, C. A. Morris, J. A. Spudich, and H. L. Sweeney. Role of the lever arm in the processive stepping of myosin V . Proceedings of the National Academy of Sciences of the United States of America, 99:14159, 2002.

[39] T. Sakamoto, A. Yildiz, P. R. Selvin, and J. R. Sellers. Step-size is determined by neck length in myosin V. Biochemistry, 44:16203, 2005.

[40] D. E. Hannemann, W. Cao, A. O. Olivares, J. P. Robblee, and E. M. de la Cruz. Magnesium, ADP, and actin binding linkage of myosin V: evidence for multiple myosin V-ADP and actomyosin V-ADP states. Biochemistry, 44:8826, 2005.

[41] D. N. Krementsov, E. B. Krementsova, and K. M. Trybus. Myosin V: regulation by calcium, calmodulin, and the tail domain . The Journal of Cell Biology, 164:878, 2004.

[42] H. Lu, E. B. Krementsova, and K. M. Trybus. Regulation of myosin V processivity by calcium at the single molecule level . The Journal of Biological Chemistry, 281:31987, 2006.

[43] J. R. Moore, E. B. Krementsova, K. M. Trybus, and D. M. Warshaw. Myosin V exhibits a high duty cycle and large unitary displacement . The Journal of Cell Biology, 155:625, 2001.

[44] M. Rief, R. S. Rock, A. D. Mehta, M. S. Mooseker, R. E. Cheney, and J. A. Spudich. Myosin-V stepping kinetics: A molecular model for processivity. Proceedings of the National Academy of Sciences of the United States of America, 97:9482, 2000.

[45] A. E-M. Clemen, M. Vilfan, J. Jaud, J. Zhang, M. Bärmann, and M. Rief. Force-dependent stepping kinetics of myosin-V. Biophysical Journal, 88:4402, 2005.

[46] J. Gebhardt, A. E-M. Clemen, J. Jaud, and M. Rief. Myosin-V is a mechanical ratchet. Proceedings of the National Academy of Sciences of the United States of America, 103:8680, 2006.

[47] G. Cappello, P. Pierobon, C. Symonds, L. Busoni, J. C. M. Gebhardt, J. Prost, and M. Rief. Myosin V stepping mechanism. Proceedings of the National Academy of Sciences of the United States of America, 104:15328–15333, 2007.

[48] E. de La Cruz, A. M. Wells, S. S. Rosenfeld, M. E. Ostap, and H. L. Sweeney. The kinetic mechanism of myosin V. Proceedings of the National Academy of Sciences of the United States of America, 96:13726, 1999.

[49] M. L. Walker, S. A. Burgess, J. R. Sellers, F. Wang, J. A. Hammer III, J. Trinick, and P. J. Knight. Two-headed binding of a processive myosin to f-actin. Nature, 405:804, 2000.

[50] M. Sun, M. B. Rose, S. K. Ananthanarayanan, D. J. Jacobs, and C. M. Yengo. Characterization of the pre-force-generation state in the actomyosin cross-bridge cycle. Proceedings of the National Academy of Sciences of the United States of America, 105:8631, 2008.

[51] M. Cecchini, A. Houdusse, and M. Karplus. Allosteric communication in Myosin V: from small conformational changes to large directed movements. PLoS Computational Biology, 4:1, 2008.

[52] K Shiroguchi. Myosin V walks by lever action and Brownian motion. Science, 316:1208, 2007.

[53] S. Uemura, H. Higuchi, A. O. Olivares, E. M. de la Cruz, and S. Ishiwata. Mechanochemical coupling of two substeps in a single myosin V motor. Nature structural & molecular biology, 11:877, 2004.

[54] C. Veigel, S. Schmitz, F. Wang, and J. R. Sellers. Load-dependent kinetics of myosin-V can explain its high processivity. Nature cell biology, 7:861, 2005.

[55] J. Sellers and C. Veigel. Direct observation of the myosin-Va power stroke and its reversal. Nature structural & molecular Biology, 17:590, 2010.

[56] T. Okada, H. Tanaka, A. Hikikoshi Iwane, K. Kitamura, M. Ikebe, and T. Yanagida. The diffusive search mechanism of processive myosin class-v motor involves directional steps along actin subunits. Biochemical and Biophysical Research Communications, 354:379, 2007.

[57] A. Yildiz, J. E. Forkey, S. A. McKinney, T. Ha, Y. E. Goldman, and P. R. Selvin. Myosin V walks hand-over-hand: Single fluorophore imaging with 1.5-nm localization. Science, 300:2061, 2003.

[58] D. M. Warshaw, G. G. Kennedy, S. S. Work, E. B. Krementsova, S. Beck, and K. M. Trybus. Differential labeling of myosin V heads with quantum dots allows direct visualization of hand-over-hand processivity. Biophysical Journal : Biophysical Letters, page L30, 2005.

[59] A. R. Dunn and J. A. Spudich. Dynamics of the unbound head during myosin V processive translocation. Nature structural & molecular biology, 14:246, 2007.

[60] G. Kirchhoff. Über die Auflösung der Gleichungen, auf welche man bei der Untersuchung der linearen Verteilung galvanischer Ströme geführt wird. Annalen der Physik und Chemie, 148:497, 1847.

[61] N. G. van Kampen. Stochastic processes in physics and chemistry. Elsevier, revised and enlarged edition, 1992.

[62] L. Volkmann. Fundamente der Graphentheorie. Springer, 1996.

[63] T. L. Hill. Free energy transduction and biochemical cycle kinetics. Springer, 1989.

[64] T. L. Hill and Y. Chen. Stochastics of cycle completions (fluxes) in bio-chemical kinetic diagrams. Proceedings of the National Academy of Sciences of the United States of America, 72:1291, 1975.

[65] B. Derrida. Velocity and diffusion constant of a periodic one-dimensional hopping model. Journal of Statistical Physics, 31:433, 1983.

[66] K. Svoboda, P. Mitra, and S. Block. Fluctuation analysis of motor protein movement and single enzyme-kinetics. Proceedings of the National Academy of Sciences of the United States of America, 91:11782, 1994.

[67] S. Liepelt and R. Lipowsky. Kinesin's network of chemomechanical motor cycles. Physical Review Letters, 98:258102, 2007.

[68] J. Schnakenberg. Network theory of microscopic and macroscopic behavior of master equation systems. Reviews of Modern Physics, 48:4, 1976.

[69] L. Jiu-li, C. van den Broeck, and G. Nicolis. Stability criteria and fluctuations around nonequilibrium states. Z. Phys. B, Condensed Matter, 56:165, 1984.

[70] J. L. Lebowitz and H. Spohn. A Gallavotti-Cohen-type symmetry in the large deviation functional for stochastic dynamics. Journal of Statistical Physics, 95:1, 1999.

[71] C. Maes and M. H. van Vieren. A markov model for kinesin. Journal of Statistical Physics, 112:1, 2003.

[72] S. Liepelt and R. Lipowsky. Steady-state balance conditions for molecular motor cycles and stochastic nonequilibrium processes. Europhysics Letters, 77:6, 2007.

[73] R. Lipowsky and S. Liepelt. Chemomechanical Coupling of Molecular Motors: Thermodynamics, Network Representations, and Balance Conditions. Journal of Statistical Physics, 130:39, 2008. Erratum: *Journal of Statistical Physics*, 135:777, 2009.

[74] T. L. Hill and R. M. Simmons. Free-energy levels and entropy production associated with biochemical kinetic diagrams. Proceedings of the National Academy of Sciences of the United States of America, 73:95, 1976.

[75] D. Tsygankov, M. Linden, and M. E. Fisher. Back-stepping, hidden substeps, and conditional dwell times in molecular motors. Physical Review E, 75:021909, 2007.

[76] A. Valleriani, S. Liepelt, and R. Lipowsky. Dwell time distributions for kinesin's mechanical steps. Europhysics Letters, 82:28011, 2008.

[77] J.-C. Liao, J. A. Spudich, D. Parker, and S. L. Delp. Extending the absorbing boundary method to fit dwell-time distributions of molecular motors with complex kinetic pathways. Proceedings of the National Academy of Sciences of the United States of America, 104:3171, 2007.

[78] C. Gardiner. Handbook of Stochastic Methods: a handbook for the natural and social sciences. Springer, 2009.

[79] R. Zwanzig. Nonequilibrium Statistical Mechanics. Oxford University Press, 2001.

[80] D. Keller and C. Bustamante. The mechanochemistry of molecular motors. Biophysical Journal, 78:541, 2000.

[81] G. Lattanzi and A. Maritan. Force dependence of the Michaelis constant in a two-state ratchet model for molecular motors. Physical Review Letters, 86:1134, 2001.

[82] G. Lattanzi and A. Maritan. Force dependent transition rates in chemical kinetics models for motor proteins. The Journal of Chemical Physics, 117:10339, 2002.

[83] G. Lattanzi and A. Maritan. Master equation approach to molecular motors. Physical review. E, 64:061905, 2001.

[84] R. Lipowsky and T. Harms. Molecular motors and nonuniform ratchets. European Biophysics Journal, 29:542, 2000.

[85] R. Lipowsky and N. Jaster. Molecular motor cycles: From ratchets to networks. Journal of Statistical Physics, 110:1141, 2003.

[86] R. P. Feynman. The Feynman Lectures on Physics, Vol. 1. Addison-Wesley, 1963.

[87] H. Risken. The Fokker-Planck equation : methods of solution and applications. Springer, 2nd edition, 1989.

[88] F. Jülicher. Statistical physics of active processes in cells. Physica A, 369:185, 2006.

[89] T. Sakamoto, M. R. Webb, E. Forgacs, H. D. White, and J. R. Sellers. Direct observation of the mechanochemical coupling in Myosin Va during processive movement. Nature, 455:128, 2008.

[90] C. Veigel, F. Wang, M. L. Bartoo, J. R. Sellers, and J. E. Molloy. The gated gait of the processive molecular motor, myosin V. Nature cell biology, 4:59, 2002.

[91] N. M. Kad, K. M. Trybus, and D. M. Warshaw. Load and Pi control flux through the branched kinetic cycle of myosin V. The Journal of Biological Chemistry, 283:17477, 2008.

[92] S. S. Rosenfeld and H. L. Sweeney. A model of myosin V processivity. The Journal of Biological Chemistry, 279:40100, 2004.

[93] Y. Oguchi, S. V. Mikhailenko, T. Ohki, A. O. Olivares, E. M. de la Cruz, and S. Ishiwata. Load-dependent ADP binding to myosins V and VI: implications for subunit coordination and function. Proceedings of the National Academy of Sciences of the United States of America, 105:7714, 2008.

[94] K. I. Skau, R. B. Hoyle, and M. S. Turner. A kinetic model describing the processivity of myosin-V. Biophysical Journal, 91:2475, 2006.

[95] A Vilfan. Elastic lever-arm model for myosin V. Biophysical Journal, 88:3792, 2005.

[96] E. M. Craig and H. Linke. Mechanochemical model for myosin V. Proceedings of the National Academy of Sciences of the United States of America, 106:18261, 2009.

[97] A. B. Kolomeisky and M. E. Fisher. A simple kinetic model describes the processivity of myosin-V. Biophysical Journal, 84:1642, 2003.

[98] D. Tsygankov and M. E. Fisher. Mechanoenzymes under superstall and large assisting loads reveal structural features. Proceedings of the National Academy of Sciences of the United States of America, 104:19321, 2007.

[99] R. Dean Astumian. Thermodynamics and kinetics of molecular motors. Biophysical Journal, 98:2401, 2010.

[100] E. Forgacs, S. Cartwright, T. Sakamoto, J. R. Sellers, J. E. T. Corrie, M. R. Webb, and H. D. White. Kinetics of ADP dissociation from the trail actomyosin V following the power stroke. The Journal of Biological Chemistry, 283:766, 2008.

[101] T. J. Purcell, H. L. Sweeney, and J. A. Spudich. A force-dependent state controls the coordination of processive myosin V. Proceedings of the National Academy of Sciences of the United States of America, 102:13873–13878, 2005.

[102] J. Robblee, W. Cao, A. Henn, D. Hannemann, and E. de la Cruz. Thermodynamics of nucleotide binding to actomyosin V and VI: A positive heat capacity change accompanies strong ADP binding. Biochemistry, 44:10238, 2005.

[103] A. L. Friedmann, M. A. Geeves, D. J. Manstein, and J. A. Spudich. Kinetic characterization of myosin head fragments with long-lived myosin-ATP states. Biochemistry, page 9679, 1998.

[104] J. E. Forkey, M. E. Quinian, M. A. Shaw, J. E. T. Corrie, and Y. E. Goldman. Three-dimensional structural dynamics of myosin V by single-molecule fluorescence polarization. Nature, 422:399, 2003.

[105] Y. Komori and A. H. Iwane. Myosin-V makes two Brownian 90 degrees rotations per 36-nm step. Nature structural & molecular biology, 14:968, 2007.

[106] N. J. Carter and R. A. Cross. Mechanics of the kinesin step. Nature, 435:308, 2005.

[107] D. T. Gillespie. Exact stochastic simulation of coupled chemical reactions. The Journal of Physical Chemistry, 81:2340, 1977.

[108] E. de la Cruz, H. L. Sweeney, and M. E. Ostap. ADP inhibition of myosin V ATPase activity. Biophysical Journal, 79:1524, 2000.

[109] M. Ali, H. Lu, C. Bookwalter, D. Warshaw, and K. Trybus. Myosin V and Kinesin act as tethers to enhance each others' processivity. Proceedings of the National Academy of Sciences of the United States of America, 105:4691, 2008.

[110] F. Berger, M. J. I. Mueller, and R. Lipowsky. Enhancement of the processivity of kinesin-transported cargo by myosin V. Europhysics Letters, 87:28002, 2009.

[111] E. L. F. Holzbaur and Y. E. Goldman. Coordination of molecular motors: from in vitro assays to intracellular dynamics. Current Opinion in Cell Biology, 22:4, 2010.

[112] G. E. Snyder, T. Sakamoto, J. A. Hammer III, J. R. Sellers, and P. R. Selvin. Nanometer localization of single green fluorescent proteins: Evidence that myosin V walks hand-over-hand via telemark configuration. Biophysical Journal, 87:1776, 2004.

[113] J. A. Spudich and R. S. Rock. A crossbridge too far. Nature cell biology, 4:E8, 2002.

[114] M. J. I. Müller, S. Klumpp, and R. Lipowsky. Tug-of-war as a cooperative mechanism for bidirectional cargo transport by molecular motors. Proceedings of the National Academy of Sciences of the United States of America, 105:4609, 2008.

[115] P. Pierobon, S. Achouri, S. Courty, A. Dunn, J. Spudich, and M. Dahan. Velocity, processivity, and individual steps of single Myosin V molecules in live cells. Biophysical Journal, 96:4268, 2009.

[116] Y. E. Goldman and C. Veigel. Drunk or sober? Myosin V walks the (quantum) dotted line in cells. Biophysical Journal, 97:399, 2009.

[117] S. Nelson, M. Ali, K. Trybus, and D. Warshaw. Random walk of processive, quantum dot-labeled myosin Va molecules within the actin cortex of COS-7 cells. Biophysical Journal, 97:509, 2009.

[118] K. Thirumurugan, T. Sakamoto, J. A. Hammer III, J. R. Sellers, and P. J. Knight. The cargo-binding domain regulates structure and activity of myosin 5. Nature, 442:212, 2006.

[119] J. A. III Hammer and X. Wu. Slip sliding away with myosin v. Proceedings of the National Academy of Sciences of the United States of America, 104:5255, 2007.

[120] M. Ali, E. Krementsova, G. Kennedy, R. Mahaffy, T. Pollard, and K. Trybus. Myosin Va maneuvers through actin intersections and diffuses along microtubules. Proceedings of the National Academy of Sciences of the United States of America, 104:4332, 2007.

[121] V. Varga, C. Leduc, V. Bormuth, S. Diez, and J. Howard. Kinesin-8 Motors act cooperatively to mediate length-dependent microtubule depolymerization. Cell, 138:1174, 2009.

summasummarum.

Das letzte Element der Arbeit möchte hier ernst und genau genommen werden. Vorsichtig und aus der Ferne betrachtet und gegens Licht gehalten, dasjenige der Wahr- und Weisheit, erweist es sich als hübsches Gebilde, welches für sich allein nicht existieren kann, sondern durch andere getragen wird. Man nennt es also Unterstützung, ohne die das Unterfangen Doktorarbeit nicht halb so spannend geworden wäre, und die mir die Zeit in Berlin im allgemeinen und Golm im Speziellen in ein so schönes Technicolor gefärbt haben.

Ich bedanke mich bei Prof. Lipowsky für das Thema, höchste Diskussionskultur, die nicht selten mit einem 'Hut ab' endet, dessen Begeisterung für die Wissenschaft weit über die biologische (Ur)suppe hinausreicht und alle Bereiche von der künstlichen Intelligenz bis zur klassischen Betrachtungen von Instabilitäten und Energie- und Impulserhaltung auf glattem Grund reicht. Auch die wissenschaftlich-taktische Unterstützung aus Schwaben, die von Florian Berger, Stefan Klumpp und Corina -Fastschwaben- Keller zur Verfügung gestellt worden ist, lässt sich nur über den hohen Klee loben, denn sie hat mir in regelmässigen Abständen die Augen geöffnet, den Weg gezeigt, oder vor dem Abgrund bewahrt, oder auch Ferien eingehandelt.

Der grösste Dank ergeht an die gesamte Golm-Crew, explizit eingeschlossen und genannt Peter Westermeier, die sich nicht nur durch ihre brillante Wissenschaft auszeichnet, die irgendwo zwischen Schwein und Bombenkunde angesiedelt ist, sondern, ausser-

dem durch einen hartnäcken Hang zum Extremexperiment in jedwedem Brandenburger Terrain. Für die Begleitung durch die Welt der Wissenschaft in allen Lebenslagen bis an die Grenzen Hamburgs und zurück in die Äste vom Apfelbaum in Golm, möcht ich Lorbeer verteilen über Caro, Flo, Rolandski, Corina, Thomas, Carlus, et al.

Ich verbleibe in andächtiger Bewunderung für Lebensrat und -Künste von meinen drei Weisen Neo, Anne, und Robert, die mich seit Jahren an ihrem unerschöpflichen Wissen zu allem teilhaben lassen, und jederzeit noch einen Notanker in Form von Betten, Futter, und Bier in der Tasche haben. Dass die Gravitation im allgemeinen überschätzt wird, ist bekannt, wird aber, ob Kegel oder Frankenjura, eindrucksvoll bewiesen von Stefan, Nick, Micha, und Johannes, die auch, danke dafür, den letzten Fels hochtreiben. An die Expertin für Luft- und Raumfahrttechnik, und das Lektorium dieser Schrift, Frau A-Punkt, ein HelmAuf!

Für die Besten zwei, die absolut im Wind und auch dagegen, seit Jahren sozusagen, mit an Bord sind, Dani und Mama, danke.